

**DESIGN AND DEVELOP AN ACTIVE MIXER  
EXTRUDER FOR INK BASED 3D PRINTER**

**CHEAH CHOON KIT**

**UNIVERSITI TUNKU ABDUL RAHMAN**

**DESIGN AND DEVELOP AN ACTIVE MIXER FOR  
INK BASED 3D PRINTER**

**CHEAH CHOON KIT**

**A project report submitted in partial fulfilment of the  
requirements for the award of Bachelor of Engineering  
(Honours) Mechanical Engineering**

**Lee Kong Chian Faculty of Engineering and Science  
Universiti Tunku Abdul Rahman**

**September 2022**

**DECLARATION**

I hereby declare that this project report is based on my original work except for citations and quotations which have been duly acknowledged. I also declare that it has not been previously and concurrently submitted for any other degree or award at UTAR or other institutions.

Signature :   
\_\_\_\_\_

Name : Cheah Choon Kit  
\_\_\_\_\_

ID No. : 1705842  
\_\_\_\_\_

Date : 12/6/2022  
\_\_\_\_\_

**APPROVAL FOR SUBMISSION**

I certify that this project report entitled “**DESIGN AND DEVELOP AN ACTIVE MIXER FOR INK BASED 3D PRINTER**” was prepared by **CHEAH CHOON KIT** has met the required standard for submission in partial fulfilment of the requirements for the award of Bachelor of Engineering (Honours) Mechanical Engineering at Universiti Tunku Abdul Rahman.

Approved by,

Signature : TJY  
\_\_\_\_\_

Supervisor : Ir Dr Tey Jing Yuen  
\_\_\_\_\_

Date : 12/9/2022  
\_\_\_\_\_

Signature : \_\_\_\_\_

Co-Supervisor : \_\_\_\_\_

Date : \_\_\_\_\_

The copyright of this report belongs to the author under the terms of the copyright Act 1987 as qualified by Intellectual Property Policy of Universiti Tunku Abdul Rahman. Due acknowledgement shall always be made of the use of any material contained in, or derived from, this report.

© 2022, Cheah Choon Kit. All right reserved.

## ACKNOWLEDGEMENTS

I would like to thank everyone who had contributed to the successful completion of this project. I would like to express my gratitude to my research supervisor, Dr. Tey Jing Yuen for his invaluable advice, guidance and his enormous patience throughout the development of the research. I would also like to express my appreciation to Universiti Tunku Abdul Rahman for providing sufficient resources to conduct this research. In addition, I would like to express my gratitude to my senior, Mr Lim Jeng Jit for the advice and guidance on the research and also Mr Chew Zen Wei, for guiding me on the fabrication job.

## ABSTRACT

Nowadays, 3D printing is essential for manufacturing micro-scale materials. Direct Ink Writing (DIW) is the most versatile form of additive manufacturing for producing microscale materials with ink formulations. The ink formulation for DIW exhibits a shear-thinning behaviour when deposited through the nozzle tip. Most DIW commercial printers cannot print soft materials with specific properties uniformly. So, the project focus will be on designing and developing an active mixer to blend two viscous silicone ink formulations into a homogeneous solution. In order to demonstrate the active mixer performance, a prototype was fabricated in the workshop, which consists of a dc motor, mixing chamber, motor housing, and rotating impeller. Then, both experimental and CFD fluid modelling with Ansys Fluent are carried out to evaluate the prototype performance in silicone mixing. When the impeller isn't rotating, there isn't any applied shear rate at the silicone that produces a heterogeneous ink profile. During 12 rpm rotation, the impeller applies a shear rate to the silicone that promotes mixing due to lower viscosity. As the impeller speed increases from 12 to 24 rpm, the fluid viscosity reduces from 93.72 to 81.11 Pa.s which improves the mixing rate. Overall, it takes 2 s and 1 s to achieve a steady mixing state for the prototype performance. At 24 rpm speed, the active mixer can reduce the pressure of non-Newtonian mixing, which increases the fluid residence time. So, the output produced can be more homogeneous at 28,000 Pa, unlike 0 rpm and 12 rpm where the pressure fluctuates. Lastly, different blue silicone ink inlet velocities are simulated at 1mm/s, 3mm/s, and 5mm/s to determine the output material composition without changing the impeller and red silicone ink flow rate. Lastly, it was found that the red ink volume fraction will decrease at the output as more blue silicone ink flows into the mixing chamber. For the contribution, the design can help save raw material and energy costs and expand business opportunities to develop new products.

## TABLE OF CONTENTS

<b>DECLARATION</b>		<b>i</b>
<b>APPROVAL FOR SUBMISSION</b>		<b>ii</b>
<b>ACKNOWLEDGEMENTS</b>		<b>iv</b>
<b>ABSTRACT</b>		<b>v</b>
<b>TABLE OF CONTENTS</b>		<b>vi</b>
<b>LIST OF TABLES</b>		<b>viii</b>
<b>LIST OF FIGURES</b>		<b>ix</b>
<b>LIST OF SYMBOLS / ABBREVIATIONS</b>		<b>xii</b>
<b>LIST OF APPENDICES</b>		<b>xiii</b>
<b>CHAPTER</b>		
<b>1</b>	<b>INTRODUCTION</b>	<b>1</b>
1.1	General Introduction	1
1.2	Importance of the Study	2
1.3	Problem Statement	2
1.4	Aim and Objectives	4
1.5	Scope and Limitation of the Study	4
1.6	Contribution of study	4
1.7	Outline of the Report	5
<b>2</b>	<b>LITERATURE REVIEW</b>	<b>6</b>
2.1	Direct Ink Writing (DIW)	6
2.2	Non-Newtonian fluids	7
2.3	Mathematical model for non-Newtonian fluids	7
2.4	Non-Newtonian fluid mixing process	10
2.5	Active and Passive Mixing Approach	11
2.5.1	Integrated hybrid mixer for sequential injection	13
2.5.2	DIW with the cooling jacket approach	14
2.6	Design consideration of active mixer design	15



2.7	Governing dimensionless parameters for the mixing process:	16
2.8	CFD modelling for the Non-Newtonian fluid	18
2.8.1	Volume of fluid simulation (VOF) for multiphase flow	20
2.9	Summary of the literature review	22
<b>3</b>	<b>METHODOLOGY AND WORK PLAN</b>	<b>23</b>
3.1	Introduction	23
3.2	Active mixer design concept	25
3.3	Active mixer simulation setup	26
3.4	Experimental Design Study	30
3.5	Prototype Performance Analysis	31
<b>4</b>	<b>RESULTS AND DISCUSSION</b>	<b>33</b>
4.1	Introduction	33
4.2	Grid Independent test	33
4.3	Ink homogeneity of the mixture from different speed of impeller	34
4.3.1	Velocity and Pressure Profile analysis	40
4.3.2	Impact of flow rate on the output	44
4.4	Summary	47
<b>5</b>	<b>CONCLUSIONS AND RECOMMENDATIONS</b>	<b>49</b>
5.1	Conclusions	49
5.2	Recommendations for future work	51
	<b>REFERENCES</b>	<b>52</b>
	<b>APPENDICES</b>	<b>56</b>
	<b>APPENDIX</b>	<b>56</b>

**LIST OF TABLES**

Table 2.1: The effect of gird size and time step on mean velocity	21
Table 3.1: Lists of components for the active mixer design.	25
Table 3.2: Silicone ink properties for simulation setup.	27
Table 3.3: Overall setup for Fluent model and boundary conditions definition.	29
Table 3.4: Calculation and Plane Settings for CFD fluid modeling.	32
Table 4.1: Independent grid test with different element size with 24 rpm rotational speed.	34
Table 4.2: Comparison of the ink mixing with different rotational speed (rpm) based on the volume fraction legend in Figure 4.3.	36
Table 4.3: Wall shear stress and computation of shear rate and viscosity in different rotational speed from Figure 3.3.	39
Table 4.4: Comparison of velocity profile at Plane 1 cross section of the fluid domain.	44
Table 4.5: Average velocity computed at the fluid domain outlet.	44
Table 4.7: Result summary for prototype performance at different speeds.	48
Table 4.8: Results obtained from different blue silicone ink inlet velocities at 24 rpm impeller speed.	48

## LIST OF FIGURES

Figure 1.1: Schematic diagram of active mixing in DIW. (Rocha et al, 2020)	3
Figure 2.1: Graph of viscosity vs Stress (Science Learning Hub, 2010)	7
Figure 2.2: Graph of Shear Stress vs Shear Rate (Wilkens, et al., 2003)	8
Figure 2.3: Hershel-Bulkey model of non-Newtonian fluid (Malvern, 2017)	9
Figure 2.4: Semilog plot of $\tau$ against $\log(\gamma)$ (Kelessidis, et al, 2006)	10
Figure 2.5: Active mixer that has rotating impeller (Ober, et al., 2015)	12
Figure 2.6: Active Mixer for mixing reactive materials. (Golobic, et al, 2019)	12
Figure 2.7: Hybrid active mixer design (Hassan & Selvaganapathy, 2021)	13
Figure 2.8: Time taken to reach a steady state mixing with and without floating static mixer (Hassan & Selvaganapathy, 2021).	14
Figure 2.9: Ink-based 3D printer with cooling jacket. (Dogan & Yigit, 2020)	15
Figure 2.10: Different result of homogeneity during mixing at different rotational speed (rpm). (Golobic, et al., 2019)	15
Figure 2.11 : The plot of residence to mixing time ratio against the mixer speed.	16
Figure 2.12: Overview of the Material point Method (MPM) for viscoelastic fluid. (Stomakin, et al., 2013)	19
Figure 2.13: Structured Mesh and Domain from the six bladed impeller (Dular et al, 2006)	21
Figure 3.1: Flowchart of the project.	24
Figure 3.2: Exploded view of the active mixer design.	26
Figure 3.3: Curve-fitting of the silicone ink rheology data into Hershel-Bulkley model with shear rate and viscosity.	26
Figure 3.4: Fluid domain with defined boundary conditions.	27

Figure 3.5: Meshing of the fluid domains.	28
Figure 3.6: Half of the fluid domain is patched with secondary phase.	30
Figure 3.7: Hardware setup for the experimental work.	31
Figure 3.8: Plane 1 created with YZ method.	32
Figure 3.9: Plane 2 created with three points method.	32
Figure 4.1(a) and (b): Red ink (left) and blue Ink (right) homogeneity for each phase without any rotation at Plane 1.	35
Figure 4.2 (a) & (b): Dark blue striation in the silicone sample (left) with a distinct interface of blue and red dye across the ink profile (right).	35
Figure 4.3: Default legend for the red ink volume fraction.	37
Figure 4.4 (a) & (b): Homogeneous purple silicone sample (left) without any distinct interface of blue and red dye colour across the ink profile (right)	37
Figure 4.5: Plot of wall shear stress against flow time in different rotational speed at the rotating wall.	38
Figure 4.6: Red ink volume fraction at the fluid domain outlet in different rotational speeds.	39
Figure 4.7: Blue ink volume fraction at the fluid domain outlet in different rotational speeds.	40
Figure 4.8: Pressure Profile of the mixing chamber at 24 rpm at Plane 1.	40
Figure 4.9: Plot of average pressure vs flow time at different rotational speeds at the Plane 1.	42
Figure 4.10: Plot of torque vs flow time at different rotational speeds from the rotating wall.	42
Figure 4.11: Tangential velocity profile across the velocity profile during rotation 12 rpm.	43
Figure 4.12: Plot of red ink volume fraction at different blue silicone ink inlet velocity with impeller speed of 24 rpm at the outlet.	45
Figure 4.13: Plot of average pressure over flow time at different blue silicone ink velocities at 24 rpm — Measured at Plane 1.	46

Figure 4.14: Plot of torque over flow time at different blue silicone ink velocities at 24 rpm —Measured at the fluid domain rotating wall. 46

Figure 4.15: Plot of wall shear stress over flow time at different blue silicone ink velocities at 24 rpm —Measured at the fluid domain rotating wall 47

**LIST OF SYMBOLS / ABBREVIATIONS**

$\eta$	viscosity of the fluid (m <sup>2</sup> /s)
$k$	consistency index of the fluid
$\dot{\gamma}$	shear rate of the fluid (s <sup>-1</sup> )
$n$	flow behaviour index
$\tau$	shear stress (N/m <sup>2</sup> )
$\tau_0$	yield stress (N/m <sup>2</sup> )
$D$	diffusion coefficient
$\frac{\partial c}{\partial x}$	difference of concentration between a particular length of the channel.
$j$	Diffusion flux

DIW	Direct Ink Writing
FDM	Fused Deposition Method
CFD	Computational Fluid Dynamics
SPH	Smooth Particle Hydrodynamics
MPM	Material Point Method
VOF	Volume of Fluids

**LIST OF APPENDICES**

Appendix A: Pictures	56
Appendix B: Tables	58
Appendix C: Engineering Drawings	88
Appendix D: Costing of the design	92

## CHAPTER 1

### INTRODUCTION

#### 1.1 General Introduction

Nowadays, 3D printing has become the driving force of fabrication at a micro-scale level which helps to advance different sciences and technologies in material science, chemistry, physics and biology. During the Covid 19 pandemic, all manufacturing industries are implied to minimize human interaction at the production site. 3D printing can help facilitate the emergency response towards the event of a disruption in production and supply chain. 3D printing can serve many benefits compared to traditional manufacturing methods since it simplifies the operation and production line. Material waste and production time can also be reduced with 3D printing.

Among all the 3D printing technologies, the most versatile method for the fabrication of materials at the micro-scale is Direct Ink Writing (DIW). The ink is deposited through the nozzle with computer aided control during the printing of product architecture. The ink formulation will exhibit its shear thinning properties and solidify when the ink is deposited in the form of gel or pastes. For such printing, no heating process is required compared to Fused Deposition Modelling (FDM) which helps to save energy.

Currently, mixing highly viscous fluids at a micro-scale level is well-known for different kinds of industry, especially additive manufacturing. DIW can fabricate new materials by combining different material ink formulations together. Besides, the material properties can be manipulated based on the printing parameter like inlet flow rate and rotational speed of the impeller. However, the ink compositions are mainly very viscous fluids with deficient Reynolds number ( $Re$ ) where no turbulence is applied. For the passive mixer, the flow parameters can only be controlled with characteristic mixing length and flow rate. Therefore, an active mixing approach can be introduced for DIW printing technology to develop the new material with an efficient mixing mechanism.



In this project, the active mixer design for DIW will be developed to cater for two inputs of ink formulation. With multiple flow inlets connected for mixing, the ink composition from the printed material can be varied by controlling the pulsatile input applied to each respective syringe with phase angle. From the design, the Computational Fluid Dynamics (CFD) simulation will be conducted as a proof of concept to evaluate the mixer performance with the available rheology data of the inks.

## **1.2 Importance of the Study**

The study of this project will focus on developing the active mixer for the ink-based 3D printer. The mixer ink extruder can provide a more effective solution for mixing viscous ink, which will save costs in creating new material through one fabrication step. At the same time, the printed output material's physical properties can be controlled in any application by varying the input composition. The choice of Direct ink Writing (DIW) provides flexibility in developing new materials that save cost and energy. Especially during Covid 19 pandemic time, many manufacturing firms that rely on the global supply chain were forced to shut down and stop production indefinitely due to the shortage of raw materials and labour available. However, the production rate can be improved with DIW by simplifying the processing steps of the product with lesser raw materials. At the same time, DIW can help fabricates components with greater quality and accuracy to be delivered.

## **1.3 Problem Statement**

Golobic (2019) mentioned that mixing highly viscous fluid in a short timescale and low volume depends on the material flow rate and rheology data. These yield stress inks demonstrate a shear-thinning behaviour under a high shear rate. By incorporating the active mixing approach into DIW, it can homogenize any different viscous ink formulations by mixing them efficiently. As a result, new material can be formulated efficiently from non-Newtonian mixing.

At the same time, the prototype can provide the specific material properties from the mixing for different applications by adjusting the input flow rate of syringes. So, the adjustment helps to vary the material composition across the output ink formulation at extrusion. For achieving this functionality, an external power source is essential to apply sufficient shear energy from the mixing impeller to reduce the ink viscosity significantly in Figure 1.1. As the ink viscosity decreases, the homogenized formulation will flow through the nozzle for the 3D printing process by ink deposition layer-by-layer.

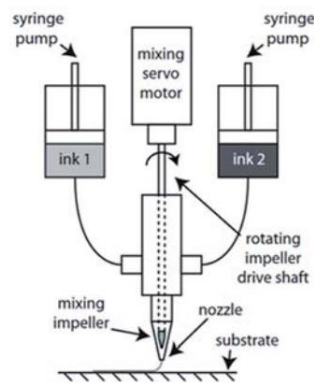


Figure 1.1: Schematic diagram of active mixing in DIW. (Rocha et al, 2020)

Currently, there are several challenges in manufacturing soft parts for flexible machine components. Conventional fabrications like injection molding or casting cannot control the material variability that fulfills the required specification or tolerances by the clients. Despite the availability of commercial DIW technology, Dogan and Yigit (2020) stated that most of them cannot print soft materials with specific properties uniformly. Also, there is not much study on how the mixing pressure affects the prototype performance for the DIW active mixing. Besides, Direct ink writing applies to a wide range of material fabrication into a small model with high complexity, especially silicone ink. In order to resolve the limitation of silicone printing, the project will cover the analysis of silicone printing at both static and active mixing methods. Through experimental and simulation work, the study will provide an extension of DIW behind the importance of developing the active mixer for non-Newtonian mixing.

#### **1.4 Aim and Objectives**

In this project, the aim is to develop an effective active mixer to allow effective mixing of highly viscous fluids. Thus, the following objectives are listed:

- 1) To design an active mixer to mix highly viscous ink formulation insitu during 3D printing.
- 2) To evaluate the performance of the active mixer through fluid modelling (CFD).
- 3) To test the design prototype printing performance with different impeller speeds in the experiment.

#### **1.5 Scope and Limitation of the Study**

The primary focus of this study is to develop an active mixer for the in-situ mixing of two ink formulations at the same time. The active mixer should be able to mix different dye colours of silicone ink during 3D printing. Besides that, the ink mixer should consist of good serviceability where the prototype can be opened up to clean any trapped inks within the mixing chamber. However, there are still some limitations which is applied to the project as listed below:

- 1) The active mixer will be focusing on the silicone ink mixing for DIW.
- 2) Heating and cooling process will not be taken into account for the active mixer design.

#### **1.6 Contribution of study**

In Malaysia, most conventional fabrication techniques like forging, machining, and casting are likely to have high energy consumption in fabricating materials. Besides, they limit the complexity of the product for the end-users. The active mixer eliminates the need to assemble components which is cost-saving for producing new material efficiently (Rocha et al, 2020). Thus, it expands the opportunities for business organizations to develop new products. Aside from mass-customizing any design models with complex architecture, the active mixing approach also allows the flexible adjustment of material properties to cater to different needs like wearable sensors, soft robotics, and electronics. In

the future, the mixer can provide a more eco-friendly manufacturing environment that eliminates large energy consumption and reduces the consumption of raw materials for processing.

### **1.7 Outline of the Report**

Chapter One of the report will describe the outline of the project with background information on the studies. It also highlights the purpose, aims, scope as well as problem statement of the study. Chapter 2 is the detailed literature review of the project. Relevant researches are made for the design and fabrication of the ink extruder with an active mixing mechanism. Chapter 3 shows the methodology of the prototype design as well as the experimental setup for obtaining the result. Lastly, Chapter 4 will discuss the result obtained by both experimental and simulation work.

## CHAPTER 2

### LITERATURE REVIEW

#### 2.1 Direct Ink Writing (DIW)

From the ISO/ASTM 52900, Price (2013) stated that there are different types of 3D printing techniques (e.g. Photopolymerisation, Binder Jetting, Material Jetting, Material Extrusion, Powder Bed Fusion, Sheet Lamination, and Directed Energy Deposition). Yang et al (2021) had explained direct ink writing (DIW) is the most versatile additive manufacturing among the 3D printing techniques. During DIW, the object is deposited layer by layer in the form of viscoelastic pastes. Unlike FDM, DIW relies on the paste deposition with specific properties from the syringe cartridge. Each complex fluid consists of a portion of powdered materials with additive added into the liquid. The concentration of the fluid is adjusted so that the paste can exhibit a shear-thinning effect and yield stress.

One of the benefits is that DIW applies to any type of materials (metal, polymer, rubber or composite) according to Rocha, et al (2020). It also allows high-resolution printing at a micro-scale which saves up the costs of operation like the manufacturing of electronic components. For DIW, mixing approach can be implemented to mix different ink compositions before extruding through the nozzle to create new material. So, rapid switching of the material composition is possible during the printing process.

Even though DIW offers flexibility in material fabrication, there are several challenges faced for DIW. First and foremost, Shahzad and Lazoglu (2021) explained that the viscosity of prepared ink has to demonstrate shear-thinning behaviour to extrude through the small nozzle hole. At the same time, the fluid viscosity, yield strength, and stiffness have to be enough to retain the shape rigidity of the printed material. In addition, the gas bubbles have to be removed as the pores may affect the mechanical properties of the printed object. In order to overcome this issue, reducing the printing layer height helps minimize the pore size and porosity. (Buj-Corral, et al, 2018)

Despite the challenges faced, DIW allows the fabrication of complex shapes without mould or traditional operations. Thus, it can offer a more sustainable solution for a wide range of fields without excluding construction and transportation. Although it serves as a potential for market solution, there is still a barrier for upscaling the design for mass production. This means that solving the design upscaling issue can improve the economy. (Rocha et al, 2020)

## 2.2 Non-Newtonian fluids

Non-Newtonian fluids are fluids that don't have constant viscosity like Newtonian fluid. Science Learning Hub (2010) stated that these fluids have a non-linear relationship between the shear stress and shear rate. They are likely to alter their viscosity when subjected to particular stress. For shear thickening fluid, their viscosity is likely to be greater when force is applied and vice versa for shear thinning fluid. Since non-Newtonian fluid demonstrates both viscous and elastic property at the same time, it is also known as viscoelastic fluid. For the properties of non-Newtonian fluid, they can be defined by different types of mathematical model like the power-law and Herschel-Bulkley Model.

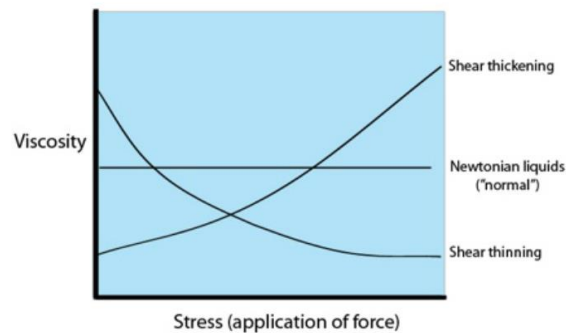


Figure 2.1: Graph of viscosity vs Stress (Science Learning Hub, 2010)

## 2.3 Mathematical model for non-Newtonian fluids

The power-law equation is the most common mathematical model for non-Newtonian fluid. The equation is modelled with a relationship between shear stress,  $\tau$  and shear rate,  $\dot{\gamma}$ .

$$\eta = k \cdot \dot{\gamma}^{n-1} \quad (2.1)$$

$$\tau = k \cdot \dot{\gamma}^n \quad (2.2)$$

where

$\eta$  = viscosity of the fluid ( $\text{m}^2/\text{s}$ )

$k$  = consistency index of the fluid

$\dot{\gamma}$  = shear rate of the fluid ( $s^{-1}$ )

$n$  = flow behaviour index

$\tau$  = shear stress ( $N/m^2$ )

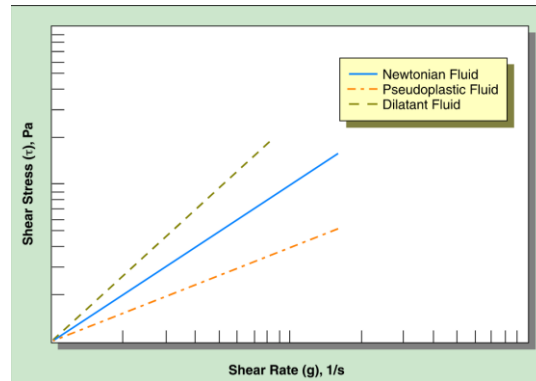


Figure 2.2: Graph of Shear Stress vs Shear Rate (Wilkins, et al., 2003)

According to the power-law model, the flow index,  $n$  will determine the characteristics of the fluid. When  $n = 1$ , the fluid will behave like the Newtonian fluid. When  $n < 1$ , the fluid will exhibit its shear-thinning effect where its viscosity decreases along with the shear rate as pseudoplastic fluid. However, the shear stress will be greater as the shear strain increases. As for  $n > 1$ , the fluid will exhibit its shear-thickening effect where its viscosity increases along with the shear rate as dilatant fluid. Despite the power-law model being commonly used, it can only be applied to a certain range of shear rate,  $\dot{\gamma}$ . For example, the shear-thinning fluids will act as Newtonian fluid when the shear rate is either too high or low. Besides, the power-law model doesn't apply for fluid that has yield stress which can lead to a major error according to Kelessidis et al (2006).

From Figure 2.3, Herschel-Bulkley model is a generalized and non-linear model for the non-Newtonian fluid. The model integrates both the power-law and Bingham plastic rheological behaviour into a single relation. Therefore, Herschel-Bulkley model describes the yield stress fluid behaviour. When the shear rate is applied, the fluid deforms elastically like a spring mechanism. When the fluid reached its critical strain, the fluid will then begin to show its shear-thinning effect. (Malvern 2017). At a high shear rate, the fluid behaves

like a power-law fluid. The mathematical equation of Herschel-Bulkley model is stated in Equation (2.3) and (2.4) where  $\tau_0$  is the non-Newtonian yield stress of the fluid.

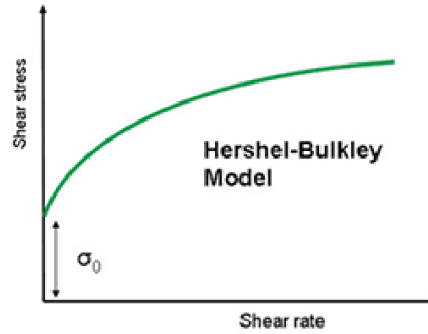


Figure 2.3:Herschel-Bulkley model of non-Newtonian fluid (Malvern, 2017)

$$\tau = \tau_0 + k \cdot \dot{\gamma}^n \quad (2.3)$$

$$\eta = k * \dot{\gamma}^{n-1} + \frac{\tau_0}{\dot{\gamma}} \quad (2.4)$$

$$\ln(\tau - \tau_0) = \ln k + n \ln \dot{\gamma} \quad (2.5)$$

Based on Equation 2.3, the three parameters (yield stress,  $\tau_0$  consistency,  $k$  and flow index,  $n$ ) can be approximated through the non-linear regression of the data obtained from the concentric cylinder geometry by the linearized model from Equation (2.5). However, the non-linear fitting of data may provide negative yield stress that is meaningless from the best fit. So, the condition where yield stress,  $\tau_0 > 0$  must be imposed to obtain the optimal estimation of the three parameters. Possibly, the solution obtained might appear non-unique.

In addition, the usage of the correlation coefficient ( $R^2$ ) over the non-linear fitting may impact the final result like pressure drop or velocity profile of the non-Newtonian fluid despite the slight difference of 0.002 for the  $R^2$ . Therefore, another better approach is to assume a proper value for the yield stress,  $\tau_0$  from the semilog graph, where the y-intercept from the graph indicates the yield stress. (Kelessidis et al, 2006)



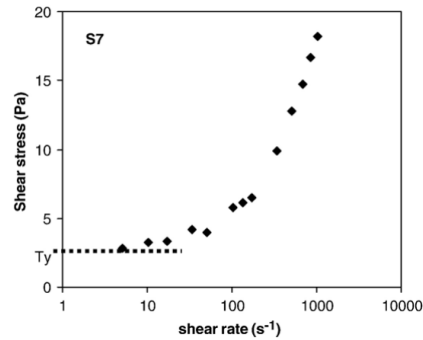


Figure 2.4: Semilog plot of  $\tau$  against  $\log(\dot{\gamma})$  (Kelessidis, et al, 2006)

## 2.4 Non-Newtonian fluid mixing process

Mixing non-Newtonian fluids is necessary in many applications like paint, medical equipments, etc. In DIW, mixing non-Newtonian fluids for multi-material can pose a challenge in 3D printing due to its low Reynold's number (Re). Therefore, no turbulence can be applied because the inertial force plays a minimal role in laminar flow. Usually, laminar flow is smooth without fluctuation according to Capretto et al (2011). Despite their characteristic, high viscous ink like yield stress fluid are essential for retaining the structure and texture of the product during fabrication.

Mixing mechanism involving fluids with low Re will undergo breaking, folding and stretching process with other fluids known as chaotic advection. Either passive or active mixing approaches can cause chaotic advection among dissimilar fluids. When the flow passes through a particular cross section, the concentration of all fluids will change over time. Eventually, the mixing will complete as the chaotic advection continues among the different fluids. (Nguyen, 2007).

Wendell et al (2013) had realized that the yield stress non-Newtonian fluid will have slower mixing compared to Newtonian fluid due to intermittent stretching during the mixing process. Malvern (2017) had provided an important insight on the yield stress had to be exceeded for the fluid to behave as if power law fluid. Thus, applying higher velocity on the non-Newtonian fluid will improve the mixing of highly viscous ink formulations that comes to terms with Malvern (2017)'s statement from the earlier section.

## 2.5 Active and Passive Mixing Approach

To develop a new material, mixing approach can be implemented in DIW method to fabricate material at a micro-scale. The micromixer design can be either passive or active configuration. For the passive mixer, the mixing mechanism solely relies on chaotic advection without external power source. So, the fluids are mixed through the molecular diffusion like Brownian motion over to what Capretto (2019) have said. Literally, Brownian motion was defined under Fick's law mathematical equation as shown below.

$$j = -D \frac{\partial c}{\partial x} \quad (2.6)$$

where

$D$  = diffusion coefficient

$\frac{\partial c}{\partial x}$  = difference of concentration between a particular length of the channel.

$j$  = Diffusion flux

With this mixing mechanism, passive micromixer had posed a limitation that the chaotic advection can only be manipulated by varying the flow rate and mixing channel geometry. Ober et al (2015) explained that introducing grooved walls to the mixing channel can enhance chaotic advection. However, the passive micromixer needs a very long mixing channel to achieve homogeneity during the non-Newtonian mixing. This is to ensure the fluid residence time,  $t_{res}$  is longer than the mixing time,  $t_{mix}$  for effective mixing. To this extent, the design concept isn't practical with such a long microchannel to channel the mixed inks as the output.

In order to address the limitation of the passive mixer, external energy source can be added to aid mixing of the non-Newtonian fluids in the active mixing approach. Active mixer can improve the mixing efficiency that reduces the mixing time and pressure drop. In Figure 2.5, the rotating impeller applies shear rate independently to control the non-Newtonian mixing independently. Golobic (2019) emphasized the increasing shear rate helps to maximize the contact area between the distinct fluids during mixing. Therefore, it helps simplify the design with a smaller size while reducing the pressure drop during ink extrusion, unlike the passive mixer.

At the same time, a compact mixer design also allows rapid material switching to control the respective involved input content. From Figure 2.5, material switching can produce an object that has a varying material composition gradient along the length. Meanwhile, Ober, et al (2015) demonstrated that the resistivity of the printed structure was altered to adjust the LED light brightness with applied voltage (Appendix A-1) by varying the composition of silver nanoparticle and carbon colloidal inks. Moreover, the active mixer framework shown in Figure 2.5 also able to vary the concentration of fluorescent polystyrene particles across the silicone ink profile profile at Appendix A-2 by varying the input flow rate from the inlets.

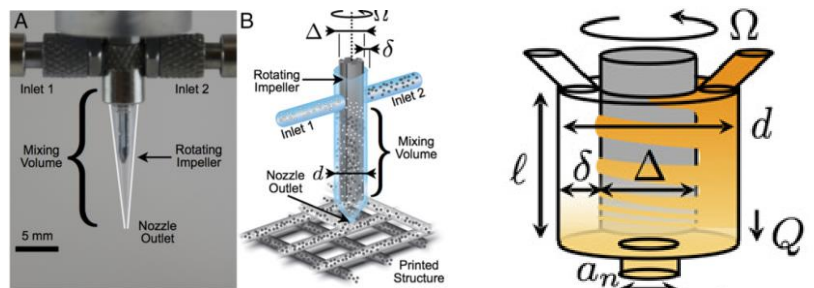


Figure 2.5: Active mixer that has rotating impeller (Ober, et al., 2015)

Based on Figure 2.6, active mixing can improve the safe working condition especially handling reactive materials for mixing. Needless to say, a faster mixing time than the reaction time among materials can prevent the occurrence of any involuntary reaction. At the same time, Golobic (2019) stated that the active mixer can tailor the energy release of thermite by varying the aluminium and copper oxide composition in the printed structure.

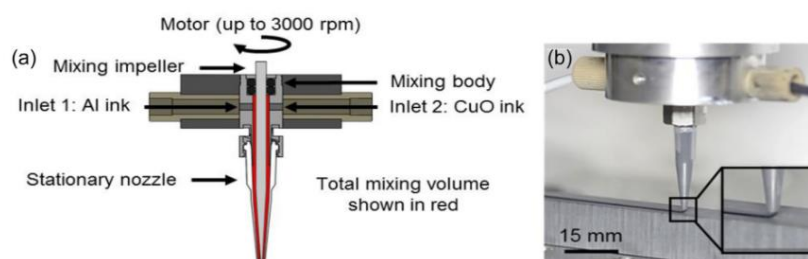


Figure 2.6: Active Mixer for mixing reactive materials. (Golobic, et al, 2019)

### 2.5.1 Integrated hybrid mixer for sequential injection

From Figure 2.7, the hybrid mixing system integrates the features of both active and passive mixers. The positive pumps force the UV silicone inks into the mixing chamber at all inlets. The solenoid valve connected to a pressure source controls the applied pressure through the inlet channel. Hassan and Selvaganapathy (2021) emphasized that the grooved static mixer helps to enhance chaotic advection among the fluids since it reduces the mixing chamber volume. At the silicone ink deposition, the specimen will be exposed to UV light illumination from the optical bundle below the nozzle tip for the curing process. This approach can save time for fabricating the rotating impeller that requires an electric motor to aid the non-Newtonian mixing. Furthermore, there are check valves to prevent any inks backflow within the mixing chamber.

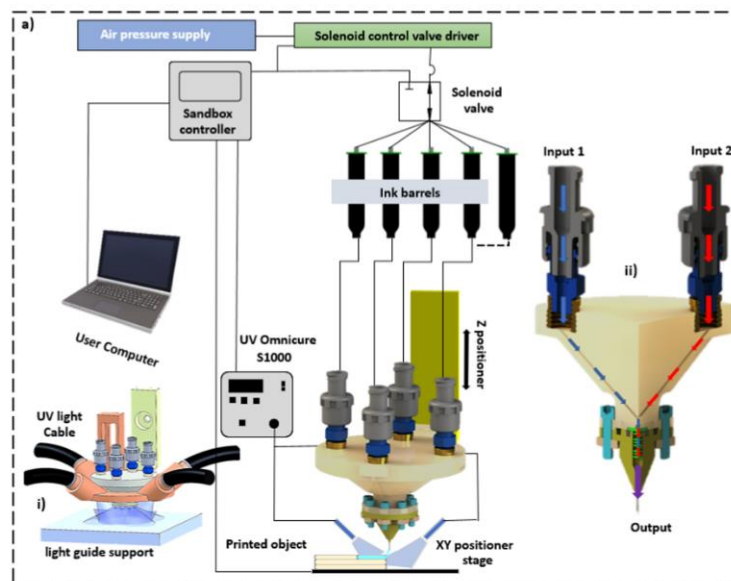


Figure 2.7: Hybrid active mixer design (Hassan & Selvaganapathy, 2021)

In this work, different silicone ink colours are mixed by applying pneumatic signal to the inlets to achieve a steady state mixing. The design of steep inlet channel in the manifold prevent ink stagnation or accumulation when entering the mixing zone. Moreover, the expanding section at the mixing zone from the inlet increases the interfacial area for chaotic advection among different inputs.

From the study, it was shown that the floating static mixer reduces the time for reaching steady state from 10s to 4s in Figure 2.8. However, there is no shear energy being applied to promote non-Newtonian mixing when the inputs reached the mixing zone. Due to the small inlet channel and mixing zone in micro-scale dimension, high pneumatic pressure is required to promote silicone mixing due to the limitation of geometry for the mixer.

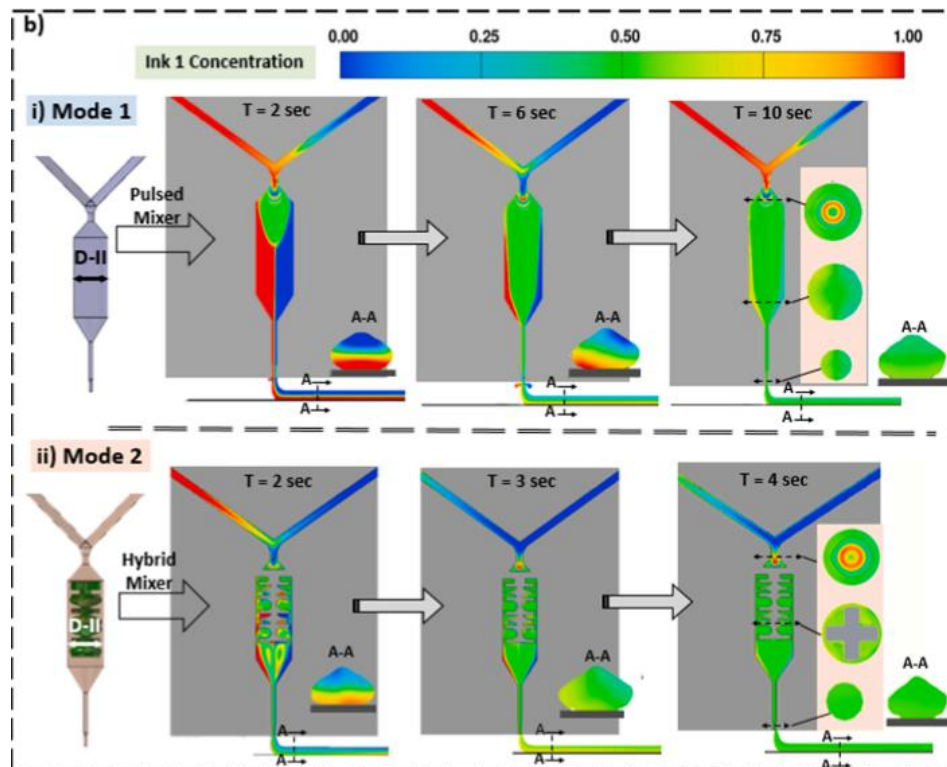


Figure 2.8: Time taken to reach a steady state mixing with and without floating static mixer (Hassan & Selvaganapathy, 2021).

### 2.5.2 DIW with the cooling jacket approach

According to Figure 2.9, the active mixer integrates heating and cooling modules in the design. The electric heater heats the surrounding air so the fans can direct hot air to the deposited ink for the curing process. At the same time, a controller helps to maintain the work surface at about 50 °C temperature. Besides, the in-line active mixer was positioned within the cavity of the cooling jacket. So, the fluid distribution cap will distribute the fluids into the cavity with pump; hence, helping to regulate the temperature of the viscous elastomer ink to prevent solidification due to temperature rise. Otherwise, clogging will occur, which disrupts the mixer's performance. (Dogan & Yigit, 2020)

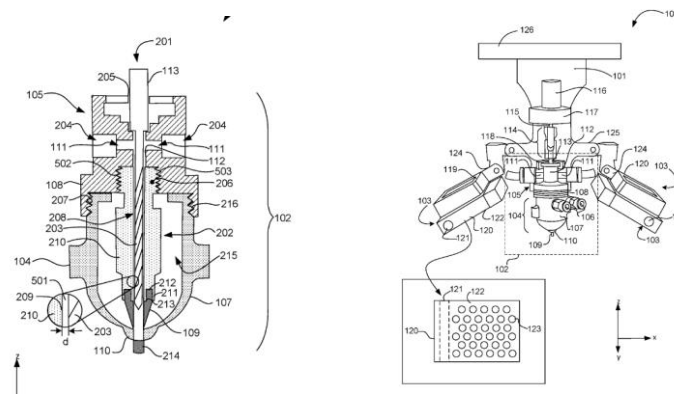


Figure 2.9: Ink-based 3D printer with cooling jacket. (Dogan & Yigit, 2020)

## 2.6 Design consideration of active mixer design

There are some design considerations when designing the active mixer. Firstly, the gap between the rotating impeller and the mixing chamber wall should prevent clogging during the fluids mixing. However, the gap size shall be small enough to induce sufficient shear rate for homogeneous non-Newtonian mixing. The speed of the rotating impeller will determine the homogeneity of the mixing among two or more different inks. Figure 2.10 shows the visible striations appear at the nozzle tip at 100rpm. As the rotational velocity increases, the striation among the mixture becomes less visible until the homogeneity at 1000rpm. At the same time, the output homogeneity becomes more uniform at higher mixer speed due to higher residence to mixing time ratio based on Figure 2.11. (Golobic, et al., 2019)

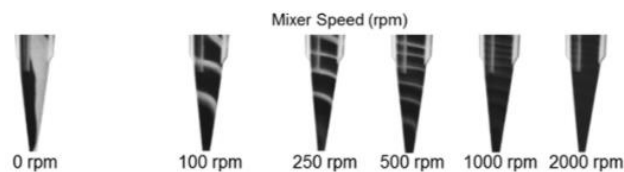


Figure 2.10: Different result of homogeneity during mixing at different rotational speed (rpm). (Golobic, et al., 2019)

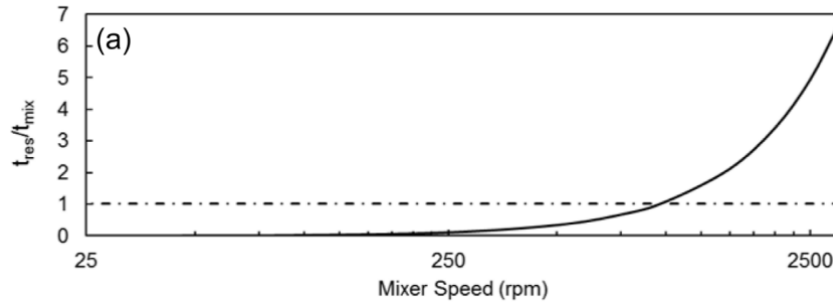


Figure 2.11 : The plot of residence to mixing time ratio against the mixer speed.

## 2.7 Governing dimensionless parameters for the mixing process:

Some governing dimensionless parameters help to define the fluid characteristic during the mixing process. For the Newtonian fluid, the type of fluid flow whether it is turbulent or laminar is determined by the Reynolds number ( $Re$ ) as shown in the equation below. The Reynolds number ( $Re$ ) also depends on the computation of the channel hydraulic diameter,  $D_h$ .

$$Re = \frac{\rho u D_h}{\mu} = \frac{\mu D_h}{\nu} \quad (2.7)$$

$$D_h = \frac{4A}{P} \quad (2.8)$$

where

$Re$  = Reynolds Number

$\rho$  = fluid density

$u$  = fluid velocity

$D_h$  = hydraulic diameter of the mixing channel

$\nu$  = kinematic viscosity

$A$  = Area of the cross-section

$P$  = Perimeter of the cross-section

$$Pe = \frac{Q}{adD} \quad (2.9)$$

$$St = \frac{f D_h}{U} \quad (2.10)$$

$$l/d \geq Pe \quad (2.11)$$

Where

$Pe$  = Peclet number

$St$  = Strouhal number

$f$  = frequency (Hz)

$U$  = mean velocity (m/s)

$Q$  = flow rate ( $\text{m}^3/\text{s}$ )

$D$  = diffusion coefficient ( $\text{m}^2/\text{s}$ )

$l$  = length of the mixing channel (m)

$d$  = diameter of the channel (m)

In the micromixer design, the Peclet number (Pe) and Strouhal number (St) also define the fluid characteristic. The Strouhal number is the ratio of subjected disturbance on the fluid flow to the changes of velocity in active mixing, according to Hassan and Selvaganapathy (2021). A higher St number indicates a faster mixing process among the fluids at a higher frequency. However, the parameter shall be optimal because incomplete mixing can occur when the Strouhal number (St) is too high. On the other hand, Peclet number represents the ratio of advective mixing to the diffusive mixing among the fluids. From Equation 2.10, the flow rate,  $Q$  and the diameter of the mixing chamber,  $d$  can be varied to determine its value. Ober et al (2015) had explained that the length to the diameter of the microchannel ratio should at least be equivalent to the Peclet number to make way for effective mixing among the viscous inks from Equation 2.11.

$$Bi = \frac{\tau_y}{\tau} \quad (2.12)$$

Where

$Bi$  = Bingham number

$\tau_y$  = yield stress, Pa

$\tau$  = viscous stress of fluid, Pa

From Equation 2.12, Bingham number, is defined as the ratio of the subjected yield stress over the viscous stress among the fluids. From the passive mixer, there is a tradeoff for determining the suitable flow rate of the inks. High input flow rate ensures that the viscous ink can be fluidized while low input flow rate ensure sufficient mixing among the inks. On the other hand, active mixer is able to induce a varying shear rate according to impeller diameter, size gap and rotational speed as the  $Bi$  number can be controlled independently from flow rate for the non-Newtonian mixing.



## 2.8 CFD modelling for the Non-Newtonian fluid

One of the solutions to model the viscoelastic fluid is Smooth Particle Hydrodynamics (SPH). SPH is a Lagrangian particle method for fluid structure interaction and had been used for problems involving incompressible fluid. Ansys(2021) mentioned that SPH helps to resolve all the governing equations of the particular fluid model unlike any classical method.

Uljad (2021) mentioned that there is an open-source library known as SPLisHSPlasH for defining the physical properties of a wide range of materials for the SPH method. The library consists of multiple pressure and viscosity solvers for fluid simulation. It also caters to the incompressibility of the flow. One of the alternative models for physically based fluid simulation is the least square material square method. Generally, discretization of the non-Newtonian fluids in terms of their properties can be very difficult. These fluids can undergo complex changes like large strain rate, large deformation, and changes in viscosity in terms of their characteristics.

Ram (2015) explained that neither Lagrangian or Eulerian approaches can resolve these fluids since they are catered for solid and fluid behaviour respectively. Therefore, Material point method (MPM) was selected to cater to non-Newtonian fluids problem. Figure 2.11 shows that MPM consists of Eulerian grid to resolve any changes of shape or collision among the fluids while the Lagrangian helps to keep track of the mass, momentum and deformation of the particles. Initially, the deformation of the body can be interpreted as  $x = \phi(X)$  where  $X$  is the undeformed state of the body. Then, the deformation gradient can be defined as  $F = \partial\phi/\partial X$ . The body deformation occurs following the law of conservation of mass and momentum as well as the elasto-plastic constitutive relation as shown below. (Stomakhin et al, 2013)

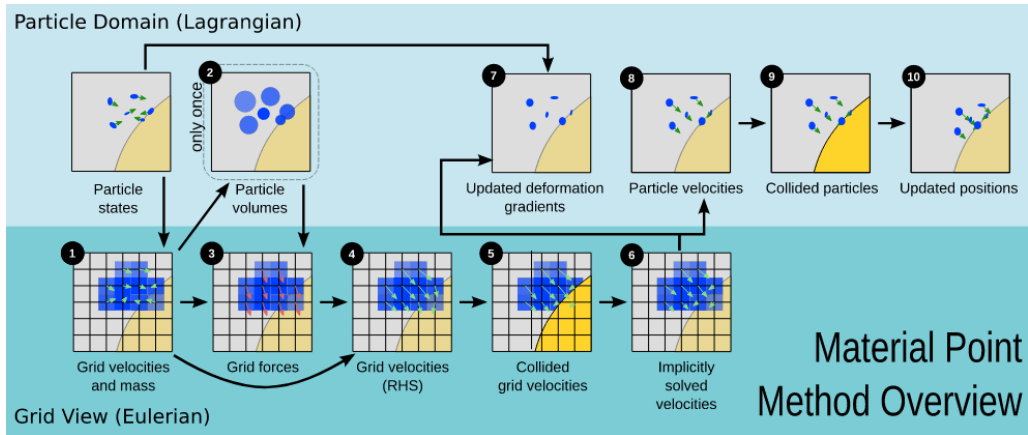


Figure 2.12: Overview of the Material point Method (MPM) for viscoelastic fluid. (Stomakin, et al., 2013)

$$\frac{d\rho}{dt} = 0, \text{ No changes of density over time} \quad (2.13)$$

$$\rho \frac{dv}{dt} = \nabla \cdot \sigma + \rho g, \text{ Conservation of mass and momentum} \quad (2.14)$$

$$\sigma = \frac{1}{J} \frac{\partial \Psi}{\partial F_E} F_E^T, \text{ Elasto-plastic constitutive relation} \quad (2.15)$$

Where

$\rho$  = Density

$t$  = time

$\sigma$  = Cauchy stress

$g$  = Gravitational acceleration

$\Psi$  = Elasto-plastic potential energy density

$F_E^T$  = Deformation part of the deformation gradient  $F$

$J$  = Determinant of  $F$ ,  $\det(F)$

From the MPM method, particles are utilized to track the mass, momentum and deformation gradient of the material. The main parameters of the particles are position,  $x_p$  velocity,  $v_p$  and deformation gradient,  $F_p$ . With Lagrangian approach, it helps to simplify the discretization of the  $\frac{d\rho}{dt}$  and  $\rho \frac{dv}{dt}$  terms. However, one of the limitations of the Lagrangian approach is the lack of mesh connectivity between particles which can be resolved by the Eulerian grid as shown in Figure 2.10.

### 2.8.1 Volume of fluid simulation (VOF) for multiphase flow

During the non-Newtonian mixing, the fluid viscosity will affect the torque applied to the rotating impeller. If the fluid viscosity changes too much, the torque will exceed the maximum motor torque. Thus, it is necessary to carry out torque measurement under the function of rotational frequency. The equation below expresses the computation of the shear rate.

$$\dot{\gamma} = K_s N \quad (2.16)$$

Where

$K_s$  = Geometry constant of the impeller

$N$  = rotational frequency of the impeller ( $s^{-1}$ )

As a result, the Re of the non-Newtonian fluid and apparent viscosity,  $\eta_a$  can be defined as below.

$$\eta_a = k. (K_s N)^{n-1} \quad (2.17)$$

$$Re = \frac{\rho N D_h}{\eta_a} = \frac{\rho D_h}{k K_s^{n-1} N^{n-2}} \quad (2.18)$$

Dular et al (2006) explained that the rotating impeller forms the vortex during the non-Newtonian mixing: Pressure gradient respective to impeller wall distance forms the vortex. Clearly, it indicates that fluid rotates faster as it gets nearer to the impeller while slower at the free surface. During rotation, the deeper part of the impeller will have higher pressure built up compared to the free surface.

For the VOF method, Dular et al (2006) had conducted an unsteady numerical simulation of the mixing process on Carboxymethyl cellulose – CMC with the 6 blades impeller on different rotating frequencies,  $N$ . Due to the presence of air, the shear rate dependence was demonstrated with the power-law equation from Equation 2.1. In the simulation, the multiphase flow model was selected due to the presence of the free surface between CMC and air.

According to Figure 2.12, the simulation model used the structured mesh for the impeller with one-sixth of the model to save computational time. During the simulation, two parameters which are the time steps and the grid size will affect the mean velocity (m/s). As a result, the fluid mean velocity increases when either the grid size increases or the time step reduces based on Table 2.2 tabulation of result.

Table 2.1: The effect of grid size and time step on mean velocity

Grid size	Time step ( $10^{-3}$ s)	Mean velocity (m/s)
~ 100000	1	0.0798
~ 225000	1	0.0821
~ 800000	1	0.0852
~ 225000	0.5	0.0834

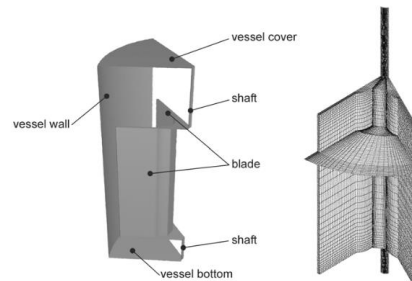


Figure 2.13: Structured Mesh and Domain from the six bladed impeller (Dular et al, 2006)

While working on the VOF simulation, there are several boundary conditions to be applied. Especially for the rotating impeller active mixer, the pressure outlet shall be subjected to the atmospheric pressure (1 bar). Since the non-Newtonian fluid flow is fully developed, there will be no turbulence model applied. The vessel wall, bottom, shaft and also the blades, will be subjected to the no-slip condition where there will be zero velocity at the wall surface. Lastly, the room temperature will be set for fluid and the wall.

## 2.9 Summary of the literature review

In the overall summary, Hershel-Bulkley helps to define the suitable parameter for running the non-Newtonian mixing for direct ink writing. Passive mixer performance is limited to the mixing channel geometry and flow rate, unlike the active mixer can apply a sufficient shear force to the fluids that reduce the viscosity for an efficient mixing mechanism. Based on some active mixer designs, the input flow rate can be adjusted to change the output material composition, which determines the specific properties of the material, like the intensity of LED brightness and the fluorescent concentration gradient across the printed ink profile. For the hybrid mixer, the inlet manifold and mixing chamber are difficult to fabricate due to the small inlet channel and mixing zone at the microscale dimension. On the other hand, the heating and cooling module help to accelerate the elastomer curing time but greater complexity to the design.

As for the governing parameter, the active mixer helps to eliminate the Bingham number constraint on the viscous ink flow by applying shear rate independently from the external power source. One method of modelling the non-Newtonian fluid is the MPM which integrates both the Eulerian and Lagrangian approaches to keep track of the mass, momentum, and deformation of the particles. Next, the VOF model helps to identify the torque requirement, pressure gradient, and velocity profile in non-Newtonian mixing. During the active mixing, a vortex is formed around the impeller that enhances the mixing. Aside from simulation, the grid size determines the result accuracy and convergence criteria. The larger the number of grids, the more accurate the result will be.

## CHAPTER 3

### METHODOLOGY AND WORK PLAN

#### 3.1 Introduction

In this project, the existing active mixer design was reviewed from different research journals as per Figure 3.1. Then, the design concept is developed for the active mixer using Solidwork software. When the design is finalized, the simulation work will be carried up using computational fluid dynamics (CFD) with Ansys software. Before the simulation work, Hershel-Bulkley non-Newtonian fluid model is utilized to curve-fit the metal ink raw data obtained from the rheometer. After that, the viscosity of the material can be defined based on the data obtained from the curve fitting. In addition, the fluid domain of the active mixer will be created so the inlets, outlet, outer and rotating wall can be defined for simulation work. After data curve-fitting and fluid domain generation, the setup for the simulation work will be proceeded with Volume of Fluid (VOF) method to obtain results regarding multiphase flow. The objective is to check the homogeneity of the solution after the mixing process.

While the simulation work in progress, all the materials will be sourced and purchased for constructing the prototype of the active mixer, as per the design concept. Some components like motor housing, rotating impeller and mixing chamber have to be fabricated from aluminium block with the available machining equipment. After that, standard parts like screws, nuts and bearing are used for assembling different parts together for the prototype of the active mixer. This is followed up by testing the functionality of the prototype in the experimental study as well as fluid modelling through CFD simulation. From the prototype, different rotating speed from DC motor will be used to determine the mixing performance of the non-Newtonian inks for homogeneity of mixing.

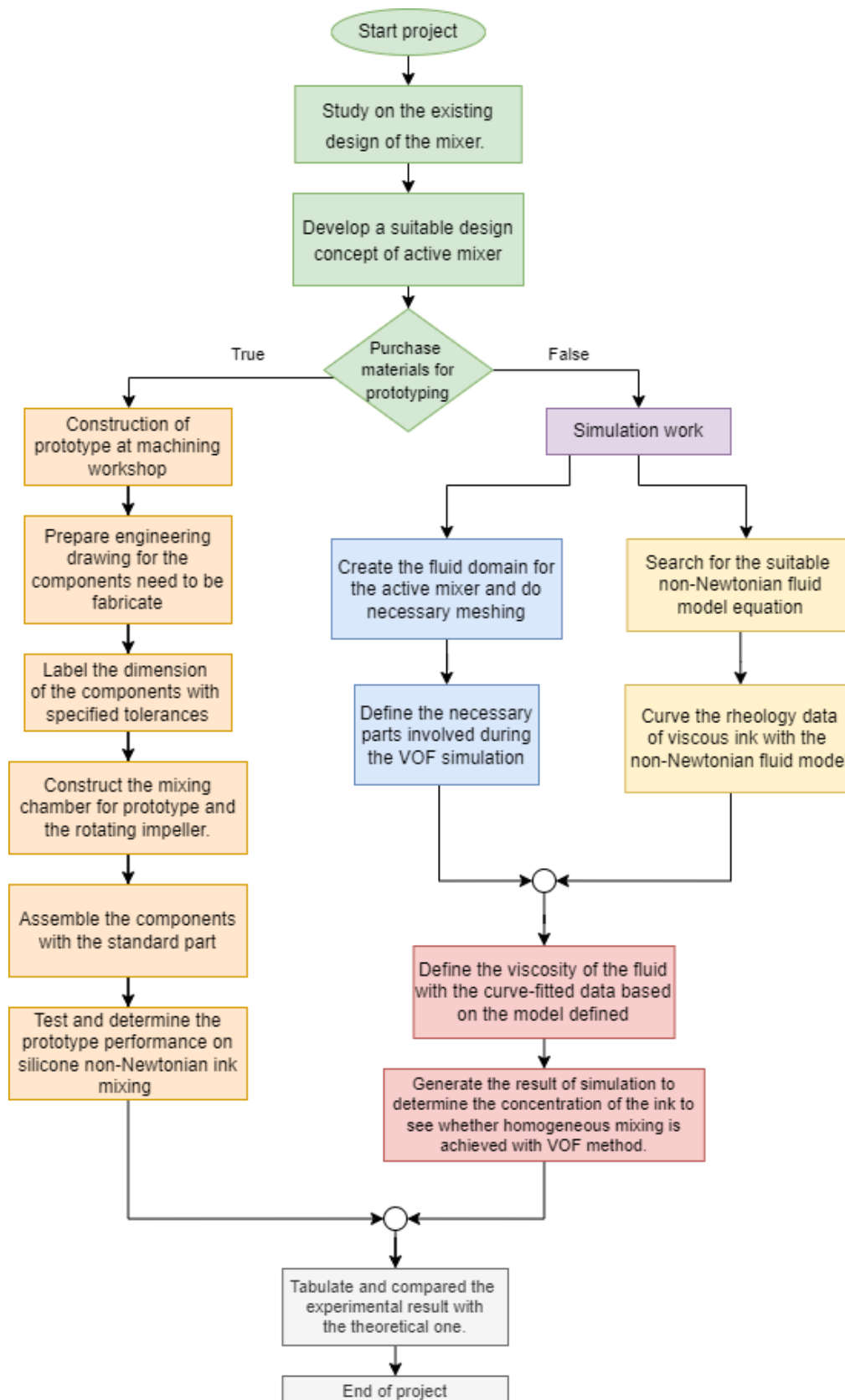


Figure 3.1: Flowchart of the project.

### 3.2 Active mixer design concept

Table 3.1 lists a few components in the active mixer design concept labelled in Figure 3.2. The mixing chamber has two inlets to blend different ink formulations. For the two other sides, there are two pressure plugs utilized to seal the two larger holes for mixing two non-Newtonian ink due to fabrication errors. Another two sides are connected with a tube fitting to a G1/4 male thread connector for silicone ink entry during 3D printing. Inside the mixing chamber, the DC motor will rotate the impeller at high angular velocity to achieve a homogeneous solution at the printed ink specimen.

Next, the bearing holds the rotating impeller in position to avoid misalignment of the rotating impeller. Besides, the Teflon seal below helps to prevent non-Newtonian flow from leaking onto the bearing and motor. Furthermore, the motor housing helps to support the motor position with two set screws to ensure that the DC motor can align the impeller in a center position. The Luer lock to G1/4 adapter fitting will be mounted below the mixing chamber for the ink to deposit through the dispensing nozzle during 3D printing time. In addition, a metal bracket helps to hold the prototype at the support plate with bolts and nuts.

Table 3.1: Lists of components for the active mixer design.

Item No	Part Name	Quantity
1	Mixing Chamber	1
2	Teflon seal	1
3	606ZZ radial ball bearing	1
4	Rotating Impeller	1
5	G1/4 to Luer lock fitting	1
6	Dispensing nozzle	1
7	DC motor	1
8	Motor housing	1
9	Pressure Plug	2
10	Mounting Bracket	1
11	Support Plate	1
12	High Pressure Tube Fitting to G1/4 Male Connector	2



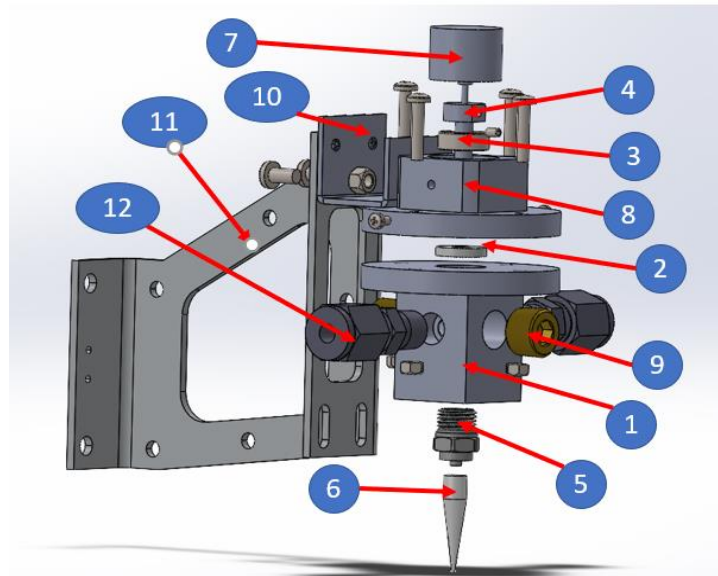


Figure 3.2: Exploded view of the active mixer design.

### 3.3 Active mixer simulation setup

First and foremost, the shear rate and viscosity of the silicone ink is obtained from the rheology data as shown in Table B-1. Then, these data points are plotted in the Matlab to curve-fit these data points with Hershel-Bulkley equation in Figure 3.3. To obtain reasonable data, conditions must be imposed to ensure that the parameters of consistency index,  $k$ ; flow behaviour index,  $n$ ; and non-Newtonian yield stress,  $\tau_0$  are greater than zero. By imposing these conditions, the three parameters computed from Hershel-Bulkley equation is shown in Table 3.2. The graph indicates very high viscosity of silicone ink at zero shear rate.

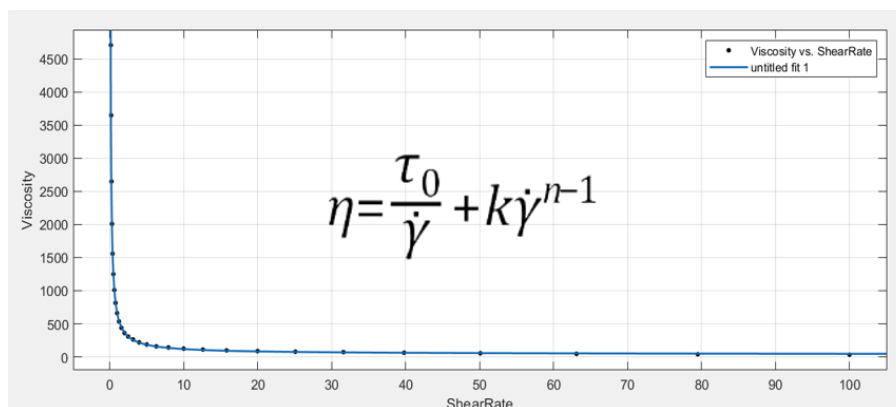


Figure 3.3: Curve-fitting of the silicone ink rheology data into Hershel-Bulkley model with shear rate and viscosity.

Table 3.2: Silicone ink properties for simulation setup.

Defined Parameter	Silicone Ink
Consistency Index, $k$	90.58
Power Law Index, $n$	0.8266
Yield Stress, $\tau_0$	575.5 Pa
Ink Density	1028.6 kg/m <sup>3</sup>

Computational Fluid Dynamics (CFD) is a technique that analyzes systems involving fluid flow by using numerical methods. CFD can conduct simulation studies in various industries like heat transfer, chemical experiments, machinery, and other aspects. The three elements for computing the result from the engineering problem in CFD are pre-processor, solver, and post-processor. In this project, CFD is used to visualize the homogeneity of the non-Newtonian mixing from different dye colours of the inks. Firstly, the active mixer Solidwork is imported into Ansys software for creating the fluid domain for CFD simulation. Next, a few boundary conditions are defined in the fluid domain as per Figure 3.4 — inlet 1, inlet 2, rotating wall, outer wall, and outlet. Later on, the condition for every boundary condition are defined in the simulation setup in Table 3.3.

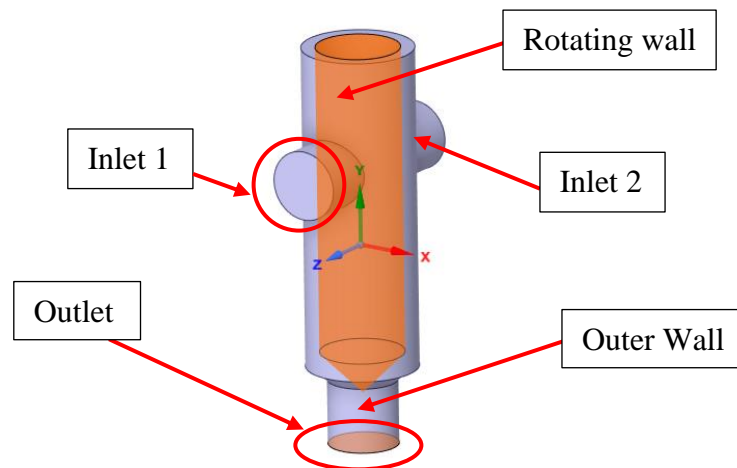


Figure 3.4: Fluid domain with defined boundary conditions.

After defining the boundary conditions, the meshing grid in Figure 3.5 helps to separate the fluid domain into smaller elements. From the figure, all the boundary conditions are meshed with tetrahedrons shape. From the tetrahedrons shape, patch conforming method is selected to support for 3D inflation at all the boundary conditions. While using inflation method for mesh definition, some hard points like sharp corners are likely to be ignored and doesn't support for 3D inflation. When the mesh element size becomes smaller with more node, the result becomes more accurate but takes a longer time to run the simulation. So, the suitable mesh size has to be determined to obtain accurate result with lesser computational time for simulation at the same time.

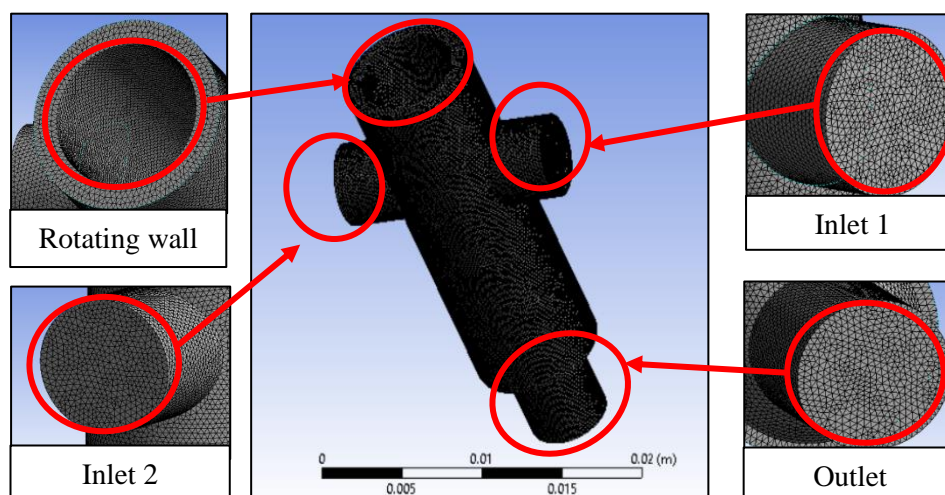


Figure 3.5: Meshing of the fluid domains.

After the meshing, the fluid model viscosity for silicone ink is considered laminar flow. For the material, the three parameter values obtained from curve-fitting (Table 3.2) define the ink viscosity under the Hershel-Bulkley model. The volume of fluid (VOF) model is selected to model the mixing performance of the active mixer to simulate the output solution homogeneity. Implicit volume fraction formulation is selected. It is because it provides a much more stable result for larger time step size because of the Courant number stability criterion that limits the computation in the explicit formulation. Moreover, “Dispersed” interface modelling is selected since the inks interpenetrate within the mixing chamber during mixing. Finally, the same silicone properties (Figure 3.2) assign the primary and secondary phases in the multiphase model.

Table 3.3: Overall setup for Fluent model and boundary conditions definition.

General						
Gravity	X	0.00 m/s <sup>2</sup>	Y	-9.81 m/s <sup>2</sup>	Z	0.00 m/s <sup>2</sup>
Time	Transient					
Model Setup for Multiphase Flow						
Viscous Model			Laminar			
Multiphase Model			Volume of Fluid			
Volume Fraction Formulation			Implicit			
Body Force Formulation			Enabled			
Number of Eulerian Phase			2			
Interface Modelling			Dispersed			
Primary phase material (Red Ink)			Silicone Ink			
Secondary phase material (Blue Ink)			Silicone Ink			
Surface Tension Coefficient			0.00023 N/m			
Phase Interaction			Adhesion Option: Wall Adhesion Model: Continuum Surface Force			
Boundary Conditions Definition						
Inlet 1	Velocity		1 mm/s			
	Blue Ink Volume Fraction		0.00			
Inlet2	Velocity		1 mm/s			
	Blue Ink Volume Fraction		1.00			
Rotating Wall Speed			0 rpm/ 12 rpm/ 24 rpm			
Outer Wall			Static Wall Setting with no-slip condition			
Outlet			Outlet pressure flow: 1 bar			

After that, the boundary condition is defined for each inlet with a velocity of 1mm/s into the mixing chamber. For inlet 2, the blue ink volume fraction is assigned as 1.0. Then, different rotational speeds in Table 3.3 are determined to obtain multiple results from the non-Newtonian mixing simulation. Also, the pressure outlet boundary condition will be subject to an atmospheric pressure of 1 bar. In Figure 3.5, half of the model is marked as the blue ink phase while the remaining region will represent the red ink phase. In the end, the red and blue silicone ink will enter the mixing chamber through inlet 1 and 2 respectively to visualize the prototype performance. During the simulation, the green colour will indicate the well-mixed region of the silicone colours.

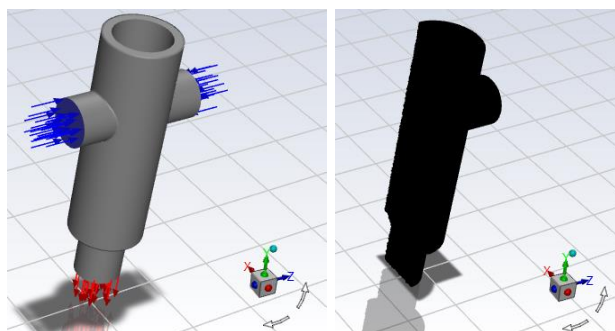


Figure 3.6: Half of the fluid domain is patched with secondary phase.

### 3.4 Experimental Design Study

In order to test the functionality of the prototype, the metal bracket holds the prototype at the printer device in Figure 3.6. The DC motor was connected to the motor controller to adjust the impeller rotational speed with the potentiometer (red square). Besides, the stepper motor will push the plunger of each syringe to pump the inks through the water hose to the mixing chamber. The silicone ink is mixed with red and blue dye in each syringe to observe the mixing result of the printed specimen. While printing, the output ink mixture is deposited through the nozzle on the printing platform.

In this project, the prototype extrudes the ink mixture through the nozzle tip after the non-Newtonian mixing in the chamber. When there is no rotation from the impeller, there will be a distinct layer of each respective colour across the ink profile that signifies the inhomogeneity from mixing the fluids.

Therefore, the appropriate rotational speed is required to provide a homogeneous solution for the printed profile. So, the different rotational speed of the impeller is applied to evaluate the prototype performance on silicone dyes mixing.

After printing the silicone sample with different impeller speeds, the dye colour distribution will be captured and examined under the SEM (Scanning Electronic Microscope). Based on the capture, the magnification factor helps to focus the image at good quality for result analysis on the image captured.

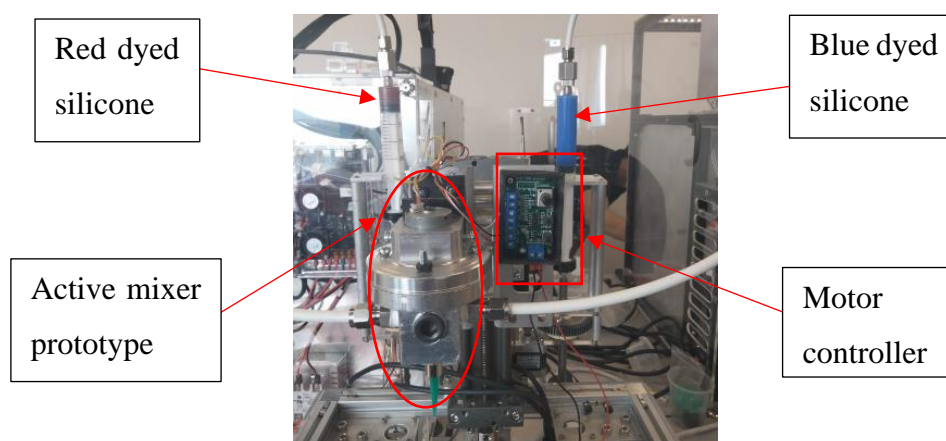


Figure 3.7: Hardware setup for the experimental work.

### 3.5 Prototype Performance Analysis

When carrying out the fluid modelling at different rotating impeller speeds (0 rpm, 12rpm and 24 rpm), each simulation test run data is saved in 200 time steps in Table 3.4. So, prototype performance is analyzed over the 10 seconds flow time. According to Figure 3.7, Plane 1 is created across the fluid domain at the X-point origin to obtain the average pressure, primary and secondary phase volume fraction distribution over the total flow time. Next, Plane 2 in Figure 3.8 is created around the fluid domain outlet with 3 point method at the YZ plane for computing each phase volume fraction after 10 seconds. Based on different time steps, various involved parameters (torque, pressure, etc.), these data will be plotted in the graph for comparison at different impeller speed in Chapter 4.

Table 3.4: Calculation and Plane Settings for CFD fluid modeling.

Calculation Settings						
No of time steps		200				
Time step size		0.05 s				
No of iteration per time step		20				
Plane 1						
Method		YZ Plane				
X position		0.00 mm				
Plane 2						
Point 1	X	0.00 mm	Y	-6.8694 mm	Z	3.9904 mm
Point 2	X	0.00 mm	Y	-6.9066 mm	Z	-4.5715 mm
Point 3	X	0.00 mm	Y	15.0600 mm	Z	-3.7530 mm

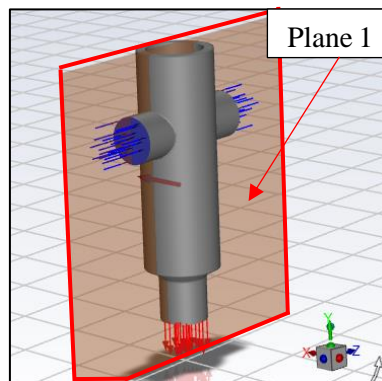


Figure 3.8: Plane 1 created with YZ method.

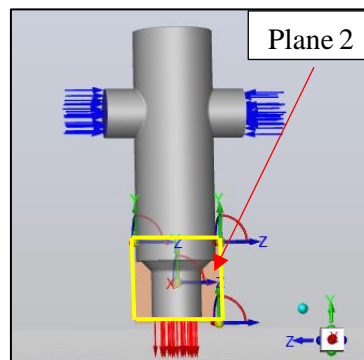


Figure 3.9: Plane 2 created with three points method.

## CHAPTER 4

### RESULTS AND DISCUSSION

#### 4.1 Introduction

In order to prove the design concept, both the experimental study and CFD fluid modelling have proceeded. From the CAD assembly file of the prototype, the fluid simulation flow model is created with the defined boundary to obtain the theoretical result of the design. Before conducting a simulation run, an independent-grid test was being carried out to ensure that a suitable mesh size was used to obtain an accurate result. After the active mixer prototype fabrication, the experimental prototype testing is proceeded on its performance at mixing different dyed silicone inks at different impeller speeds.

#### 4.2 Grid Independent test

The grid-independent test helps to determine the suitable mesh size for CFD fluid modelling. According to Table 1.4, there are five different mesh sizes tested with 24 rpm impeller rotational speed. A converged solution was obtained from the result for every mesh size. As the mesh element size gets smaller, the number of nodes and element for the calculation activities become greater. From 2 mm to 0.35 mm mesh size, the wall shear rate and torque at the rotating wall changed by 1-4% of its value for every mesh size decrement. When the element size decreases to 0.21 mm from 0.35 mm, the number of nodes and elements increases significantly. At the same time, there is less than a 1% value change for the wall shear stress and torque at the rotating wall. So, it is safe to conclude that a 0.2 mm mesh size is reasonable for CFD fluid modelling.



Table 4.1: Independent grid test with different element size with 24 rpm rotational speed.

Mesh Size, mm	No of nodes	No of elements	Wall Shear Stress, Pa	Change of value in percent	Torque, Nmm	Change of value in percent
2.00	2694	10162	1533.361	NIL	1.857	NIL
0.75	4318	17245	1581.922	3.16%	1.877	1.08%
0.50	11479	50163	1641.509	3.77%	1.950	3.89%
0.35	29264	137201	1702.705	3.72%	1.924	-1.33%
0.20	101964	506313	1690.278	-0.69%	1.934	0.52%

### 4.3 Ink homogeneity of the mixture from different speed of impeller

The active mixer performance testing involves different mixing scenarios at different rotational speeds (0 rpm, 12 rpm, and 24 rpm). In the test, the motor operates at 24 rpm during the maximum power from the motor controller. As the speed gets lower than 12 rpm, the viscous force from the silicone ink dominates the rotational force at the impeller that curb the active mixing approach at lower motor power. All the silicone ink flow will be laminar due to the low Reynold number. In the mixing chamber, the fluid will interpenetrate with each other in chaotic advection as the volume fraction from the respective inks start to spread across the volume depending on the impeller speed. However, the homogeneity within the mixture depends on the shear energy applied in low-volume mixing.

When there is no rotation from the impeller, all the fluid surfaces that touch the impeller and inner wall of the mixing chamber are considered stationary walls. Based on Figure 4.1 below, a distinct interface of different dye colours across the silicone ink profile without rotation from the impeller. Without shear energy from the impeller, there is a heterogeneous solution obtained from the extruder. A distinct layer of two dye colours is formed across the ink profile as the viscous flow travels downward to the nozzle. Das (2022) explained that viscosity consists of the resistance of the fluid to slide over each other during fluid motion. For the silicone ink, there are high intermolecular forces that hold the particles inside that results to low diffusion coefficient. So, the diffusion flux will be very low based on Fick's law of diffusion explained by Capretto (2019).

Therefore, a short mixing channel length is not applicable for the static mixing approach to obtain a homogeneous solution from non-Newtonian mixing. In Figure 4.2(a), the dark-blue visible striation appears in the silicone sample due to a distinct layer interface of red and blue dyes across the deposited silicone ink profile as shown in Figure 4.2 (b).

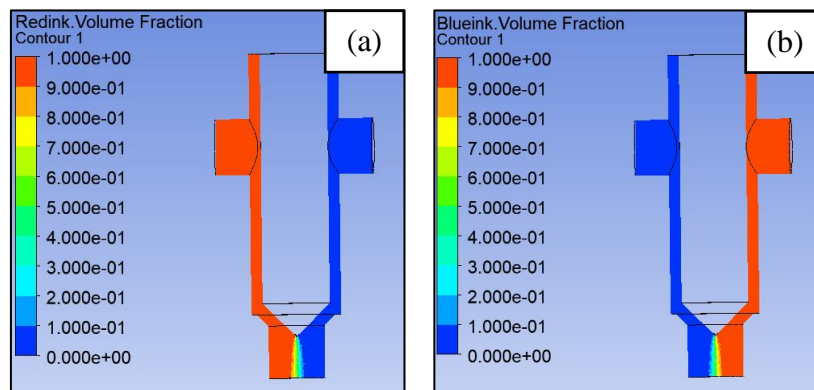


Figure 4.1(a) and (b): Red ink (left) and blue Ink (right) homogeneity for each phase without any rotation at Plane 1.

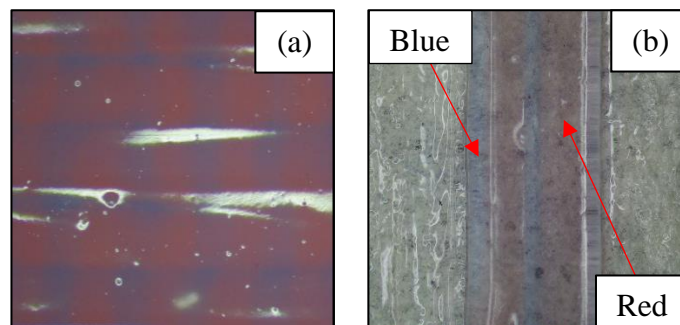
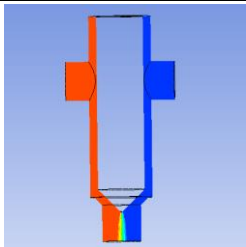
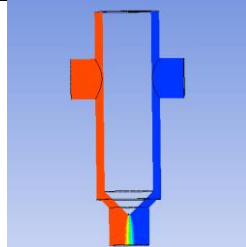
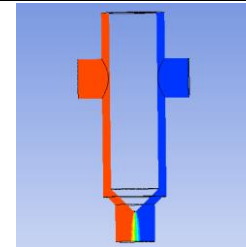
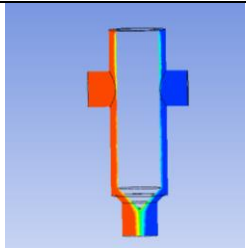
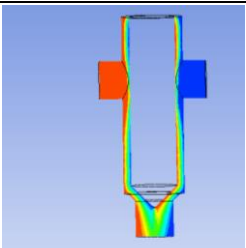
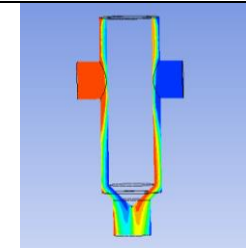
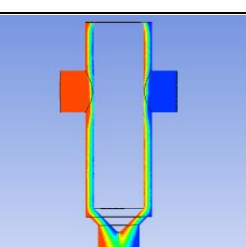
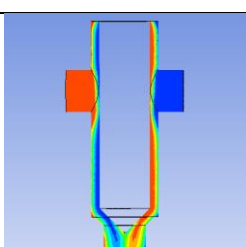
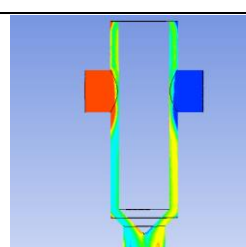


Figure 4.2 (a) & (b): Dark blue striation in the silicone sample (left) with a distinct interface of blue and red dye across the ink profile (right).

After that, the motor controller helps to adjust the impeller at different rotational speeds of 12 rpm and 24 rpm. When the impeller is rotating, the impeller applies shear energy to the silicone ink formulation. With sufficient shear rate applied, it helps the ink formulations to overcome the yield stress based on the Hershel-Bulkley rheology model to exhibit its shear-thinning behaviour. So, the non-Newtonian mixing has improved significantly in a low volume compared to the static mixing approach.

According to Table 4.1, CFD simulation evaluates the prototype mixing performance at different rotational speeds at a two-second interval. As the impeller rotational speed increases, the different dyed silicone colours mixing will be more efficient because higher shear energy applied from the DC motor will provide a greater shear rate at the fluid region near the rotating impeller. During mixing time, the fluid flow implies the no-slip condition at the wall surface. During the rotation, the silicone ink is sheared from the impeller surface to the inner wall within the mixing chamber. So, a higher impeller rotational speed provides a more consistent flow of homogeneous solution.

Table 4.2: Comparison of the ink mixing with different rotational speed (rpm) based on the volume fraction legend in Figure 4.3.

Rotational Speed (rpm)	Flow Time		
	2s	4s	6s
0			
12			
24			

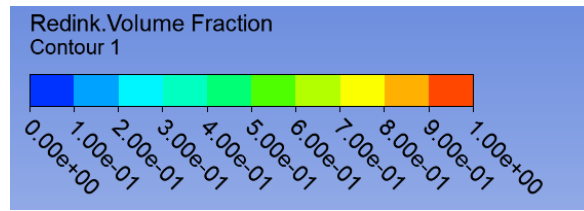


Figure 4.3: Default legend for the red ink volume fraction.

At different rotational speeds, Plane 2 (Figure 3.8) is created near the outlet to compute the average volume fraction of red and blue ink. The computed average volume fraction for each ink is approximately 0.5. So, it indicates that the two dye colours from each silicone ink are blended evenly to produce a homogeneous ink profile in Table 4.2. In the experimental testing, a purple homogeneous solution printed sample is obtained by mixing red and blue dyed silicone inks when the motor rotates the impeller at different rotational speeds (12 rpm and 24 rpm) in Figure 4.4(a). So, there is no distinct interface of two different dye colours across the printing profile in Figure 4.4(b). When the shear rate is applied, the ink viscosity has reduced for silicone mixing of different dye colours.

Table 4.2: Average volume fraction computation for each ink from the Plane 2.

Rotational Speed (rpm)	Red ink Volume Fraction	Blue Ink Volume Fraction
12	0.505082	0.494918
24	0.505289	0.494711

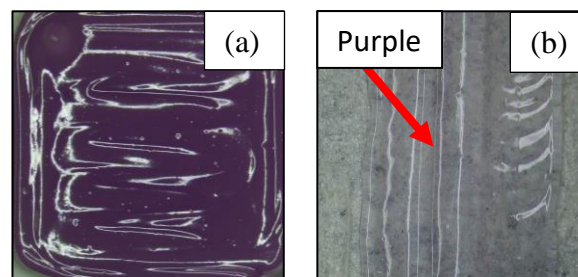


Figure 4.4 (a) & (b): Homogeneous purple silicone sample (left) without any distinct interface of blue and red dye colour across the ink profile (right)

In Figure 4.5, the wall shear stress is measured at the rotating wall of the fluid domain when the mixing subjects to rotation at 12 rpm and 24 rpm. Wall shear stress defines the force per area unit exerted by the solid boundary in a tangential direction. Based on the graph, the measured wall shear stress at 12 rpm and 24 rpm are approximately 1,455.19 Pa and 1,690.28 Pa respectively as listed in Table 4.2. The wall shear stress and fluid viscosity are under the function of shear rate in the Hershel-Bulkley rheology model from Equations 2.3 and 2.4. Based on the computed result for shear rate and fluid viscosity, this validates non-Newtonian fluid shear-thinning property according to the rheology data (Table B-I). During rotation, the fluid flow surface that contacts the impeller surface will experience the highest shear rate. So, the shear stress at that point is the greatest. As the rotational speed increases, it will promote fluid deformation among the silicone inks in mixing due to a higher shear rate.

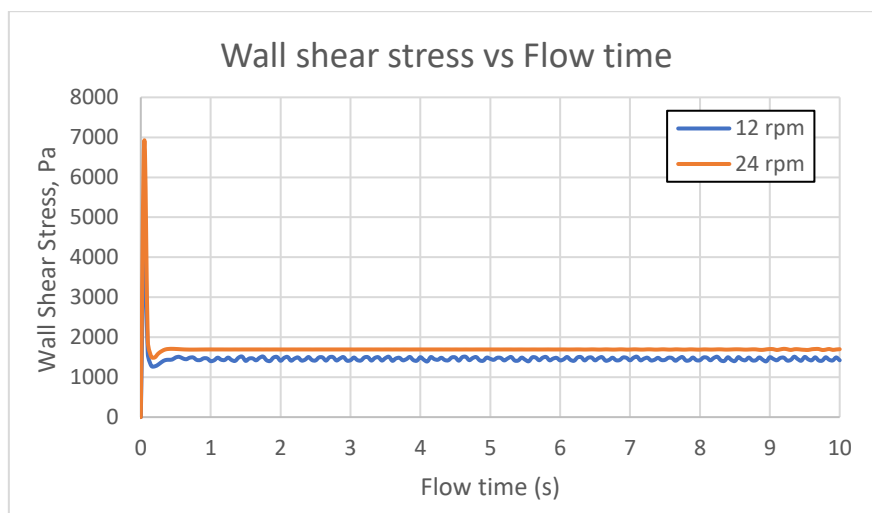


Figure 4.5: Plot of wall shear stress against flow time in different rotational speed at the rotating wall.

Table 4.3: Wall shear stress and computation of shear rate and viscosity in different rotational speed from Figure 3.3.

<b>Rotational speed (rpm)</b>	<b>Wall shear stress (Pa)</b>	<b>Shear Rate (1/s)</b>	<b>Viscosity (Pa.s)</b>
12	1,455.19	15.65	93.72
24	1,690.28	20.84	81.11

Based on Figure 4.6 and 4.7, the graphs representing average volume fraction for both inks at the fluid outlet (Figure 3.4) are plotted separately at the fluid domain outlet (Figure 3.4). From the methodology, half of the fluid domain is marked with blue ink during the initialization of solution. When mixing begins, there is a steep increment of red ink volume fraction by 0.35 and vice versa for blue ink volume fraction. As the mixing proceeds, output produced will eventually reach a well-mixed steady state with 0.5 volume fraction at the outlet for each respective inks. At 12rpm, the average volume fraction reaches about 0.5 at 2 s while 24rpm speed achieve this average value at outlet during 1 s flow time. So, the active mixer can shorten the time taken to achieve a steady-state mixing compared to hybrid mixer developed by Hassan and Selvaganapathy (2021).

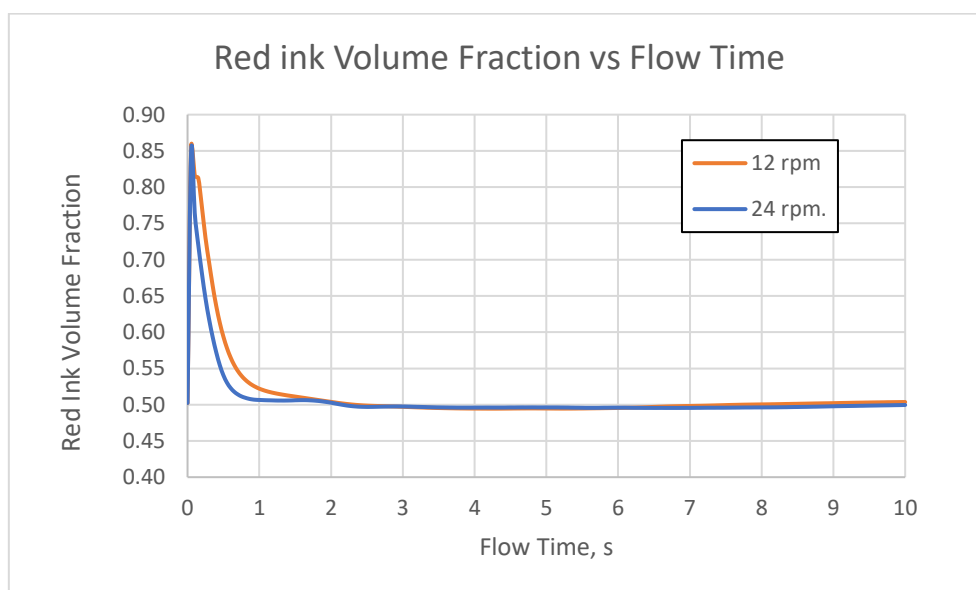


Figure 4.6: Red ink volume fraction at the fluid domain outlet in different rotational speeds.

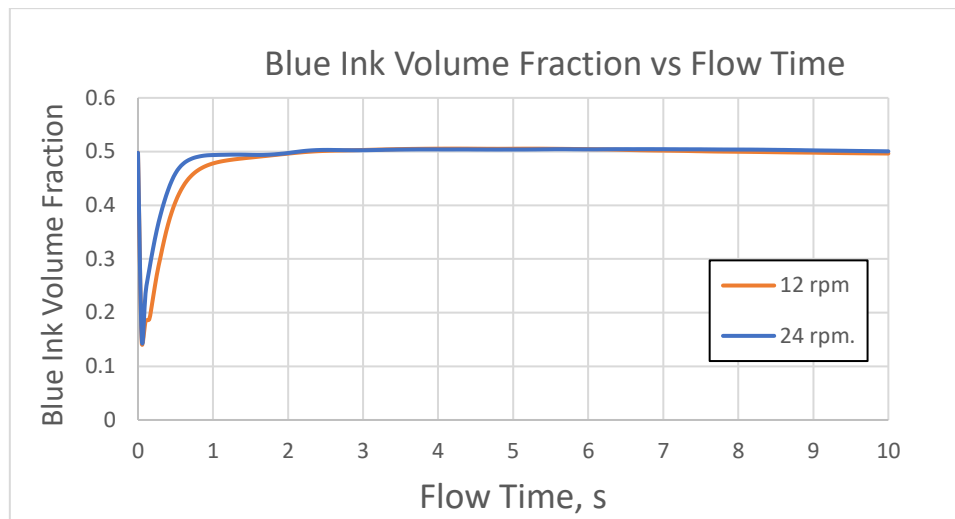


Figure 4.7: Blue ink volume fraction at the fluid domain outlet in different rotational speeds.

#### 4.3.1 Velocity and Pressure Profile analysis

Based on the simulation results, Plane 1 from Figure 3.7 displays the pressure profile from the bottom to the top of the mixing chamber during the mixing time in Figure 4.8. When the inks from each inlet mix together, the pressure is higher near the top of the wall. As the fluid passes down the channel due to sequential injection from the syringes, the pressure decreases as it approaches the outlet where the atmospheric pressure is about 1 bar. In Figure 4.8, a pressure gradient is observed at Plane 1 contour of the simulation from the inner chamber to the outlet. So, the silicone ink will have a pressure flow during the extrusion process due to the pressure gradient.

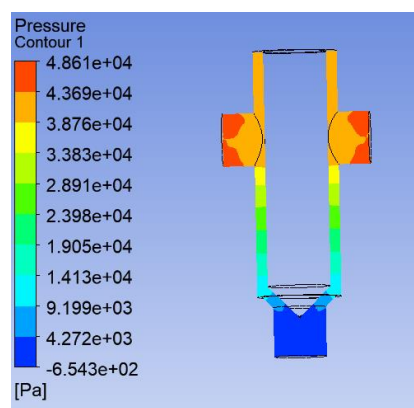


Figure 4.8: Pressure Profile of the mixing chamber at 24 rpm at Plane 1.

During operation, the average pressure at Plane 1 will continue to fluctuate along the flow time in Figure 4.8. When there is no rotation, the pressure fluctuation is very significant. The estimated peak pressure value is about 55000 Pa without the impeller rotating in mixing. With applied external power from the DC motor, the pressure fluctuation reduces to a range between 30,000 Pa and 40,000 Pa. As a result, Bernoulli's principle indicates that pressure is inversely proportional to velocity.

When there is rotation, the impeller transfers the kinetic energy to the fluid during mixing. While implying the energy conservation law, the pressure will decrease due to higher velocity. It is because the total sum of potential and kinetic energy; and energy associated with fluid pressure are constant. Therefore, the inner pressure of the mixing chamber decreases with the active mixing approach compared to the static mixing approach. As the impeller rotational speed increases to 24 rpm, the pressure fluctuation reduces as the pressure across the time remains around 28,000 Pa before it begins to fluctuate a bit at 6 s flow time. According to Golobic et al (2019), higher impeller rotational speed manages to prolong the residence time of the fluid for mixing before the ink deposition. Due to lower pressure gradient flow, the silicone inks will be mixed at longer time within the mixing chamber to achieve better uniformity of material composition at the final output.

For static mixing approach, no torque is applied from the motor power as inks are pushed from the syringes by the stepper motors into the mixing chamber. As the DC motor power is activated, the rotating impeller applies torque to the fluid during the non-Newtonian mixing. Initially, the torque reaches the peak value around 0.05 s flow time before it decreases due to high silicone ink viscosity before applying any shear rate. As the fluid viscosity decreases, the torque becomes lower. As the motor power increases, the torque applied to the fluids becomes greater: 24rpm with 1.93 Nmm and 12 rpm with approximately 1.4 Nmm. So, it indicates higher power is required for higher rotating impeller speed for the non-Newtonian mixing based on Figure 4.10.



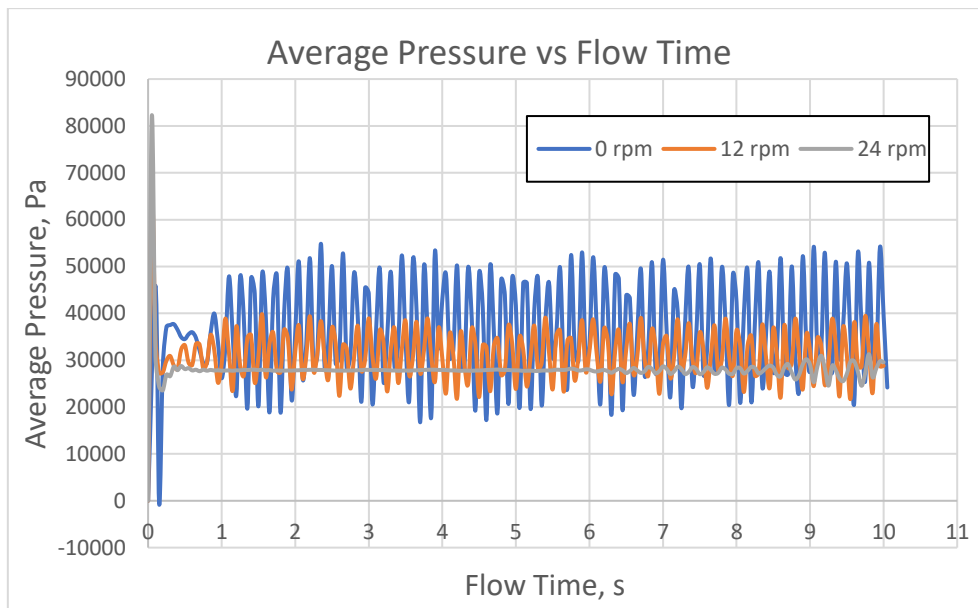


Figure 4.9: Plot of average pressure vs flow time at different rotational speeds at the Plane 1.

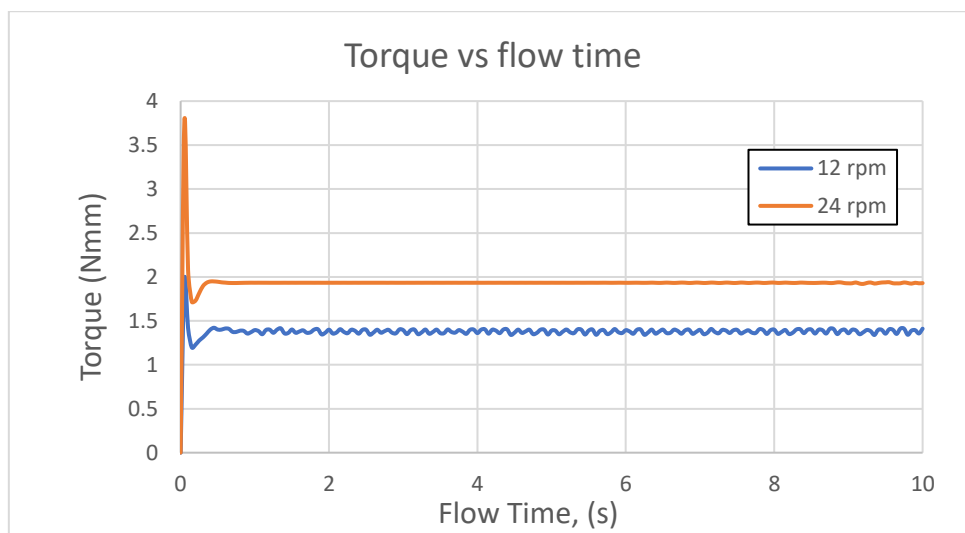


Figure 4.10: Plot of torque vs flow time at different rotational speeds from the rotating wall.

When the impeller rotates, Dular et al (2006) mentioned that the tangential velocity in the silicone mixing changes depending on the point distance from the impeller surface. As the point gets nearer to the impeller, the tangential velocity rises; therefore, forming a vortex around the impeller in Figure 4.11. It shows that the tangential velocity is inversely proportional to the vortex radius from Figure 4.8. Oladebeye and Boloji (2004) stated that the forced vortex formed by the rotation develops a parabolic profile that pushes the

fluid down to the nozzle. Therefore, the middle of the flow has a higher velocity at the outlet. Due to the no-slip condition, there is no relative movement at the wall surface due to direct contact with the stationary wall surface.

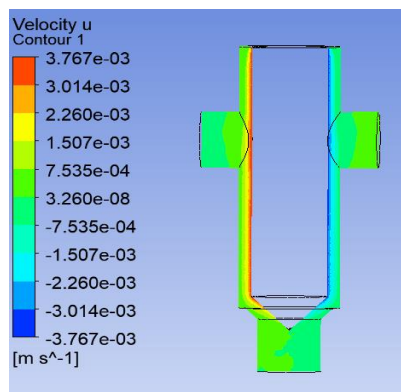


Figure 4.11: Tangential velocity profile across the velocity profile during rotation 12 rpm.

On the other hand, the impeller acts as the wall boundary condition when the impeller is not rotating. As the fluid extrudes along the path, the velocity increases as the cross-sectional area get smaller. In both cases, the fluid extrusion velocity gets significantly higher when the silicone extrudes through the nozzle hole. Based on Table 4.4, the average outlet velocity reduces when the rotational speed increases from 0 to 12 rpm. One of the factors is the pressure drop in the inner chamber from the rotating impeller. As the impeller rotates, the fluid circulates the rotating impeller in Figure 4.11. As the fluid rotates at 12 rpm, the vortex reduces the downward velocity of silicone flow in Table 4.3. This data supports the research work by Golobic et al (2015) that the silicone ink residence time becomes longer for sufficient silicone mixing. However, the average outlet velocity increases when the rotational speed rises to 24 rpm; thus, a higher rotational speed from the impeller can reduce the mixing chamber pressure while increasing the output velocity.

Table 4.4: Comparison of velocity profile at Plane 1 cross section of the fluid domain.

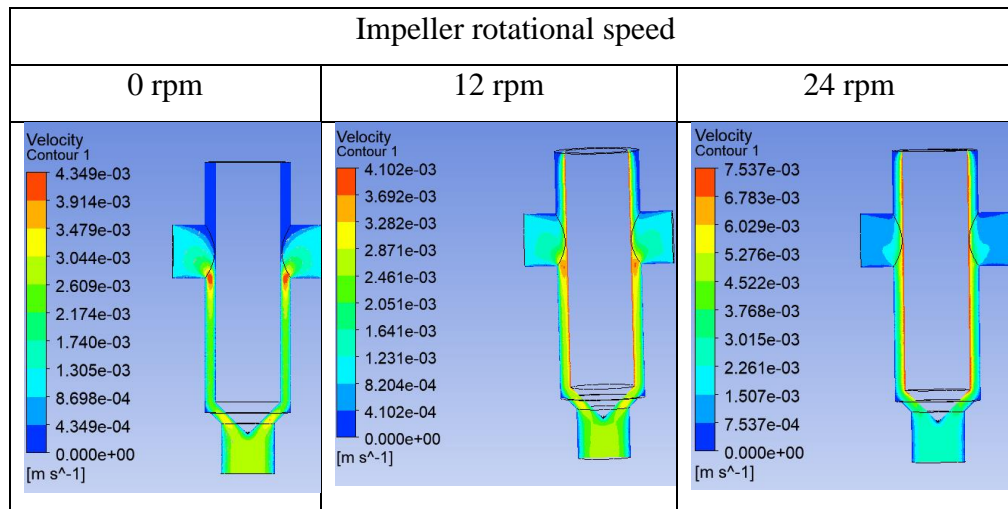


Table 4.5: Average velocity computed at the fluid domain outlet.

Rotational Speed, rpm	Average velocity, mm/s
0	2.1592
12	1.8490
24	2.0076

### 4.3.2 Impact of flow rate on the output

The active mixer can vary the composition of different ink formulation inputs at the output by adjusting the inlet velocity at any silicone flow. In the simulation, the ratio between the inlet velocity of blue ink to red silicone ink is adjusted according to Table 4.5. At the same time, the impeller rotational speed remains at 24 rpm, and the red silicone flow at inlet 1 (Figure 3.4) remains at 1mm/s. From Figure 4.12, the red ink volume function across the flow time is plotted at different blue silicone ink inlet velocities in the mixing chamber. As the velocity increases, the average red ink volume fraction at the outlet decreases as more blue silicone ink is pumped into the mixing chamber over the flow time. The average value of red and blue ink volume fractions from the outlet at 10 s are listed in Table 4.2. According to Ober (2015), the inlet velocity or flow rate of any input ink can be varied to control the output material composition.

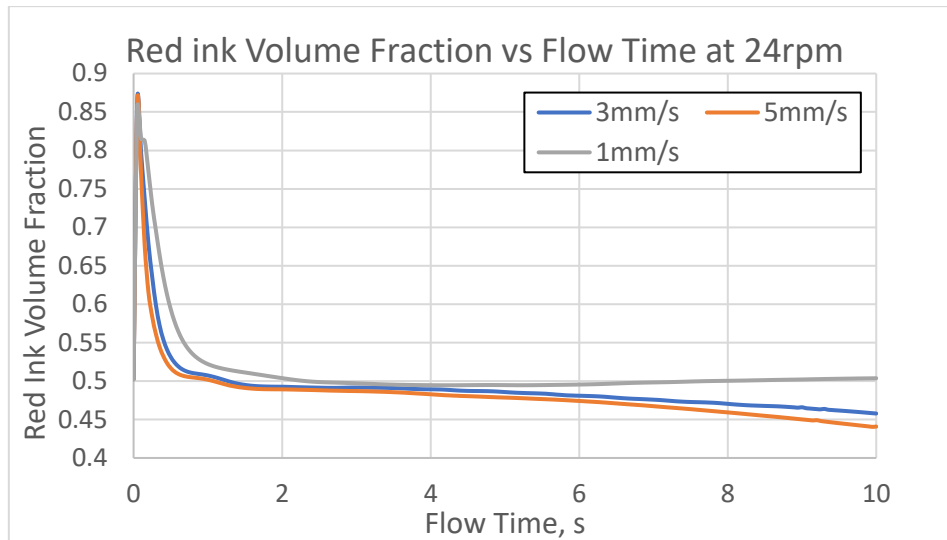


Figure 4.12: Plot of red ink volume fraction at different blue silicone ink inlet velocity with impeller speed of 24 rpm at the outlet.

As more blue silicone ink flows into the mixing chamber, there will be more pressure building up inside the mixing chamber. As the velocity for blue silicone ink increases, more silicone is being pumped into the mixing chamber. At the same time, additional pressure builds up in the non-Newtonian mixing. So, the outlet velocity at the fluid domain increases. In Figure 4.13, the average pressure increases to around 42,000 Pa and 55,000 Pa when the blue silicone inlet velocity increases to 3 mm/s and 5mm/s respectively. As more fluids build up in the mixing chamber, higher torque is required to blend the respective ink together due to extra power needed. In order to achieve a uniform output, higher impeller speed is needed from the dc motor to reduce the mixing chamber inner pressure; therefore, the fluid residence time will increase for a more uniform output at the silicone ink profile.

As a result, higher torque provides higher rotating force that applies higher wall shear stress to the fluid during the silicone mixing in Figure 4.15. As the blue silicone ink flow increases further, the flow becomes more pressurized that higher shear rate is applied compared to 3mm/s velocity. Therefore, the torque required for the non-Newtonian flow decreases at 5mm/s in Figure 4.14. All the measured value of torque, wall shear stress and respective ink colour volume fraction by the end are listed in Table 4.5.

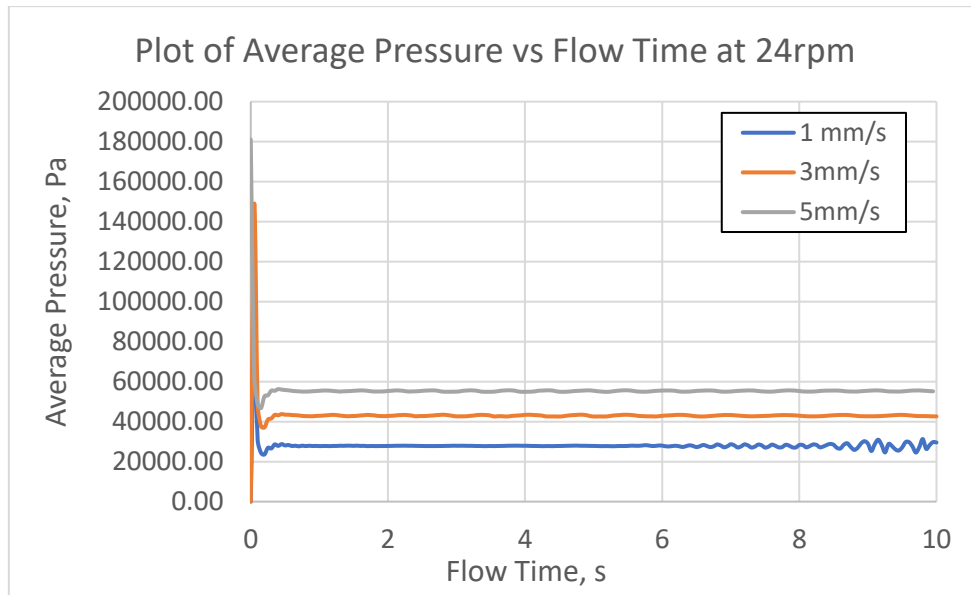


Figure 4.13: Plot of average pressure over flow time at different blue silicone ink velocities at 24 rpm — Measured at Plane 1.

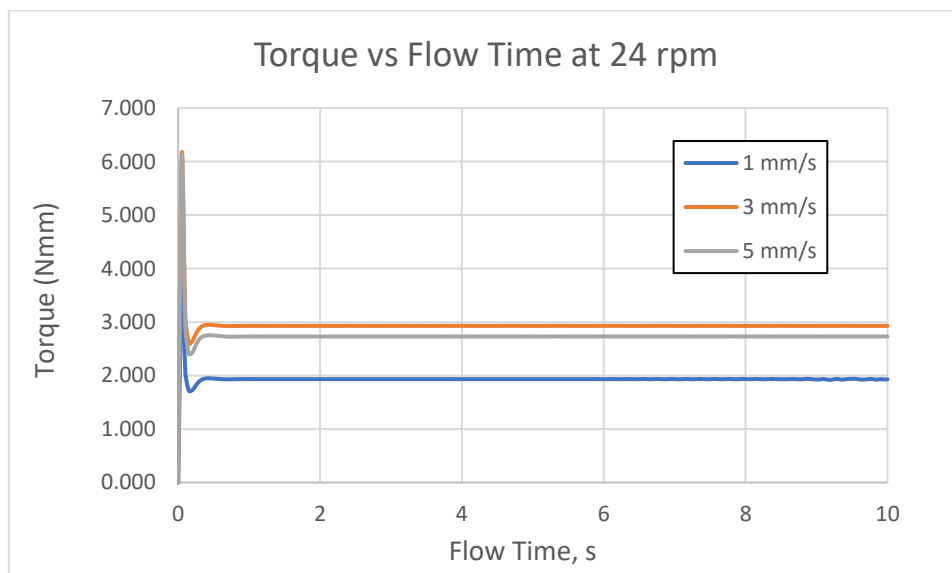


Figure 4.14: Plot of torque over flow time at different blue silicone ink velocities at 24 rpm — Measured at the fluid domain rotating wall.

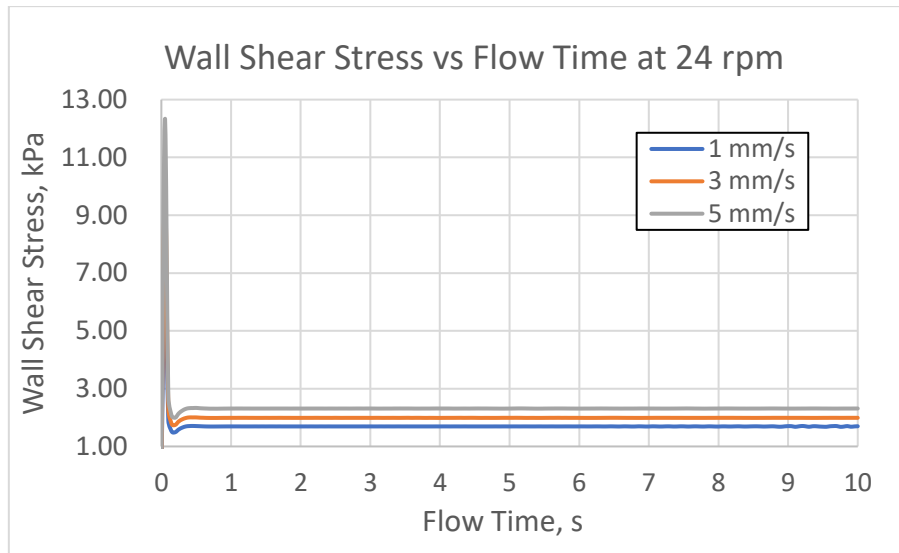


Figure 4.15: Plot of wall shear stress over flow time at different blue silicone ink velocities at 24 rpm —Measured at the fluid domain rotating wall

#### 4.4 Summary

A total of three impeller rotational speeds (0 rpm, 12 rpm and 24 rpm) were being experimented in the prototype testing and evaluated through CFD fluid modelling. In the static mixing approach, there is no dye colour mixing among the silicone inks due to zero shear rate from the impeller. When the impeller rotates at either 12 rpm or 24 rpm rotational speed, shear rate is applied to the silicone that reduces the viscosity. Therefore, it promotes the mixing performance that produces a purple homogeneous solution at 0.5 volume fraction. For 12 rpm or 24 rpm mixing, a well-mixed steady state output can be achieved by 2s and 1s respectively which proved to be efficient compared to the hybrid mixer with floating static mixer. As the rotational speed becomes greater, the torque applied to the fluid domain gets larger. At the same time, the wall shear stress becomes higher; therefore, it results to higher shear rate but lower viscosity. At the same time, the pressure will decrease which promote the residence time in the mixing chamber for mixing. Although the impeller rotation reduces the mixing pressure and outlet velocity of silicone printing, the outlet velocity can still be increased with larger impeller speed. The overall result of prototype performance at different speeds are summarized in Table 4.7. Furthermore, the input velocity ratio between different inlets can be adjusted to vary the concentration of output as shown in Table 4.8,

Table 4.6: Result summary for prototype performance at different speeds.

Impeller Speed, rpm	0 rpm	12 rpm	24 rpm
Shear Rate (1/s)	0	15.65	93.72
Viscosity, Pa.s	To infinity	20.84	81.11
Torque (Nmm)	0	1.4	1.93
Wall Shear Stress (Rotating wall) , Pa	0	1,455.19	1,690.28
Average Pressure, Pa	20,000 -55,000	22,000- 40,000	28,000
Outlet average velocity, mm/s	2.1592	1.8490	2.0076
Time taken to reach steady mixing state, s	0	2	1

Table 4.7: Results obtained from different blue silicone ink inlet velocities at 24 rpm impeller speed.

Velocity Ratio of blue to red ink flow	1:1	3:1	5:1
Red Ink Volume Fraction	0.505289	0.457807	0.440839
Blue Ink Volume Fraction	0.505289	0.542193	0.559161
Torque, Nmm	1.9294	2.9294	2.7305
Wall Shear Stress, kPa	1.70	1.99	2.31
Average Pressure, Pa	28,000	42,000	55,000

## CHAPTER 5

### CONCLUSIONS AND RECOMMENDATIONS

#### 5.1 Conclusions

In this project, the first objective is to design an active mixer to produce a homogeneous solution from different silicone ink formulations. The active mixer design concept was developed with Solidwork before the prototype was fabricated in the mechanical workshop. The prototype design has several essential components like a mixing chamber, rotating impeller, motor housing, etc. After the fabrication process, the prototype has proceeded with experimental testing. The heterogeneous ink profile was observed with a distinct interface between red and blue dye colours without rotation from the impeller. Due to the applied rotational speed at either 12 rpm or 24 rpm, the mixer can provide a sufficient shear rate on the fluids to blend the dye colours into a purple homogeneous solution.

Besides that, CFD is used to evaluate the prototype performance with fluid modelling. At 12rpm, the measured wall shear stress from the impeller is 1,455.19 Pa with an estimated shear rate of 15.65 s<sup>-1</sup>; therefore, the silicone ink viscosity will reduce to 93.72 Pa.s significantly from the initial state. Also, it minimizes the pressure fluctuation from 0 rpm mixing from 20,000- 55,000 Pa to 22,000- 40,000 Pa. As the impeller speed increases to 24 rpm from 12 rpm, the shear stress increases up to 1,690.28 Pa with an estimated shear rate of 20.84 s<sup>-1</sup> and 81.11 Pa.s viscosity. At 24 rpm operation, the pressure fluctuation is greatly reduced where the pressure remains around 28,000 Pa along the flow time. So, the residence time of silicone can be promoted to produce a more uniform output mentioned by Golobic et al (2019). So, an active mixer promotes the uniformity of the output in terms of material properties. Higher mixing pressure will reduce the fluid residence time which affects the output homogeneity from mixing.



Even though the outlet velocity is reduced as the impeller rotates at 12 rpm from 0 rpm, the printing speed can be adjusted by varying the impeller speed — a higher impeller speed provides a higher printing speed. Lastly, it was observed that it takes about 2 s and 1 s for the prototype to achieve a steady mixing with a 0.5 volume fraction at 12 rpm and 24 rpm impeller speeds respectively, which serves as a more efficient solution than the hybrid and static mixer.

Without changing the rotational speed of 24 rpm, the change of blue to red silicone inlet velocity ratio can change the output composition of the dye colours. When the ratio increases, the red ink volume fraction decreases as more blue silicone ink flows into the mixing chamber. When more fluids build up in the mixing, the pressure increases along with torque and wall shear stress. At 5:1 blue to red silicone inlet velocity, the pressure increases up to 55,000 Pa. This indicates that higher impeller speed is needed to raise the fluid residence time for the printed silicone output. Later, the torque will increase from 1.9294 Nmm to 2.9294 Nmm at 3mm.s blue silicone ink inlet velocity. As the blue silicone velocity increases to 5mm/s, the torque value will decline to 2.7305 Nmm due to the additional shear rate applied from the higher inlet velocity for the blue silicone ink.

In conclusion, the outcome shows that an active mixing approach is necessary to blend different ink formulations compared to a static mixing approach that requires a longer mixing channel length for obtaining a homogeneous solution. For DIW, active mixing can combine different kinds of material properties efficiently. The rotating impeller is essential to reduce the mixing pressure for higher fluid residence time in the chamber to provide a more uniform output in terms of material properties to cater to different needs like soft components for the machine or internal structure. The design consideration can be applied in the future for better product serviceability.

## 5.2 Recommendations for future work

From the project current findings, there are several aspects for the work to be improved in the future. The first aspect is the fabrication and assembling process of the components. First and foremost, the bearing shall be press-fitted with the rotating impeller rather than loose fitting to minimize the possibility of fluid leakage in the upward direction. Besides, the Teflon seal at the bearing below shall consist of a minimal gap hole from the rotating impeller without disrupting the impeller performance.

Next, the four holes at the motor housing and mixing chamber can be fabricated more accurately in the future for better connection. Therefore, it allows proper mounting of the dc motor in the housing that rotates the impeller during the non-Newtonian mixing. So, the impeller body won't distort easily from the center alignment in the mixing chamber to improve the product reliability during non-Newtonian mixing.

As for the mixing chamber, design improvement is applicable in the future; for instance, it can cater to up to four inlets to allow a more flexible adjustment of the material composition by varying the flow rate at each input. After usage, the silicone ink within the chamber shall be isolated from the atmosphere to prevent curing due to moisture air content.

## REFERENCES

- Anon., 2004. Design, Construction and Performance Testing of a Forced Vortex Equipment for use in the Fluid Mechanics Laboratory.. *International Journal of Science and Technological Research*, 1(1&2), pp. 132-144.
- Ansys, 2021. *Ansys LS-DYNA Smooth*. [Online] Available at: <https://www.ansys.com/content/dam/product/structures/ls-dyna/ls-dyna-smooth-particle-hydrodynamics.pdf> [Accessed 5 February 2022].
- Britannica, T. Editors of Encyclopaedia , 2018. *Vickers hardness*. [Online] Available at: <https://www.britannica.com/science/Vickers-hardness> [Accessed 23 April 2022].
- Buj-Corral, I., Bagheri, A. & Petit-Rojo, O., 2018. 3D Printing of Porous Scaffolds with Controlled Porosity and Pore Size Values. *Materials*, 11(9), p. 1532.
- Capretto, L., Cheng, W., Hill, M. & Zhang, X., 2011. *Micromixing Within Microfluidic Devices*. [Online] Available at: [https://www.researchgate.net/profile/Xunli-Zhang/publication/51083035\\_Micromixing\\_Within\\_Microfluidic\\_Devices/links/02e7e51adea4e65bef000000/Micromixing-Within-Microfluidic-Devices.pdf](https://www.researchgate.net/profile/Xunli-Zhang/publication/51083035_Micromixing_Within_Microfluidic_Devices/links/02e7e51adea4e65bef000000/Micromixing-Within-Microfluidic-Devices.pdf) [Accessed 2nd July 2022].
- Das, S., 2022. *Diffusion Coefficient And Viscosity: Relationship And Impacts*. [Online] Available at: <https://lambdageeks.com/diffusion-coefficient-and-viscosity/> [Accessed 11 September 2022].
- Dogan, Y. O. & Yigit, M., 2020. *Extrusion System for 3-D Printing of Viscous Elastomers*. Oregon, Patent No. 0298492.
- Dular, M. et al., 2006. Numerical Simulation And Experimental Study Of Non-Newtonian Mixing Flow With A Free Surface. *Brazilian Journal of Chemical Engineering*, 23(4), pp. 473-486.
- Dutrow, B. L. & Clark, C. M., 2018. *X-ray Powder Diffraction (XRD)*. [Online] Available at: [https://serc.carleton.edu/msu\\_nanotech/methods/XRD.html](https://serc.carleton.edu/msu_nanotech/methods/XRD.html) [Accessed 23 April 2022].

EKU Online, 2020. *The Seven Wastes of Lean Manufacturing*. [Online] Available at: <https://safetymanagement.eku.edu/blog/the-seven-wastes-of-lean-manufacturing/#:~:text=Under%20the%20lean%20manufacturing%20system,processing%2C%20waiting%2C%20and%20transport.>

[Accessed 23 April 2022].

Equbal, A., Akhter, S., Sood, A. K. & Equbal, I., 2021. The usefulness of additive manufacturing (AM) in Covid 19. *Annals of 3D Printed Medicine*, Volume 2, p. p100013.

Gaget, L., 2018. *How can 3D printing be an asset for lean manufacturing?*. [Online] Available at: <https://www.sculpteo.com/blog/2018/03/20/how-can-3d-printing-be-an-asset-for-lean-manufacturing/> [Accessed 20 April 2022].

Golobic, A. M. et al., 2019. Active Mixing of Reactive Materials for 3D Printing. *Advanced Engineering Materials*, 21(8), p. 1900147.

Hassan, I. & Selvaganapathy, P. R., 2021. *A microfluidic printhead with integrated hybrid mixing by sequential injection for multimaterial 3D printing*. [Online]. Available at: <https://www.sciencedirect.com/science/article/pii/S2214860421007065> [Accessed 19 February 2022].

Kelessidis, V. C., Maglione, R., Tsamantaki, C. & Aspirtakis, Y., 2006. Optimal determination of rheological parameters for Herschel–Bulkley drilling fluids and impact on pressure drop, velocity profiles and penetration rates during drilling. *Journal of Petroleum Science and Engineering*, 53(3), pp. 203-224.

Malvern, 2017. *Understanding Yield Stress Measurement*. [Online] Available at: <https://www.azom.com/article.aspx?ArticleID=14417> [Accessed 15 February 2022].

M, S., 2020. *Tolerances: Types And Difference Between Unilateral & Bilateral Tolerances*. [Online] Available at: <https://www.theengineerspost.com/tolerances-types/> [Accessed 29 March 2022].

Nanakoudis, A., 2019. *EDX Analysis with SEM: How Does it Work?*. [Online] Available at: <https://www.thermofisher.com/blog/microscopy/edx-analysis-with-sem-how-does-it-work/> [Accessed 23 April 2022].

NASA John H. Glenn Research Center, 2016. *In-Situ Mixing, Degassing, Decavitation, and Extrusion Modules for Fused Deposition Modeling 3D Printers*. [Online] Available at: <https://www.techbriefs.com/component/content/article/tb/pub/briefs/manufacturing-prototyping/23682> [Accessed 29 January 2022].

Nguyen, N. T., 2007. Mixing in Microscale. In: S. Hardt & F. Schonfeld, eds. *Microfluidic Technologies for Miniaturized Analysis Systems*. Boston: Springer, pp. 117-155.

NTN Global, n.d. *Ball and Roller Bearing*. [Online] Available at: <https://www.ntnglobal.com/en/products/catalog/pdf/2203E.pdf> [Accessed 22 April 2022].

Ober, T. J., Foresti, D. & Lewis, J. A., 2015. Active mixing of complex fluids at the microscale. *Proceedings of the National Academy of Sciences*, 112(40), pp. 12293-12298.

Oladebeye, D. H. & Bolaji, B. O., 2004. Design, Construction and Performance Testing of a Forced Vortex Equipment for use in the Fluid Mechanics Laboratory. *International Journal of Science and Technological Research* , 1(1&2), pp. 132-144.

Price, A., 2013. *Additive Manufacturing – Standards..* [Online] Available at: <https://www.nottingham.ac.uk/research/groups/advanced-manufacturing-technology-research-group/documents/manufacturing-metrology-team/qcam-17/bsi.pdf> [Accessed 20 April 2022].

Ram, D. et al., 2015. *A material point method for viscoelastic fluids, foams and sponges*. Los Angeles, California, SCA 2015 Proceedings of the 14th ACM SIGGRAPH / Eurographics Symposium on Computer Animation.

Rocha, V. G., Saiz, E., Tirichenki, L. S. & Tunon, E. G., 2020. Direct Ink writing advances in multi-material structures for a sustainable future. *Journal of Materials Chemistry A*, 8(31), pp. 15646-15657.

Science Learning Hub, 2010. *Non-Newtonian fluids*. [Online] Available at: <https://www.sciencelearn.org.nz/resources/1502-non-newtonian-fluids> [Accessed 5 February 2022].

Shahzad, A. & Lazoglu, I., 2021. Direct ink writing (DIW) of structural and functional ceramics: Recent achievements and future challenges. *Composites Part B: Engineering*, Volume 225, p. 109249.

Stomakhin, A. et al., 2013. A material point method for snow simulation. *ACM Transactions on Graphics (TOG)*, 32(4), pp. 1-10.

The Engineers Post, 2019. *Difference Between Unilateral & Bilateral..* [Online] Available at: <https://www.theengineerspost.com/tolerances-types/> [Accessed 2022 March 29].

Uljad, B. et al., 2021. *Mobile 3D Printing Robot Simulation with Viscoelastic Fluid*. [Online] Available at: <https://arxiv.org/abs/2110.04412> [Accessed 5th February 2022].

Wendell, D. M., Pigeonneau, F., Gouillart, E. & Jop, P., 2013. Intermittent Flow In Yield-Stress Fluids Slows Down Chaotic Mixing. *Physical Review E*, 88(2), p. 023024.

Wilkins, R. J., Henry, C. & Gates, L. E., 2003. *How to Scale-Up Mixing Processes in Non-Newtonian Fluids*. [Online] Available at: <http://web.ist.utl.pt/ist11061/leq-II/Documentos/OpUnitarias/How%20to%20Scale-Up%20Mixing%20Processes%20in%20Non-Newtonian%20Fluids.pdf> [Accessed 14 February 2022].

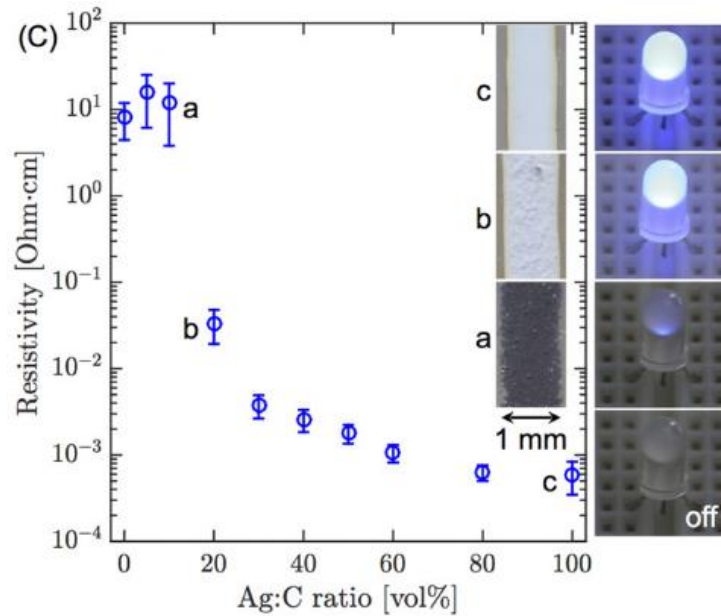
Xie, J. & Jin, Y. C., 2016. Parameter determination for the Cross rheology. *Engineering Applications of Computational Fluid Mechanics*, 10(1), pp. 111-129.

Yang, G. et al., 2021. Direct-ink-writing (DIW) 3D printing functional composite materials based on supra-molecular interaction.. *Composites Science and Technology*, Volume 215, p. 109013.

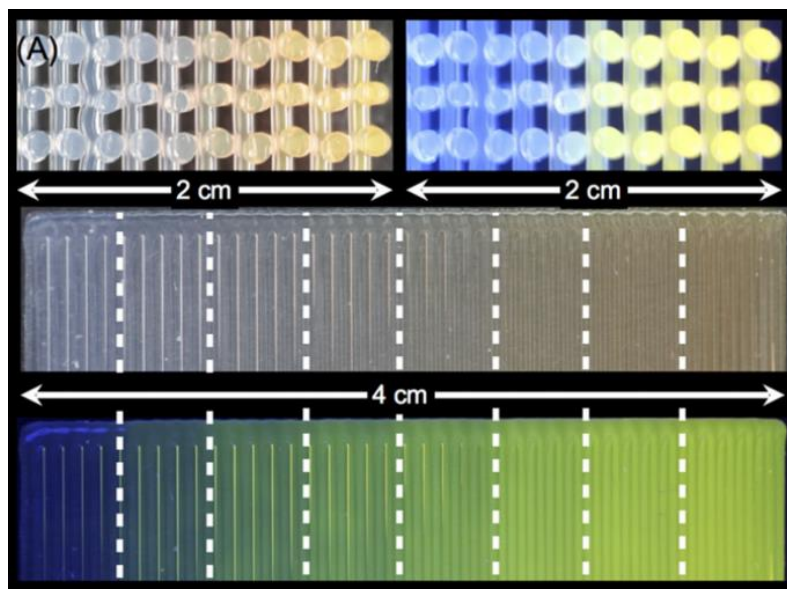
## APPENDICES

## Appendix A: Pictures

## APPENDIX



Appendix A-1: Resistivity of the printed material is controlled by varying the composition of silver and carbon inks.



Appendix A-2: Compositional gradient of the fluorescent pigment along the printed structure. (Ober, et al, 2015)



Appendix A-3: Printed silicone sample at different impeller speeds



## Appendix B: Tables

Table B- 1: Rheology data for the silicone ink.

Meas. Pts.	Shear Rate	Shear Stress	Viscosity	Speed	Torque	Status
	[1/s]	[Pa]	[Pa·s]	[1/min]	[ $\mu$ Nm]	[ ]
1	0.0991	132	1,330	0.0757	406	Dy_auto
2	0.126	428	3,400	0.0962	1,310	Dy_auto
3	0.158	746	4,710	0.121	2,290	Dy_auto
4	0.2	729	3,650	0.152	2,240	Dy_auto
5	0.251	667	2,650	0.192	2,050	Dy_auto
6	0.316	635	2,010	0.242	1,950	Dy_auto
7	0.398	623	1,560	0.304	1,910	Dy_auto
8	0.501	627	1,250	0.383	1,920	Dy_auto
9	0.631	636	1,010	0.482	1,950	Dy_auto
10	0.795	648	815	0.607	1,990	Dy_auto
11	1	661	661	0.764	2,030	Dy_auto
12	1.26	675	536	0.962	2,070	Dy_auto
13	1.59	694	438	1.21	2,130	Dy_auto
14	2	720	360	1.52	2,210	Dy_auto
15	2.51	770	307	1.92	2,360	Dy_auto
16	3.16	833	263	2.42	2,550	Dy_auto
17	3.98	873	219	3.04	2,680	Dy_auto
18	5.01	937	187	3.83	2,880	Dy_auto
19	6.31	1,000	159	4.82	3,080	Dy_auto
20	7.94	1,120	142	6.07	3,450	Dy_auto
21	10	1,240	124	7.64	3,800	Dy_auto
22	12.6	1,400	111	9.62	4,290	Dy_auto
23	15.8	1,560	98.4	12.1	4,780	Dy_auto
24	20	1,750	87.5	15.2	5,350	Dy_auto
25	25.1	1,960	78	19.2	6,010	Dy_auto
26	31.6	2,270	71.6	24.2	6,950	Dy_auto
27	39.8	2,490	62.6	30.4	7,650	Dy_auto
28	50.1	2,740	54.6	38.3	8,400	Dy_auto
29	63.1	2,930	46.4	48.2	8,980	Dy_auto
30	79.5	3,130	39.4	60.7	9,610	Dy_auto
31	100	3,300	33	76.4	10,100	Dy_auto

Table B-2: Results of wall shear stress at different rotational speeds  
(Figure 3.7).

Rotational Speed of impeller			
12 RPM		24 rpm	
Flow time (s)	Wall Shear Stress (Pa)	Flow time (s)	Wall Shear Stress (Pa)
0	0	0	0
0.05	4682.809489	0.05	6911.562337
0.1	1591.800894	0.1	1898.877152
0.15	1285.298908	0.15	1510.566859
0.2	1270.147247	0.2	1494.316647
0.25	1315.015156	0.25	1589.730425
0.3	1380.347133	0.3	1651.689138
0.35	1426.409118	0.35	1692.288148
0.4	1434.720871	0.4	1705.904013
0.45	1441.407975	0.45	1708.913064
0.5	1493.504059	0.5	1705.34299
0.55	1508.468068	0.55	1700.755239
0.6	1470.332303	0.6	1695.427429
0.65	1448.129343	0.65	1691.860013
0.7	1486.946984	0.7	1690.045338
0.75	1492.149949	0.75	1689.785308
0.8	1432.294304	0.8	1690.753093
0.85	1428.627641	0.85	1691.747364
0.9	1471.809022	0.9	1692.868936
0.95	1467.108317	0.95	1693.181379
1	1401.355821	1	1693.88708
1.05	1423.151316	1.05	1693.188215
1.1	1487.584818	1.1	1693.519399
1.15	1437.129243	1.15	1693.073016
1.2	1428.761195	1.2	1692.941246
1.25	1489.897036	1.25	1692.911339
1.3	1428.121275	1.3	1692.66909
1.35	1407.843488	1.35	1693.13942
1.4	1490.001198	1.4	1692.677741
1.45	1514.528227	1.45	1693.33439
1.5	1408.058084	1.5	1693.040697
1.55	1465.168491	1.55	1693.139029
1.6	1469.915855	1.6	1693.147104
1.65	1421.790405	1.65	1693.027525
1.7	1486.371825	1.7	1693.115067
1.75	1516.016879	1.75	1692.885662
1.8	1423.304666	1.8	1693.048122
1.85	1404.73718	1.85	1692.87488
1.9	1490.909949	1.9	1692.999818
1.95	1504.716539	1.95	1693.019054
2	1411.241443	2	1692.89992

2.05	1480.876943	2.05	1693.09527
2.1	1505.775077	2.1	1692.90906
2.15	1412.881602	2.15	1693.15431
2.2	1464.949864	2.2	1692.955202
2.25	1492.903422	2.25	1693.088808
2.3	1415.405927	2.3	1693.148395
2.35	1437.098141	2.35	1692.994329
2.4	1503.456685	2.4	1693.147871
2.45	1427.787761	2.45	1692.944919
2.5	1418.09991	2.5	1692.995996
2.55	1493.479595	2.55	1692.966218
2.6	1493.502293	2.6	1692.978524
2.65	1415.011778	2.65	1693.067607
2.7	1496.965273	2.7	1692.977607
2.75	1501.872993	2.75	1693.040901
2.8	1417.956409	2.8	1693.054063
2.85	1467.844866	2.85	1692.962859
2.9	1502.38348	2.9	1693.118595
2.95	1414.656029	2.95	1693.052011
3	1423.3802	3	1693.117788
3.05	1490.409257	3.05	1692.94529
3.1	1426.180343	3.1	1693.050111
3.15	1417.781433	3.15	1693.130871
3.2	1493.582411	3.2	1692.966236
3.25	1498.949614	3.25	1693.174299
3.3	1415.832644	3.3	1692.955034
3.35	1482.5938	3.35	1693.027612
3.4	1498.120201	3.4	1693.212984
3.45	1415.71071	3.45	1692.914952
3.5	1476.829642	3.5	1693.072332
3.55	1509.707004	3.55	1693.084405
3.6	1409.622433	3.6	1692.865529
3.65	1467.555394	3.65	1693.069124
3.7	1484.094853	3.7	1692.907316
3.75	1421.365801	3.75	1693.025993
3.8	1450.428444	3.8	1693.04777
3.85	1505.898754	3.85	1692.923161
3.9	1426.9574	3.9	1693.06082
3.95	1412.555811	3.95	1693.12466
4	1498.765179	4	1692.996036
4.05	1435.083493	4.05	1693.133063
4.1	1393.57067	4.1	1693.203462
4.15	1503.054526	4.15	1692.951857
4.2	1451.17169	4.2	1693.227363
4.25	1435.051689	4.25	1693.238231
4.3	1484.904574	4.3	1692.954588

4.35	1428.316951	4.35	1693.164743
4.4	1422.572228	4.4	1693.078423
4.45	1493.141659	4.45	1692.880831
4.5	1492.512103	4.5	1693.078951
4.55	1413.837257	4.55	1692.938697
4.6	1500.269505	4.6	1692.837337
4.65	1508.167775	4.65	1693.074977
4.7	1425.596698	4.7	1692.859573
4.75	1479.413053	4.75	1692.899315
4.8	1501.788287	4.8	1693.110432
4.85	1420.065923	4.85	1692.962207
4.9	1412.205524	4.9	1693.113331
4.95	1489.862744	4.95	1693.223739
5	1458.325535	5	1692.989873
5.05	1433.93574	5.05	1693.170594
5.1	1484.726437	5.1	1693.223817
5.15	1480.197464	5.15	1692.948191
5.2	1419.309778	5.2	1693.172784
5.25	1468.979353	5.25	1693.217986
5.3	1504.428146	5.3	1692.973644
5.35	1417.187155	5.35	1692.641946
5.4	1417.173733	5.4	1693.149793
5.45	1489.181556	5.45	1693.108498
5.5	1435.625593	5.5	1692.643784
5.55	1397.352168	5.55	1692.642531
5.6	1493.426435	5.6	1693.189922
5.65	1490.678294	5.65	1693.031443
5.7	1423.352298	5.7	1692.405848
5.75	1485.68664	5.75	1692.547848
5.8	1504.644647	5.8	1693.508828
5.85	1421.563952	5.85	1693.530599
5.9	1465.082114	5.9	1692.645336
5.95	1482.318562	5.95	1692.485703
6	1419.843981	6	1693.61625
6.05	1446.035297	6.05	1693.909724
6.1	1504.3963	6.1	1692.945618
6.15	1430.552767	6.15	1692.284432
6.2	1410.748229	6.2	1693.368323
6.25	1494.51215	6.25	1694.504242
6.3	1500.107247	6.3	1693.44545
6.35	1419.243242	6.35	1691.306203
6.4	1483.453874	6.4	1692.883281
6.45	1491.883159	6.45	1695.082751
6.5	1420.231273	6.5	1694.021579
6.55	1475.779461	6.55	1690.486633
6.6	1500.984812	6.6	1692.020341

6.65	1413.538775	6.65	1695.413576
6.7	1430.947946	6.7	1693.325876
6.75	1486.261772	6.75	1690.013826
6.8	1424.425097	6.8	1690.982177
6.85	1427.402874	6.85	1695.916254
6.9	1491.771178	6.9	1694.628252
6.95	1482.699294	6.95	1690.125172
7	1421.174944	7	1691.174027
7.05	1484.644885	7.05	1696.054033
7.1	1511.175161	7.1	1694.766679
7.15	1421.057288	7.15	1690.177542
7.2	1462.718255	7.2	1690.942615
7.25	1486.464534	7.25	1695.86721
7.3	1418.045503	7.3	1695.090714
7.35	1434.521358	7.35	1690.204379
7.4	1483.761806	7.4	1690.628518
7.45	1428.859397	7.45	1695.923212
7.5	1431.40828	7.5	1695.340309
7.55	1485.312682	7.55	1690.033719
7.6	1478.183861	7.6	1690.547655
7.65	1411.019399	7.65	1695.708166
7.7	1467.966636	7.7	1694.189444
7.75	1503.141727	7.75	1690.053437
7.8	1416.907281	7.8	1689.839205
7.85	1424.728681	7.85	1695.319647
7.9	1490.560588	7.9	1694.305191
7.95	1426.029476	7.95	1690.32396
8	1423.529486	8	1689.039551
8.05	1491.084227	8.05	1694.639932
8.1	1486.838187	8.1	1694.215079
8.15	1422.621815	8.15	1690.522643
8.2	1482.70812	8.2	1691.889118
8.25	1509.178658	8.25	1695.649015
8.3	1420.060187	8.3	1696.10126
8.35	1407.307361	8.35	1690.607817
8.4	1497.846724	8.4	1689.758452
8.45	1430.622661	8.45	1693.415372
8.5	1403.102029	8.5	1696.407646
8.55	1501.058174	8.55	1696.811968
8.6	1441.348218	8.6	1693.299853
8.65	1422.923704	8.65	1689.128544
8.7	1489.229633	8.7	1691.630158
8.75	1420.8301	8.75	1696.378207
8.8	1423.698906	8.8	1695.011946
8.85	1492.929645	8.85	1684.931717
8.9	1433.88253	8.9	1683.046544

8.95	1396.140739	8.95	1695.147699
9	1498.353327	9	1702.706158
9.05	1456.288909	9.05	1700.814982
9.1	1422.51329	9.1	1680.073163
9.15	1479.57843	9.15	1694.566605
9.2	1487.214584	9.2	1708.456201
9.25	1415.53457	9.25	1698.445245
9.3	1431.668401	9.3	1680.352008
9.35	1511.433819	9.35	1697.960372
9.4	1450.843677	9.4	1699.122242
9.45	1411.516709	9.45	1689.383948
9.5	1506.048418	9.5	1683.705333
9.55	1445.576806	9.55	1681.086413
9.6	1421.430484	9.6	1698.041931
9.65	1495.328042	9.65	1704.311608
9.7	1418.325755	9.7	1704.714931
9.75	1414.947214	9.75	1679.220077
9.8	1496.510376	9.8	1688.203865
9.85	1435.178783	9.85	1704.894319
9.9	1418.436796	9.9	1682.860732
9.95	1492.705241	9.95	1692.459202
10	1421.517922	10	1699.490251

Table B- 3: Result of torque at different rotational speeds.

Flow Time (s)	12 rpm		24 rpm	
	Torque (Nm)	Torque (Nmm)	Torque (Nm)	Torque (Nmm)
0	0.0000	0.0000	0.0000	0.0000
0.05	-0.0019	-1.9488	-0.0038	-3.7620
0.1	-0.0014	-1.4193	-0.0021	-2.0810
0.15	-0.0012	-1.1986	-0.0017	-1.7177
0.2	-0.0012	-1.2278	-0.0017	-1.7296
0.25	-0.0013	-1.2760	-0.0018	-1.8156
0.3	-0.0013	-1.3112	-0.0019	-1.8946
0.35	-0.0014	-1.3543	-0.0019	-1.9334
0.4	-0.0014	-1.4001	-0.0019	-1.9482
0.45	-0.0014	-1.4211	-0.0019	-1.9485
0.5	-0.0014	-1.4005	-0.0019	-1.9448
0.55	-0.0014	-1.4004	-0.0019	-1.9386
0.6	-0.0014	-1.4129	-0.0019	-1.9350
0.65	-0.0014	-1.4092	-0.0019	-1.9315
0.7	-0.0014	-1.3748	-0.0019	-1.9307
0.75	-0.0014	-1.3738	-0.0019	-1.9306
0.8	-0.0014	-1.3882	-0.0019	-1.9317
0.85	-0.0014	-1.3856	-0.0019	-1.9326
0.9	-0.0014	-1.3551	-0.0019	-1.9334
0.95	-0.0014	-1.3721	-0.0019	-1.9339
1	-0.0014	-1.3947	-0.0019	-1.9337
1.05	-0.0014	-1.3833	-0.0019	-1.9340
1.1	-0.0013	-1.3477	-0.0019	-1.9336
1.15	-0.0014	-1.3960	-0.0019	-1.9336
1.2	-0.0014	-1.3998	-0.0019	-1.9334
1.25	-0.0014	-1.3640	-0.0019	-1.9333
1.3	-0.0014	-1.4004	-0.0019	-1.9334
1.35	-0.0014	-1.4148	-0.0019	-1.9332
1.4	-0.0014	-1.3573	-0.0019	-1.9335
1.45	-0.0014	-1.3626	-0.0019	-1.9332
1.5	-0.0014	-1.4013	-0.0019	-1.9335
1.55	-0.0014	-1.3641	-0.0019	-1.9334
1.6	-0.0014	-1.3788	-0.0019	-1.9335
1.65	-0.0014	-1.3923	-0.0019	-1.9335
1.7	-0.0014	-1.3644	-0.0019	-1.9335
1.75	-0.0014	-1.3697	-0.0019	-1.9335
1.8	-0.0014	-1.4005	-0.0019	-1.9334
1.85	-0.0014	-1.4045	-0.0019	-1.9335
1.9	-0.0013	-1.3458	-0.0019	-1.9334
1.95	-0.0014	-1.3653	-0.0019	-1.9334
2	-0.0014	-1.3994	-0.0019	-1.9335
2.05	-0.0014	-1.3557	-0.0019	-1.9334
2.1	-0.0014	-1.3670	-0.0019	-1.9335

2.15	-0.0014	-1.4048	-0.0019	-1.9334
2.2	-0.0014	-1.3741	-0.0019	-1.9335
2.25	-0.0014	-1.3592	-0.0019	-1.9334
2.3	-0.0014	-1.3990	-0.0019	-1.9334
2.35	-0.0014	-1.3870	-0.0019	-1.9335
2.4	-0.0014	-1.3544	-0.0019	-1.9334
2.45	-0.0014	-1.3972	-0.0019	-1.9335
2.5	-0.0014	-1.3992	-0.0019	-1.9335
2.55	-0.0013	-1.3419	-0.0019	-1.9335
2.6	-0.0014	-1.3677	-0.0019	-1.9335
2.65	-0.0014	-1.3991	-0.0019	-1.9334
2.7	-0.0014	-1.3649	-0.0019	-1.9335
2.75	-0.0014	-1.3833	-0.0019	-1.9334
2.8	-0.0014	-1.3986	-0.0019	-1.9334
2.85	-0.0014	-1.3646	-0.0019	-1.9335
2.9	-0.0014	-1.3574	-0.0019	-1.9334
2.95	-0.0014	-1.4032	-0.0019	-1.9334
3	-0.0014	-1.3944	-0.0019	-1.9333
3.05	-0.0013	-1.3493	-0.0019	-1.9335
3.1	-0.0014	-1.3931	-0.0019	-1.9334
3.15	-0.0014	-1.4013	-0.0019	-1.9334
3.2	-0.0013	-1.3483	-0.0019	-1.9335
3.25	-0.0014	-1.3696	-0.0019	-1.9334
3.3	-0.0014	-1.4010	-0.0019	-1.9335
3.35	-0.0014	-1.3532	-0.0019	-1.9335
3.4	-0.0014	-1.3731	-0.0019	-1.9334
3.45	-0.0014	-1.4003	-0.0019	-1.9335
3.5	-0.0014	-1.3599	-0.0019	-1.9334
3.55	-0.0014	-1.3601	-0.0019	-1.9334
3.6	-0.0014	-1.4024	-0.0019	-1.9335
3.65	-0.0014	-1.3734	-0.0019	-1.9333
3.7	-0.0014	-1.3659	-0.0019	-1.9335
3.75	-0.0014	-1.3952	-0.0019	-1.9334
3.8	-0.0014	-1.3770	-0.0019	-1.9334
3.85	-0.0014	-1.3522	-0.0019	-1.9335
3.9	-0.0014	-1.3982	-0.0019	-1.9334
3.95	-0.0014	-1.4010	-0.0019	-1.9334
4	-0.0014	-1.3609	-0.0019	-1.9335
4.05	-0.0014	-1.3994	-0.0019	-1.9334
4.1	-0.0014	-1.4042	-0.0019	-1.9334
4.15	-0.0014	-1.3542	-0.0019	-1.9335
4.2	-0.0014	-1.3998	-0.0019	-1.9333
4.25	-0.0014	-1.3887	-0.0019	-1.9334
4.3	-0.0014	-1.3600	-0.0019	-1.9335
4.35	-0.0014	-1.4012	-0.0019	-1.9333
4.4	-0.0014	-1.4031	-0.0019	-1.9334



4.45	-0.0013	-1.3402	-0.0019	-1.9335
4.5	-0.0014	-1.3657	-0.0019	-1.9333
4.55	-0.0014	-1.4001	-0.0019	-1.9334
4.6	-0.0014	-1.3625	-0.0019	-1.9335
4.65	-0.0014	-1.3805	-0.0019	-1.9333
4.7	-0.0014	-1.3998	-0.0019	-1.9335
4.75	-0.0013	-1.3491	-0.0019	-1.9334
4.8	-0.0014	-1.3628	-0.0019	-1.9334
4.85	-0.0014	-1.3991	-0.0019	-1.9335
4.9	-0.0014	-1.3993	-0.0019	-1.9334
4.95	-0.0013	-1.3445	-0.0019	-1.9334
5	-0.0014	-1.3900	-0.0019	-1.9335
5.05	-0.0014	-1.3894	-0.0019	-1.9334
5.1	-0.0013	-1.3476	-0.0019	-1.9334
5.15	-0.0014	-1.3769	-0.0019	-1.9335
5.2	-0.0014	-1.4011	-0.0019	-1.9333
5.25	-0.0014	-1.3697	-0.0019	-1.9333
5.3	-0.0014	-1.3595	-0.0019	-1.9334
5.35	-0.0014	-1.4034	-0.0019	-1.9336
5.4	-0.0014	-1.3993	-0.0019	-1.9332
5.45	-0.0013	-1.3445	-0.0019	-1.9333
5.5	-0.0014	-1.3898	-0.0019	-1.9335
5.55	-0.0014	-1.4016	-0.0019	-1.9335
5.6	-0.0013	-1.3415	-0.0019	-1.9332
5.65	-0.0014	-1.3852	-0.0019	-1.9335
5.7	-0.0014	-1.3958	-0.0019	-1.9339
5.75	-0.0013	-1.3494	-0.0019	-1.9337
5.8	-0.0014	-1.3686	-0.0019	-1.9330
5.85	-0.0014	-1.4066	-0.0019	-1.9332
5.9	-0.0014	-1.3704	-0.0019	-1.9338
5.95	-0.0014	-1.3612	-0.0019	-1.9337
6	-0.0014	-1.3943	-0.0019	-1.9330
6.05	-0.0014	-1.3797	-0.0019	-1.9330
6.1	-0.0014	-1.3531	-0.0019	-1.9337
6.15	-0.0014	-1.3984	-0.0019	-1.9339
6.2	-0.0014	-1.4012	-0.0019	-1.9331
6.25	-0.0013	-1.3414	-0.0019	-1.9326
6.3	-0.0014	-1.3677	-0.0019	-1.9334
6.35	-0.0014	-1.4001	-0.0019	-1.9346
6.4	-0.0014	-1.3545	-0.0019	-1.9331
6.45	-0.0014	-1.3784	-0.0019	-1.9318
6.5	-0.0014	-1.4003	-0.0019	-1.9329
6.55	-0.0014	-1.3611	-0.0019	-1.9351
6.6	-0.0014	-1.3643	-0.0019	-1.9334
6.65	-0.0014	-1.3999	-0.0019	-1.9315
6.7	-0.0014	-1.3852	-0.0019	-1.9334

6.75	-0.0014	-1.3537	-0.0019	-1.9354
6.8	-0.0014	-1.3920	-0.0019	-1.9341
6.85	-0.0014	-1.4003	-0.0019	-1.9311
6.9	-0.0014	-1.3526	-0.0019	-1.9324
6.95	-0.0014	-1.3750	-0.0019	-1.9355
7	-0.0014	-1.3975	-0.0019	-1.9337
7.05	-0.0013	-1.3485	-0.0019	-1.9308
7.1	-0.0014	-1.3647	-0.0019	-1.9323
7.15	-0.0014	-1.4080	-0.0019	-1.9354
7.2	-0.0014	-1.3735	-0.0019	-1.9338
7.25	-0.0014	-1.3583	-0.0019	-1.9309
7.3	-0.0014	-1.3970	-0.0019	-1.9322
7.35	-0.0014	-1.3896	-0.0019	-1.9355
7.4	-0.0014	-1.3618	-0.0019	-1.9339
7.45	-0.0014	-1.3928	-0.0019	-1.9309
7.5	-0.0014	-1.3972	-0.0019	-1.9320
7.55	-0.0014	-1.3563	-0.0019	-1.9356
7.6	-0.0014	-1.3753	-0.0019	-1.9339
7.65	-0.0014	-1.3931	-0.0019	-1.9309
7.7	-0.0014	-1.3659	-0.0019	-1.9327
7.75	-0.0014	-1.3616	-0.0019	-1.9354
7.8	-0.0014	-1.4051	-0.0019	-1.9347
7.85	-0.0014	-1.3965	-0.0019	-1.9313
7.9	-0.0014	-1.3512	-0.0019	-1.9322
7.95	-0.0014	-1.3933	-0.0019	-1.9352
8	-0.0014	-1.4002	-0.0019	-1.9353
8.05	-0.0014	-1.3517	-0.0019	-1.9315
8.1	-0.0014	-1.3738	-0.0019	-1.9327
8.15	-0.0014	-1.3962	-0.0019	-1.9350
8.2	-0.0014	-1.3505	-0.0019	-1.9331
8.25	-0.0014	-1.3649	-0.0019	-1.9311
8.3	-0.0014	-1.4020	-0.0019	-1.9317
8.35	-0.0014	-1.4041	-0.0019	-1.9351
8.4	-0.0014	-1.3602	-0.0019	-1.9342
8.45	-0.0014	-1.3989	-0.0019	-1.9321
8.5	-0.0014	-1.4013	-0.0019	-1.9314
8.55	-0.0014	-1.3557	-0.0019	-1.9311
8.6	-0.0014	-1.3999	-0.0019	-1.9328
8.65	-0.0014	-1.3937	-0.0019	-1.9341
8.7	-0.0014	-1.3555	-0.0019	-1.9336
8.75	-0.0014	-1.4105	-0.0019	-1.9301
8.8	-0.0014	-1.4073	-0.0019	-1.9314
8.85	-0.0013	-1.3496	-0.0019	-1.9378
8.9	-0.0014	-1.3901	-0.0019	-1.9372
8.95	-0.0014	-1.4000	-0.0019	-1.9295
9	-0.0014	-1.3589	-0.0019	-1.9273

9.05	-0.0014	-1.3991	-0.0019	-1.9277
9.1	-0.0014	-1.3922	-0.0019	-1.9365
9.15	-0.0013	-1.3481	-0.0019	-1.9242
9.2	-0.0014	-1.3698	-0.0019	-1.9201
9.25	-0.0014	-1.3963	-0.0019	-1.9314
9.3	-0.0014	-1.3823	-0.0019	-1.9364
9.35	-0.0013	-1.3388	-0.0019	-1.9246
9.4	-0.0014	-1.3973	-0.0019	-1.9302
9.45	-0.0014	-1.3977	-0.0019	-1.9363
9.5	-0.0014	-1.3541	-0.0019	-1.9379
9.55	-0.0014	-1.4045	-0.0019	-1.9400
9.6	-0.0014	-1.3979	-0.0019	-1.9277
9.65	-0.0014	-1.3513	-0.0019	-1.9266
9.7	-0.0014	-1.4115	-0.0019	-1.9273
9.75	-0.0014	-1.4112	-0.0019	-1.9366
9.8	-0.0013	-1.3413	-0.0019	-1.9309
9.85	-0.0014	-1.3888	-0.0019	-1.9235
9.9	-0.0014	-1.3938	-0.0019	-1.9333
9.95	-0.0014	-1.3565	-0.0019	-1.9271
10	-0.0014	-1.4109	-0.0019	-1.9294

Table B- 4: Results of average pressure at different rotational speeds.

Rotational Speed of impeller					
0 rpm		12 rpm		24 rpm	
Flow Time,s	Pressure, Pa	Flow Time,s	Pressure, Pa	Flow Time,s	Pressure, Pa
0	-	0	-	0	-
0.1	45,919.14	0.05	65,492.77	0.05	81,929.94
0.15	652.50	0.1	34,301.64	0.1	30,961.17
0.2	28,809.22	0.15	27,319.42	0.15	24,362.40
0.25	37,118.13	0.2	27,398.98	0.2	23,578.67
0.3	37,499.09	0.25	29,937.07	0.25	26,907.56
0.35	37,694.95	0.3	30,905.11	0.3	26,589.38
0.4	36,505.87	0.35	28,860.22	0.35	28,622.57
0.45	34,924.09	0.4	28,141.47	0.4	27,872.66
0.5	34,508.46	0.45	32,337.09	0.45	28,755.14
0.55	35,530.70	0.5	33,196.00	0.5	28,098.95
0.6	35,968.35	0.55	29,470.92	0.55	28,310.71
0.65	34,810.57	0.6	28,993.10	0.6	27,809.32
0.7	32,065.39	0.65	33,450.63	0.65	27,969.38
0.75	29,415.06	0.7	33,349.43	0.7	27,650.90
0.8	29,347.37	0.75	28,242.29	0.75	27,972.45
0.85	35,842.37	0.8	29,471.97	0.8	27,764.03
0.9	39,958.15	0.85	35,396.22	0.85	27,932.60
0.95	33,817.73	0.9	32,106.92	0.9	27,798.15
1	26,142.65	0.95	25,199.09	0.95	27,856.17
1.05	32,727.42	1	29,170.79	1	27,767.31
1.1	47,899.62	1.05	38,872.68	1.05	27,787.02
1.15	35,460.54	1.1	31,419.24	1.1	27,823.51
1.2	22,549.88	1.15	23,497.44	1.15	27,753.35
1.25	47,629.98	1.2	37,225.81	1.2	27,848.19
1.3	39,378.47	1.25	28,960.73	1.25	27,827.26
1.35	19,724.62	1.3	26,649.78	1.3	27,940.92
1.4	47,385.72	1.35	34,809.08	1.35	27,903.04
1.45	44,222.42	1.4	35,356.91	1.4	27,967.00
1.5	20,141.95	1.45	25,181.20	1.45	27,978.31
1.55	48,287.08	1.5	30,895.84	1.5	27,878.96
1.6	39,395.24	1.55	39,793.33	1.55	27,988.07
1.65	18,848.58	1.6	26,418.83	1.6	27,846.85
1.7	43,201.55	1.65	33,449.03	1.65	27,898.79
1.75	48,059.78	1.7	35,915.19	1.7	27,751.23
1.8	18,846.15	1.75	27,749.52	1.75	27,812.28
1.85	40,334.95	1.8	27,442.51	1.8	27,774.20
1.9	49,179.05	1.85	36,511.82	1.85	27,772.81
1.95	21,664.42	1.9	34,708.77	1.9	27,802.17
2	35,753.69	1.95	23,760.62	1.95	27,788.16

2.05	50,997.71	2	31,754.02	2	27,842.58
2.1	26,237.54	2.05	37,400.87	2.05	27,855.33
2.15	33,372.14	2.1	26,131.41	2.1	27,919.28
2.2	51,774.54	2.15	30,818.75	2.15	27,931.80
2.25	28,840.86	2.2	39,361.75	2.2	27,947.09
2.3	30,897.87	2.25	27,611.12	2.25	27,964.31
2.35	54,862.46	2.3	31,256.80	2.3	27,920.07
2.4	28,507.35	2.35	38,358.80	2.35	27,924.94
2.45	33,922.97	2.4	30,571.67	2.4	27,887.94
2.5	50,070.70	2.45	25,873.49	2.45	27,852.57
2.55	29,324.72	2.5	36,983.39	2.5	27,822.92
2.6	31,035.43	2.55	33,598.55	2.55	27,785.85
2.65	52,809.96	2.6	22,380.99	2.6	27,788.24
2.7	28,495.24	2.65	33,250.73	2.65	27,778.39
2.75	30,872.76	2.7	32,493.59	2.7	27,790.20
2.8	48,614.71	2.75	23,955.75	2.75	27,810.07
2.85	39,301.16	2.8	30,635.23	2.8	27,817.27
2.9	21,146.13	2.85	37,360.34	2.85	27,870.49
2.95	45,385.53	2.9	27,708.24	2.9	27,888.39
3	44,209.85	2.95	30,075.20	2.95	27,952.25
3.05	20,613.59	3	38,938.63	3	27,930.28
3.1	36,536.71	3.05	30,870.88	3.05	27,929.82
3.15	49,584.01	3.1	26,154.83	3.1	27,945.68
3.2	25,503.07	3.15	36,435.92	3.15	27,894.81
3.25	34,892.12	3.2	33,896.92	3.2	27,898.76
3.3	48,839.21	3.25	23,318.48	3.25	27,855.46
3.35	28,624.42	3.3	32,391.99	3.3	27,815.23
3.4	33,366.60	3.35	36,821.68	3.35	27,803.91
3.45	52,377.21	3.4	25,171.21	3.4	27,745.85
3.5	34,409.07	3.45	32,388.43	3.45	27,775.23
3.55	21,416.91	3.5	38,432.01	3.5	27,802.46
3.6	51,388.71	3.55	26,796.43	3.55	27,766.60
3.65	40,475.41	3.6	30,620.43	3.6	27,820.99
3.7	16,852.92	3.65	38,169.38	3.65	27,842.86
3.75	50,013.28	3.7	27,204.24	3.7	27,877.71
3.8	36,020.33	3.75	32,058.24	3.75	27,937.63
3.85	17,948.68	3.8	38,918.19	3.8	27,954.56
3.9	53,275.51	3.85	30,775.61	3.85	27,974.48
3.95	32,698.19	3.9	25,438.81	3.9	27,971.78
4	43,047.07	3.95	36,986.58	3.95	27,927.33
4.05	48,258.44	4	30,328.20	4	27,922.60
4.1	30,447.80	4.05	22,930.10	4.05	27,903.77
4.15	32,146.07	4.1	35,685.68	4.1	27,826.80
4.2	50,237.25	4.15	30,991.06	4.15	27,828.47
4.25	28,817.15	4.2	21,806.25	4.2	27,788.23
4.3	28,058.31	4.25	36,084.58	4.25	27,730.27

4.35	49,705.58	4.3	28,940.26	4.3	27,773.56
4.4	38,907.25	4.35	24,838.21	4.35	27,776.59
4.45	19,331.64	4.4	36,818.64	4.4	27,739.80
4.5	48,483.21	4.45	33,443.44	4.45	27,800.25
4.55	41,277.77	4.5	22,129.92	4.5	27,818.20
4.6	17,281.76	4.55	33,212.37	4.55	27,841.71
4.65	50,033.47	4.6	32,822.00	4.6	27,910.08
4.7	36,409.62	4.65	23,369.45	4.65	27,936.74
4.75	18,741.73	4.7	33,016.98	4.7	27,974.01
4.8	47,037.00	4.75	34,680.18	4.75	28,011.76
4.85	43,923.62	4.8	26,849.53	4.8	27,939.37
4.9	20,647.55	4.85	27,857.03	4.85	27,921.16
4.95	47,475.87	4.9	37,480.32	4.9	27,910.23
5	41,642.46	4.95	33,534.80	4.95	27,853.11
5.05	19,802.66	5	23,855.30	5	27,842.25
5.1	46,496.02	5.05	34,969.56	5.05	27,807.59
5.15	46,450.23	5.1	32,225.22	5.1	27,734.39
5.2	19,592.01	5.15	24,377.95	5.15	27,759.90
5.25	40,691.29	5.2	30,798.20	5.2	27,767.25
5.3	47,432.51	5.25	37,395.41	5.25	27,718.30
5.35	20,421.64	5.3	28,237.02	5.3	27,696.25
5.4	37,944.94	5.35	29,342.20	5.35	27,784.94
5.45	46,563.96	5.4	39,067.77	5.4	27,810.24
5.5	30,561.50	5.45	31,806.34	5.45	27,795.12
5.55	35,478.39	5.5	23,774.70	5.5	27,852.07
5.6	49,831.41	5.55	35,221.38	5.55	27,982.88
5.65	28,760.81	5.6	36,335.94	5.6	27,944.42
5.7	24,188.82	5.65	23,273.70	5.65	27,908.74
5.75	52,396.61	5.7	34,165.43	5.7	28,023.85
5.8	32,219.34	5.75	34,707.03	5.75	28,211.78
5.85	29,902.89	5.8	25,674.31	5.8	28,082.49
5.9	53,022.10	5.85	30,772.46	5.85	27,811.34
5.95	29,978.31	5.9	38,523.58	5.9	27,856.69
6	33,170.47	5.95	27,519.40	5.95	28,061.32
6.05	51,975.28	6	31,884.17	6	27,984.97
6.1	36,490.33	6.05	38,736.44	6.05	27,675.46
6.15	20,758.12	6.1	31,180.91	6.1	27,598.73
6.2	49,267.95	6.15	25,500.55	6.15	27,794.28
6.25	40,832.66	6.2	36,794.36	6.2	27,920.89
6.3	18,374.71	6.25	34,101.07	6.25	27,652.73
6.35	48,247.13	6.3	22,714.32	6.3	27,323.09
6.4	47,346.79	6.35	32,050.21	6.35	27,771.06
6.45	19,302.07	6.4	36,387.99	6.4	28,163.95
6.5	43,796.48	6.45	25,317.34	6.45	27,825.92
6.55	43,231.18	6.5	32,314.10	6.5	27,258.81
6.6	22,661.59	6.55	37,700.96	6.55	27,704.88

6.65	35,609.27	6.6	26,959.39	6.6	28,343.83
6.7	49,497.71	6.65	30,714.16	6.65	27,823.06
6.75	26,874.90	6.7	39,052.51	6.7	27,284.11
6.8	32,517.24	6.75	30,170.59	6.75	27,650.21
6.85	50,910.35	6.8	26,709.19	6.8	28,568.71
6.9	27,233.52	6.85	36,661.97	6.85	28,113.91
6.95	28,881.26	6.9	32,614.05	6.9	27,183.26
7	51,381.03	6.95	22,814.41	6.95	27,672.19
7.05	36,144.22	7	33,388.23	7	28,680.49
7.1	22,140.09	7.05	35,124.21	7.05	28,149.77
7.15	44,805.71	7.1	26,168.04	7.1	27,082.73
7.2	40,403.50	7.15	30,664.74	7.15	27,605.44
7.25	19,736.28	7.2	38,714.92	7.2	28,615.45
7.3	37,581.17	7.25	28,115.68	7.25	28,141.10
7.35	49,696.27	7.3	30,770.80	7.3	27,056.10
7.4	24,669.54	7.35	37,924.90	7.35	27,491.10
7.45	34,546.31	7.4	30,329.34	7.4	28,531.26
7.5	50,444.68	7.45	27,365.96	7.45	28,144.81
7.55	27,095.00	7.5	35,919.75	7.5	27,027.96
7.6	32,357.62	7.55	32,331.46	7.55	27,477.49
7.65	51,703.60	7.6	24,108.96	7.6	28,485.52
7.7	27,518.19	7.65	30,722.93	7.65	27,923.25
7.75	27,896.45	7.7	37,444.58	7.7	27,109.44
7.8	49,734.15	7.75	27,808.18	7.75	27,278.16
7.85	38,155.60	7.8	30,100.76	7.8	28,419.76
7.9	20,532.11	7.85	38,895.71	7.85	28,027.33
7.95	48,119.65	7.9	30,697.90	7.9	27,118.87
8	42,406.26	7.95	26,760.55	7.95	27,113.35
8.05	20,866.51	8	36,386.23	8	28,311.35
8.1	39,940.41	8.05	33,076.85	8.05	28,294.11
8.15	49,096.99	8.1	23,214.36	8.1	27,167.19
8.2	21,126.67	8.15	33,101.79	8.15	27,740.77
8.25	38,079.06	8.2	35,230.08	8.2	28,573.02
8.3	50,623.11	8.25	26,701.70	8.25	28,352.62
8.35	24,316.58	8.3	27,314.65	8.3	27,163.34
8.4	35,291.56	8.35	37,633.11	8.35	27,564.21
8.45	48,825.92	8.4	30,724.15	8.4	28,336.77
8.5	27,601.61	8.45	24,095.38	8.45	28,857.88
8.55	32,396.61	8.5	36,857.12	8.5	28,414.37
8.6	51,777.26	8.55	30,781.88	8.55	26,840.31
8.65	27,513.05	8.6	22,078.31	8.6	26,586.34
8.7	26,992.03	8.65	37,486.12	8.65	28,480.12
8.75	50,019.17	8.7	28,373.68	8.7	29,183.48
8.8	30,422.16	8.75	29,289.58	8.75	27,328.35
8.85	23,486.96	8.8	38,885.68	8.8	25,875.80
8.9	52,104.81	8.85	31,499.02	8.85	26,870.63

8.95	33,251.94	8.9	23,755.38	8.9	29,110.71
9	28,044.03	8.95	35,548.62	8.95	30,210.64
9.05	54,227.56	9	31,936.23	9	29,009.12
9.1	31,325.08	9.05	24,486.52	9.05	25,300.82
9.15	31,821.69	9.1	34,767.82	9.1	28,708.74
9.2	52,957.24	9.15	33,267.36	9.15	30,965.96
9.25	29,210.50	9.2	24,697.20	9.2	28,346.58
9.3	27,391.24	9.25	29,511.39	9.25	24,568.87
9.35	51,037.04	9.3	38,822.53	9.3	28,804.90
9.4	30,577.51	9.35	33,140.02	9.35	27,829.50
9.45	37,577.53	9.4	22,285.12	9.4	26,105.70
9.5	50,672.53	9.45	37,063.24	9.45	25,537.97
9.55	34,453.57	9.5	31,029.11	9.5	27,107.38
9.6	20,878.59	9.55	21,799.62	9.55	29,771.06
9.65	52,870.84	9.6	38,059.84	9.6	29,747.36
9.7	37,230.13	9.65	28,725.95	9.65	27,557.79
9.75	25,661.90	9.7	28,622.84	9.7	24,531.15
9.8	50,777.82	9.75	39,451.17	9.75	27,317.26
9.85	31,603.52	9.8	32,003.16	9.8	31,280.20
9.9	29,621.66	9.85	23,013.43	9.85	26,370.43
9.95	54,138.20	9.9	37,683.74	9.9	28,256.46
10	39,324.78	9.95	28,774.67	9.95	29,768.15
10.05	24,166.12	10	28,812.21	10	29,567.51



Table B- 5: Results of red and blue ink volume fraction at different impeller rotational speeds.

Flow Time, s	Red ink Volume Fraction		Blue Ink Volume Fraction	
	12 rpm	24 rpm	12 rpm	24 rpm
0	0.50239	0.50239	0.49761	0.49761
0.05	0.85580	0.84782	0.15218	0.14420
0.1	0.81573	0.76451	0.23549	0.18427
0.15	0.81243	0.72014	0.27986	0.18757
0.2	0.77297	0.68137	0.31863	0.22703
0.25	0.73031	0.64675	0.35325	0.26969
0.3	0.69642	0.61797	0.38203	0.30358
0.35	0.66429	0.59341	0.40659	0.33571
0.4	0.63605	0.57217	0.42783	0.36395
0.45	0.61280	0.55439	0.44561	0.38720
0.5	0.59367	0.54049	0.45951	0.40633
0.55	0.57793	0.53028	0.46972	0.42207
0.6	0.56512	0.52305	0.47695	0.43488
0.65	0.55481	0.51785	0.48215	0.44519
0.7	0.54662	0.51421	0.48579	0.45338
0.75	0.54006	0.51147	0.48853	0.45994
0.8	0.53481	0.50968	0.49032	0.46519
0.85	0.53058	0.50825	0.49175	0.46942
0.9	0.52717	0.50730	0.49270	0.47283
0.95	0.52440	0.50673	0.49327	0.47560
1	0.52210	0.50652	0.49348	0.47790
1.05	0.52023	0.50629	0.49371	0.47977
1.1	0.51864	0.50610	0.49390	0.48136
1.15	0.51733	0.50600	0.49400	0.48267
1.2	0.51618	0.50584	0.49416	0.48382
1.25	0.51518	0.50571	0.49429	0.48482
1.3	0.51427	0.50569	0.49431	0.48573
1.35	0.51343	0.50569	0.49431	0.48657
1.4	0.51264	0.50574	0.49426	0.48736
1.45	0.51188	0.50586	0.49414	0.48812
1.5	0.51115	0.50606	0.49394	0.48885
1.55	0.51042	0.50617	0.49383	0.48958
1.6	0.50969	0.50626	0.49374	0.49031
1.65	0.50895	0.50622	0.49378	0.49105
1.7	0.50821	0.50602	0.49398	0.49179
1.75	0.50748	0.50574	0.49426	0.49252
1.8	0.50673	0.50536	0.49464	0.49327
1.85	0.50599	0.50488	0.49512	0.49401
1.9	0.50526	0.50421	0.49579	0.49474
1.95	0.50454	0.50354	0.49646	0.49546
2	0.50383	0.50273	0.49727	0.49617
2.05	0.50312	0.50179	0.49821	0.49688

2.1	0.50244	0.50085	0.49915	0.49756
2.15	0.50179	0.49998	0.50002	0.49821
2.2	0.50118	0.49915	0.50085	0.49882
2.25	0.50062	0.49846	0.50154	0.49938
2.3	0.50012	0.49792	0.50208	0.49988
2.35	0.49969	0.49749	0.50251	0.50031
2.4	0.49931	0.49718	0.50282	0.50069
2.45	0.49899	0.49701	0.50299	0.50101
2.5	0.49872	0.49693	0.50307	0.50128
2.55	0.49851	0.49695	0.50305	0.50149
2.6	0.49833	0.49703	0.50297	0.50167
2.65	0.49817	0.49714	0.50286	0.50183
2.7	0.49803	0.49727	0.50273	0.50197
2.75	0.49789	0.49739	0.50261	0.50211
2.8	0.49775	0.49747	0.50253	0.50225
2.85	0.49760	0.49754	0.50246	0.50240
2.9	0.49743	0.49759	0.50241	0.50257
2.95	0.49725	0.49758	0.50242	0.50275
3	0.49706	0.49754	0.50246	0.50294
3.05	0.49688	0.49745	0.50255	0.50312
3.1	0.49670	0.49731	0.50269	0.50330
3.15	0.49651	0.49715	0.50285	0.50349
3.2	0.49633	0.49700	0.50300	0.50367
3.25	0.49615	0.49689	0.50311	0.50385
3.3	0.49598	0.49673	0.50327	0.50402
3.35	0.49581	0.49660	0.50340	0.50419
3.4	0.49568	0.49649	0.50351	0.50432
3.45	0.49553	0.49636	0.50364	0.50447
3.5	0.49541	0.49628	0.50372	0.50459
3.55	0.49528	0.49622	0.50378	0.50472
3.6	0.49518	0.49615	0.50385	0.50482
3.65	0.49508	0.49609	0.50391	0.50492
3.7	0.49499	0.49604	0.50396	0.50501
3.75	0.49491	0.49596	0.50404	0.50509
3.8	0.49483	0.49594	0.50406	0.50517
3.85	0.49477	0.49595	0.50405	0.50523
3.9	0.49472	0.49595	0.50405	0.50528
3.95	0.49468	0.49596	0.50404	0.50532
4	0.49464	0.49601	0.50399	0.50536
4.05	0.49461	0.49605	0.50395	0.50539
4.1	0.49458	0.49604	0.50396	0.50542
4.15	0.49455	0.49607	0.50393	0.50545
4.2	0.49453	0.49607	0.50393	0.50547
4.25	0.49452	0.49603	0.50397	0.50548
4.3	0.49453	0.49603	0.50397	0.50547
4.35	0.49456	0.49603	0.50397	0.50544

4.4	0.49459	0.49603	0.50397	0.50541
4.45	0.49463	0.49610	0.50390	0.50537
4.5	0.49468	0.49618	0.50382	0.50532
4.55	0.49473	0.49616	0.50384	0.50527
4.6	0.49477	0.49620	0.50380	0.50523
4.65	0.49481	0.49627	0.50373	0.50519
4.7	0.49483	0.49623	0.50377	0.50517
4.75	0.49484	0.49625	0.50375	0.50516
4.8	0.49485	0.49628	0.50372	0.50515
4.85	0.49484	0.49624	0.50376	0.50516
4.9	0.49482	0.49623	0.50377	0.50518
4.95	0.49478	0.49623	0.50377	0.50522
5	0.49474	0.49624	0.50376	0.50526
5.05	0.49469	0.49621	0.50379	0.50531
5.1	0.49465	0.49621	0.50379	0.50535
5.15	0.49462	0.49621	0.50379	0.50538
5.2	0.49461	0.49615	0.50385	0.50539
5.25	0.49461	0.49610	0.50390	0.50539
5.3	0.49462	0.49606	0.50394	0.50538
5.35	0.49465	0.49594	0.50406	0.50535
5.4	0.49469	0.49586	0.50414	0.50531
5.45	0.49473	0.49580	0.50420	0.50527
5.5	0.49480	0.49572	0.50428	0.50520
5.55	0.49486	0.49563	0.50437	0.50514
5.6	0.49493	0.49563	0.50437	0.50507
5.65	0.49499	0.49563	0.50437	0.50501
5.7	0.49506	0.49563	0.50437	0.50494
5.75	0.49513	0.49571	0.50429	0.50487
5.8	0.49520	0.49580	0.50420	0.50480
5.85	0.49527	0.49582	0.50418	0.50473
5.9	0.49535	0.49588	0.50412	0.50465
5.95	0.49542	0.49592	0.50408	0.50458
6	0.49551	0.49592	0.50408	0.50449
6.05	0.49559	0.49593	0.50407	0.50441
6.1	0.49568	0.49591	0.50409	0.50432
6.15	0.49578	0.49583	0.50417	0.50422
6.2	0.49590	0.49573	0.50427	0.50410
6.25	0.49603	0.49568	0.50432	0.50397
6.3	0.49618	0.49566	0.50434	0.50382
6.35	0.49635	0.49558	0.50442	0.50365
6.4	0.49652	0.49556	0.50444	0.50348
6.45	0.49671	0.49555	0.50445	0.50329
6.5	0.49690	0.49553	0.50447	0.50310
6.55	0.49708	0.49553	0.50447	0.50292
6.6	0.49726	0.49554	0.50446	0.50274
6.65	0.49742	0.49552	0.50448	0.50258

6.7	0.49758	0.49551	0.50449	0.50242
6.75	0.49772	0.49552	0.50448	0.50228
6.8	0.49784	0.49553	0.50447	0.50216
6.85	0.49796	0.49552	0.50448	0.50204
6.9	0.49806	0.49555	0.50445	0.50194
6.95	0.49815	0.49557	0.50443	0.50185
7	0.49824	0.49556	0.50444	0.50176
7.05	0.49832	0.49560	0.50440	0.50168
7.1	0.49842	0.49566	0.50434	0.50158
7.15	0.49851	0.49568	0.50432	0.50149
7.2	0.49861	0.49572	0.50428	0.50139
7.25	0.49872	0.49577	0.50423	0.50128
7.3	0.49885	0.49578	0.50422	0.50115
7.35	0.49899	0.49579	0.50421	0.50101
7.4	0.49913	0.49581	0.50419	0.50087
7.45	0.49927	0.49582	0.50418	0.50073
7.5	0.49941	0.49583	0.50417	0.50059
7.55	0.49956	0.49589	0.50411	0.50044
7.6	0.49968	0.49595	0.50405	0.50032
7.65	0.49980	0.49599	0.50401	0.50020
7.7	0.49990	0.49604	0.50396	0.50010
7.75	0.50000	0.49611	0.50389	0.50000
7.8	0.50008	0.49614	0.50386	0.49992
7.85	0.50016	0.49616	0.50384	0.49984
7.9	0.50023	0.49620	0.50380	0.49977
7.95	0.50029	0.49623	0.50377	0.49971
8	0.50036	0.49624	0.50376	0.49964
8.05	0.50043	0.49627	0.50373	0.49957
8.1	0.50050	0.49629	0.50371	0.49950
8.15	0.50058	0.49632	0.50368	0.49942
8.2	0.50066	0.49637	0.50363	0.49934
8.25	0.50075	0.49643	0.50357	0.49925
8.3	0.50085	0.49650	0.50350	0.49915
8.35	0.50095	0.49656	0.50344	0.49905
8.4	0.50103	0.49667	0.50333	0.49897
8.45	0.50113	0.49675	0.50325	0.49887
8.5	0.50121	0.49682	0.50318	0.49879
8.55	0.50133	0.49691	0.50309	0.49867
8.6	0.50141	0.49698	0.50302	0.49859
8.65	0.50152	0.49705	0.50295	0.49848
8.7	0.50159	0.49717	0.50283	0.49841
8.75	0.50169	0.49726	0.50274	0.49831
8.8	0.50176	0.49735	0.50265	0.49824
8.85	0.50185	0.49746	0.50254	0.49815
8.9	0.50191	0.49758	0.50242	0.49809
8.95	0.50199	0.49768	0.50232	0.49801

9	0.50206	0.49781	0.50219	0.49794
9.05	0.50216	0.49791	0.50209	0.49784
9.1	0.50229	0.49799	0.50201	0.49771
9.15	0.50238	0.49808	0.50192	0.49762
9.2	0.50247	0.49816	0.50184	0.49753
9.25	0.50257	0.49824	0.50176	0.49743
9.3	0.50268	0.49831	0.50169	0.49732
9.35	0.50278	0.49841	0.50159	0.49722
9.4	0.50285	0.49851	0.50149	0.49715
9.45	0.50294	0.49860	0.50140	0.49706
9.5	0.50301	0.49871	0.50129	0.49699
9.55	0.50308	0.49880	0.50120	0.49692
9.6	0.50316	0.49887	0.50113	0.49684
9.65	0.50322	0.49897	0.50103	0.49678
9.7	0.50329	0.49906	0.50094	0.49671
9.75	0.50337	0.49912	0.50088	0.49663
9.8	0.50343	0.49921	0.50079	0.49657
9.85	0.50348	0.49931	0.50069	0.49652
9.9	0.50354	0.49940	0.50060	0.49646
9.95	0.50360	0.49950	0.50050	0.49640
10	0.50366	0.49960	0.50040	0.49634

Table B- 6: Results of red ink volume fraction due to different blue silicone ink inlet velocities.

Flow Time, s	Red Ink Volume Fraction			Flow Time, s	Red Ink Volume Fraction		
	1 mm/s	3 mm/s	5 mm/s		1 mm/s	3 mm/s	5 mm/s
0	0.5024	0.5024	0.5024	5.05	0.4947	0.4854	0.4784
0.05	0.8558	0.8661	0.8608	5.1	0.4947	0.4851	0.4782
0.1	0.8157	0.7987	0.7710	5.15	0.4946	0.4849	0.4780
0.15	0.8124	0.7368	0.6758	5.2	0.4946	0.4847	0.4778
0.2	0.7730	0.6791	0.6161	5.25	0.4946	0.4845	0.4776
0.25	0.7303	0.6360	0.5841	5.3	0.4946	0.4844	0.4774
0.3	0.6964	0.5993	0.5615	5.35	0.4946	0.4842	0.4772
0.35	0.6643	0.5727	0.5445	5.4	0.4947	0.4841	0.4770
0.4	0.6360	0.5542	0.5325	5.45	0.4947	0.4839	0.4768
0.45	0.6128	0.5410	0.5235	5.5	0.4948	0.4837	0.4766
0.5	0.5937	0.5314	0.5169	5.55	0.4949	0.4835	0.4764
0.55	0.5779	0.5244	0.5124	5.6	0.4949	0.4831	0.4762
0.6	0.5651	0.5193	0.5093	5.65	0.4950	0.4828	0.4760
0.65	0.5548	0.5156	0.5074	5.7	0.4951	0.4823	0.4757
0.7	0.5466	0.5132	0.5061	5.75	0.4951	0.4820	0.4755
0.75	0.5401	0.5115	0.5053	5.8	0.4952	0.4816	0.4752
0.8	0.5348	0.5104	0.5047	5.85	0.4953	0.4814	0.4750
0.85	0.5306	0.5096	0.5041	5.9	0.4953	0.4812	0.4747
0.9	0.5272	0.5089	0.5035	5.95	0.4954	0.4811	0.4744

0.95	0.5244	0.5082	0.5027	6	0.4955	0.4809	0.4741
1	0.5221	0.5073	0.5017	6.05	0.4956	0.4808	0.4738
1.05	0.5202	0.5062	0.5006	6.1	0.4957	0.4807	0.4736
1.1	0.5186	0.5049	0.4993	6.15	0.4958	0.4805	0.4733
1.15	0.5173	0.5035	0.4979	6.2	0.4959	0.4804	0.4730
1.2	0.5162	0.5020	0.4966	6.25	0.4960	0.4801	0.4727
1.25	0.5152	0.5005	0.4953	6.3	0.4962	0.4799	0.4724
1.3	0.5143	0.4991	0.4941	6.35	0.4963	0.4795	0.4720
1.35	0.5134	0.4978	0.4932	6.4	0.4965	0.4792	0.4717
1.4	0.5126	0.4967	0.4923	6.45	0.4967	0.4788	0.4713
1.45	0.5119	0.4958	0.4917	6.5	0.4969	0.4784	0.4709
1.5	0.5112	0.4950	0.4911	6.55	0.4971	0.4780	0.4706
1.55	0.5104	0.4944	0.4906	6.6	0.4973	0.4777	0.4702
1.6	0.5097	0.4938	0.4902	6.65	0.4974	0.4774	0.4699
1.65	0.5089	0.4935	0.4899	6.7	0.4976	0.4771	0.4695
1.7	0.5082	0.4932	0.4896	6.75	0.4977	0.4769	0.4692
1.75	0.5075	0.4930	0.4895	6.8	0.4978	0.4767	0.4689
1.8	0.5067	0.4929	0.4894	6.85	0.4980	0.4765	0.4685
1.85	0.5060	0.4928	0.4893	6.9	0.4981	0.4763	0.4681
1.9	0.5053	0.4927	0.4893	6.95	0.4982	0.4760	0.4677
1.95	0.5045	0.4927	0.4893	7	0.4982	0.4758	0.4673
2	0.5038	0.4926	0.4892	7.05	0.4983	0.4755	0.4669
2.05	0.5031	0.4925	0.4892	7.1	0.4984	0.4752	0.4665
2.1	0.5024	0.4924	0.4891	7.15	0.4985	0.4749	0.4661
2.15	0.5018	0.4922	0.4889	7.2	0.4986	0.4745	0.4658
2.2	0.5012	0.4921	0.4888	7.25	0.4987	0.4741	0.4654
2.25	0.5006	0.4920	0.4887	7.3	0.4989	0.4738	0.4650
2.3	0.5001	0.4919	0.4886	7.35	0.4990	0.4735	0.4646
2.35	0.4997	0.4917	0.4885	7.4	0.4991	0.4732	0.4643
2.4	0.4993	0.4916	0.4884	7.45	0.4993	0.4730	0.4639
2.45	0.4990	0.4915	0.4882	7.5	0.4994	0.4728	0.4635
2.5	0.4987	0.4914	0.4881	7.55	0.4996	0.4726	0.4631
2.55	0.4985	0.4913	0.4879	7.6	0.4997	0.4725	0.4626
2.6	0.4983	0.4912	0.4878	7.65	0.4998	0.4724	0.4622
2.65	0.4982	0.4912	0.4876	7.7	0.4999	0.4723	0.4618
2.7	0.4980	0.4912	0.4875	7.75	0.5000	0.4721	0.4614
2.75	0.4979	0.4912	0.4874	7.8	0.5001	0.4718	0.4609
2.8	0.4977	0.4913	0.4873	7.85	0.5002	0.4716	0.4605
2.85	0.4976	0.4914	0.4872	7.9	0.5002	0.4712	0.4601
2.9	0.4974	0.4915	0.4871	7.95	0.5003	0.4708	0.4597
2.95	0.4972	0.4916	0.4871	8	0.5004	0.4704	0.4593
3	0.4971	0.4916	0.4870	8.05	0.5004	0.4700	0.4588
3.05	0.4969	0.4916	0.4869	8.1	0.5005	0.4696	0.4584
3.1	0.4967	0.4915	0.4868	8.15	0.5006	0.4692	0.4580
3.15	0.4965	0.4915	0.4867	8.2	0.5007	0.4689	0.4575
3.2	0.4963	0.4914	0.4865	8.25	0.5007	0.4686	0.4571

3.25	0.4962	0.4914	0.4864	8.3	0.5008	0.4684	0.4566
3.3	0.4960	0.4913	0.4862	8.35	0.5009	0.4682	0.4561
3.35	0.4958	0.4912	0.4861	8.4	0.5010	0.4680	0.4557
3.4	0.4957	0.4912	0.4859	8.45	0.5011	0.4679	0.4552
3.45	0.4955	0.4911	0.4858	8.5	0.5012	0.4677	0.4548
3.5	0.4954	0.4909	0.4856	8.55	0.5013	0.4675	0.4544
3.55	0.4953	0.4908	0.4853	8.6	0.5014	0.4674	0.4539
3.6	0.4952	0.4905	0.4851	8.65	0.5015	0.4672	0.4535
3.65	0.4951	0.4903	0.4849	8.7	0.5016	0.4670	0.4530
3.7	0.4950	0.4901	0.4846	8.75	0.5017	0.4668	0.4526
3.75	0.4949	0.4899	0.4843	8.8	0.5018	0.4664	0.4521
3.8	0.4948	0.4897	0.4840	8.85	0.5018	0.4661	0.4516
3.85	0.4948	0.4895	0.4837	8.9	0.5019	0.4658	0.4511
3.9	0.4947	0.4894	0.4834	8.95	0.5020	0.4654	0.4506
3.95	0.4947	0.4893	0.4831	9	0.5021	0.4660	0.4502
4	0.4946	0.4893	0.4828	9.05	0.5022	0.4648	0.4497
4.05	0.4946	0.4893	0.4825	9.1	0.5023	0.4643	0.4492
4.1	0.4946	0.4892	0.4822	9.15	0.5024	0.4639	0.4488
4.15	0.4945	0.4890	0.4819	9.2	0.5025	0.4635	0.4492
4.2	0.4945	0.4888	0.4816	9.25	0.5026	0.4632	0.4481
4.25	0.4945	0.4885	0.4814	9.3	0.5027	0.4638	0.4475
4.3	0.4945	0.4881	0.4811	9.35	0.5028	0.4628	0.4469
4.35	0.4946	0.4878	0.4809	9.4	0.5029	0.4624	0.4463
4.4	0.4946	0.4876	0.4807	9.45	0.5029	0.4620	0.4457
4.45	0.4946	0.4874	0.4805	9.5	0.5030	0.4617	0.4452
4.5	0.4947	0.4872	0.4804	9.55	0.5031	0.4613	0.4447
4.55	0.4947	0.4871	0.4802	9.6	0.5032	0.4610	0.4441
4.6	0.4948	0.4871	0.4800	9.65	0.5032	0.4606	0.4436
4.65	0.4948	0.4870	0.4799	9.7	0.5033	0.4602	0.4431
4.7	0.4948	0.4870	0.4797	9.75	0.5034	0.4599	0.4426
4.75	0.4948	0.4869	0.4794	9.8	0.5034	0.4595	0.4420
4.8	0.4948	0.4868	0.4792	9.85	0.5035	0.4590	0.4415
4.85	0.4948	0.4866	0.4791	9.9	0.5035	0.4586	0.4410
4.9	0.4948	0.4864	0.4789	9.95	0.5036	0.4582	0.4405
4.95	0.4948	0.4861	0.4787	10	0.5037	0.4578	0.4408
5	0.4947	0.4857	0.4785				

Table B-7: Results for average pressure due to different blue silicone ink inlet velocities.

Flow Time, s	Pressure			Flow Time, s	Pressure		
	1 mm/s	3 mm/s	5 mm/s		1 mm/s	3 mm/s	5 mm/s
0	0.00	0.00	0.00	5.05	27807.59	42555.2	55447.03
0.05	81929.94	148509.40	181038.82	5.1	27734.39	42583.5	55224.56
0.1	30961.17	48698.92	63363.45	5.15	27759.9	42538.94	55065.89
0.15	24362.40	37676.78	48836.51	5.2	27767.25	42637.63	54942.55
0.2	23578.67	37074.01	46769.93	5.25	27718.3	42870.65	54889.6
0.25	26907.56	41007.91	52669.17	5.3	27696.25	43098.3	55024.08
0.3	26589.38	41576.19	53117.15	5.35	27784.94	43213.16	55238.9
0.35	28622.57	43391.06	55489.69	5.4	27810.24	43315.1	55444.53
0.4	27872.66	43167.93	55425.96	5.45	27795.12	43439.42	55588.57
0.45	28755.14	43760.13	56263.73	5.5	27852.07	43405.29	55661.68
0.5	28098.95	43467.00	56007.87	5.55	27982.88	43307.79	55634.69
0.55	28310.71	43456.23	55811.77	5.6	27944.42	43125.34	55495.1
0.6	27809.32	43291.78	55657.05	5.65	27908.74	42883.42	55248.33
0.65	27969.38	43221.08	55397.45	5.7	28023.85	42789.56	55038.67
0.7	27650.90	43083.52	55260.67	5.75	28211.78	42706.64	54960.56
0.75	27972.45	42854.96	55134.52	5.8	28082.49	42631.74	54968.12
0.8	27764.03	42742.15	55033.13	5.85	27811.34	42645.6	55036.62
0.85	27932.60	42714.85	55027.84	5.9	27856.69	42569.23	55202.3
0.9	27798.15	42692.57	55065.10	5.95	28061.32	42701.82	55371.05
0.95	27856.17	42835.83	55186.88	6	27984.97	42889.81	55457.2
1	27767.31	42905.71	55302.72	6.05	27675.46	43034.28	55522.27
1.05	27787.02	43012.57	55402.19	6.1	27598.73	43134.15	55566.47
1.1	27823.51	43160.94	55548.42	6.15	27794.28	43222.99	55566.12
1.15	27753.35	43282.00	55549.15	6.2	27920.89	43338.63	55504.92
1.2	27848.19	43398.87	55501.29	6.25	27652.73	43385.83	55353.37
1.25	27827.26	43280.19	55327.36	6.3	27323.09	43362.88	55078.02
1.3	27940.92	43033.17	55194.48	6.35	27771.06	43251.24	54970.55
1.35	27903.04	42881.60	55048.21	6.4	28163.95	43059.32	54989.27
1.4	27967.00	42688.59	55147.91	6.45	27825.92	42848.52	55037.57
1.45	27978.31	42756.03	55216.48	6.5	27258.81	42676.32	55202.72
1.5	27878.96	42810.82	55294.76	6.55	27704.88	42581.37	55360.61
1.55	27988.07	42903.92	55419.39	6.6	28343.83	42581.64	55452.33
1.6	27846.85	43087.88	55516.62	6.65	27823.06	42660.18	55516.58
1.65	27898.79	43198.91	55603.50	6.7	27284.11	42778.4	55572.82
1.7	27751.23	43378.36	55572.81	6.75	27650.21	42927.5	55577.74
1.75	27812.28	43261.46	55411.33	6.8	28568.71	43082.04	55511
1.8	27774.20	43138.60	55201.94	6.85	28113.91	43208.09	55296.84
1.85	27772.81	42865.66	55060.74	6.9	27183.26	43301.58	55076.05
1.9	27802.17	42786.17	55076.95	6.95	27672.19	43325.02	54962.53
1.95	27788.16	42743.40	55061.69	7	28680.49	43298.49	54992.92
2	27842.58	42831.92	55147.71	7.05	28149.77	43196.65	55054.76



2.05	27855.33	42937.63	55311.85	7.1	27082.73	43048.82	55232.33
2.1	27919.28	43026.38	55417.98	7.15	27605.44	42916.2	55363.97
2.15	27931.80	43235.53	55582.32	7.2	28615.45	42803.62	55444.35
2.2	27947.09	43279.43	55596.30	7.25	28141.1	42708	55530.36
2.25	27964.31	43357.26	55481.35	7.3	27056.1	42667.83	55584.62
2.3	27920.07	43213.49	55264.87	7.35	27491.1	42687.37	55583.85
2.35	27924.94	43021.20	55059.86	7.4	28531.26	42743.29	55501.24
2.4	27887.94	42649.45	55092.98	7.45	28144.81	42799.66	55306.81
2.45	27852.57	42759.19	55133.86	7.5	27027.96	42858.06	55143.45
2.5	27822.92	42787.98	55238.11	7.55	27477.49	42925.18	55047.09
2.55	27785.85	42813.66	55385.27	7.6	28485.52	43023.65	54990.86
2.6	27788.24	42954.54	55510.58	7.65	27923.25	43140.17	54995.19
2.65	27778.39	43039.32	55575.41	7.7	27109.44	43223.78	55133.87
2.7	27790.20	43235.20	55634.74	7.75	27278.16	43276.52	55313.43
2.75	27810.07	43334.09	55556.59	7.8	28419.76	43282.42	55471.18
2.8	27817.27	43456.72	55275.63	7.85	28027.33	43250.18	55576.09
2.85	27870.49	43338.55	54983.76	7.9	27118.87	43191.38	55618.63
2.9	27888.39	43118.43	54950.05	7.95	27113.35	43099.28	55583.46
2.95	27952.25	42845.07	54942.60	8	28311.35	42961.12	55476.39
3	27930.28	42630.83	54961.46	8.05	28294.11	42811.3	55291.36
3.05	27929.82	42655.06	54992.65	8.1	27167.19	42698.73	55102.92
3.1	27945.68	42646.81	55162.19	8.15	27740.77	42637.9	55034.89
3.15	27894.81	42685.75	55424.37	8.2	28573.02	42632.74	55017.25
3.2	27898.76	42880.77	55544.67	8.25	28352.62	42650.69	55040.11
3.25	27855.46	43033.80	55657.67	8.3	27163.34	42705.02	55155
3.3	27815.23	43286.16	55590.65	8.35	27564.21	42795.7	55324.23
3.35	27803.91	43369.49	55417.92	8.4	28336.77	42931.16	55442.41
3.4	27745.85	43353.32	55063.92	8.45	28857.88	43067.33	55492.1
3.45	27775.23	43270.00	54935.89	8.5	28414.37	43189.56	55521.34
3.5	27802.46	42993.80	54904.69	8.55	26840.31	43275.39	55544.08
3.55	27766.60	42556.05	54922.15	8.6	26586.34	43326.1	55541.22
3.6	27820.99	42722.79	54992.42	8.65	28480.12	43350.17	55458.29
3.65	27842.86	42718.21	55197.39	8.7	29183.48	43312.14	55274.08
3.7	27877.71	42610.23	55451.13	8.75	27328.35	43188.91	55119.22
3.75	27937.63	42586.96	55597.16	8.8	25875.8	42994.47	55060.27
3.8	27954.56	42828.30	55660.36	8.85	26870.63	42822.37	55041.84
3.85	27974.48	42975.87	55626.93	8.9	29110.71	42722.79	55075.19
3.9	27971.78	43058.26	55464.95	8.95	30210.64	42688.16	55198.56
3.95	27927.33	43196.64	55085.89	9	29009.12	42682.28	55326.49
4	27922.60	43390.23	54915.07	9.05	25300.82	42672.12	55431.05
4.05	27903.77	43426.65	54903.26	9.1	28708.74	42700.62	55529.67
4.1	27826.80	43383.07	54949.93	9.15	30965.96	42741.4	55599.43
4.15	27828.47	43261.25	54974.54	9.2	28346.58	42804.79	55601.26
4.2	27788.23	43175.52	55182.86	9.25	24568.87	42914.09	55494.46
4.25	27730.27	42993.70	55472.80	9.3	28804.9	43033.4	55309.67
4.3	27773.56	42629.22	55517.52	9.35	27829.5	43150.17	55119.24

4.35	27776.59	42587.45	55610.84	9.4	26105.7	43274.24	55070.5
4.4	27739.80	42585.31	55637.61	9.45	25537.97	43356.07	55051.04
4.45	27800.25	42585.62	55546.08	9.5	27107.38	43365.99	55035.7
4.5	27818.20	42545.38	55209.98	9.55	29771.06	43299.58	55116.42
4.55	27841.71	42661.32	54958.53	9.6	29747.36	43150.61	55270.43
4.6	27910.08	42923.86	54912.28	9.65	27557.79	42987.13	55410.52
4.65	27936.74	43135.51	54953.27	9.7	24531.15	42850.82	55536.27
4.7	27974.01	43263.63	55055.33	9.75	27317.26	42788.85	55578.58
4.75	28011.76	43349.47	55242.35	9.8	31280.2	42768.39	55570.74
4.8	27939.37	43459.33	55364.03	9.85	26370.43	42745.66	55495.37
4.85	27921.16	43419.94	55434.11	9.9	28256.46	42698.52	55392.09
4.9	27910.23	43184.95	55531.42	9.95	29768.15	42637.14	55252.11
4.95	27853.11	42766.74	55614.41	10	29567.51	42642.05	55144.01
5	27842.25	42572.89	55598.57				

Table B- 8 Results of torque at different blue silicone ink inlet velocities.

Flow Time	Torque (Nmm)			Flow Time	Torque (Nmm)		
	1 mm/s	3 mm/s	5 mm/s		1 mm/s	3 mm/s	5 mm/s
0	0.000	0.000	0.000	5.05	1.933	2.928	2.730
0.05	3.762	6.115	6.074	5.1	1.933	2.928	2.730
0.1	2.081	3.146	2.944	5.15	1.933	2.928	2.730
0.15	1.718	2.599	2.408	5.2	1.933	2.929	2.730
0.2	1.730	2.645	2.428	5.25	1.933	2.930	2.731
0.25	1.816	2.777	2.570	5.3	1.933	2.929	2.731
0.3	1.895	2.881	2.681	5.35	1.934	2.929	2.732
0.35	1.933	2.931	2.733	5.4	1.933	2.930	2.732
0.4	1.948	2.947	2.748	5.45	1.933	2.930	2.732
0.45	1.949	2.949	2.754	5.5	1.934	2.929	2.731
0.5	1.945	2.943	2.749	5.55	1.934	2.928	2.731
0.55	1.939	2.938	2.744	5.6	1.933	2.928	2.730
0.6	1.935	2.931	2.738	5.65	1.933	2.928	2.730
0.65	1.932	2.928	2.732	5.7	1.934	2.928	2.730
0.7	1.931	2.925	2.728	5.75	1.934	2.929	2.730
0.75	1.931	2.925	2.726	5.8	1.933	2.928	2.731
0.8	1.932	2.926	2.726	5.85	1.933	2.929	2.731
0.85	1.933	2.927	2.727	5.9	1.934	2.929	2.731
0.9	1.933	2.928	2.729	5.95	1.934	2.929	2.731
0.95	1.934	2.929	2.730	6	1.933	2.929	2.731
1	1.934	2.929	2.731	6.05	1.933	2.929	2.731
1.05	1.934	2.929	2.731	6.1	1.934	2.929	2.731
1.1	1.934	2.929	2.731	6.15	1.934	2.929	2.731
1.15	1.934	2.929	2.731	6.2	1.933	2.929	2.731
1.2	1.933	2.928	2.731	6.25	1.933	2.929	2.730
1.25	1.933	2.928	2.731	6.3	1.933	2.929	2.730
1.3	1.933	2.929	2.731	6.35	1.935	2.928	2.730
1.35	1.933	2.929	2.731	6.4	1.933	2.928	2.731

1.4	1.934	2.929	2.731	6.45	1.932	2.928	2.731
1.45	1.933	2.929	2.731	6.5	1.933	2.928	2.731
1.5	1.934	2.929	2.731	6.55	1.935	2.928	2.731
1.55	1.933	2.929	2.731	6.6	1.933	2.928	2.731
1.6	1.934	2.929	2.731	6.65	1.931	2.929	2.731
1.65	1.934	2.928	2.731	6.7	1.933	2.929	2.731
1.7	1.933	2.928	2.731	6.75	1.935	2.929	2.731
1.75	1.933	2.928	2.731	6.8	1.934	2.929	2.731
1.8	1.933	2.929	2.731	6.85	1.931	2.929	2.731
1.85	1.933	2.929	2.731	6.9	1.932	2.929	2.730
1.9	1.933	2.929	2.731	6.95	1.935	2.929	2.730
1.95	1.933	2.929	2.731	7	1.934	2.929	2.731
2	1.933	2.929	2.731	7.05	1.931	2.928	2.731
2.05	1.933	2.929	2.731	7.1	1.932	2.928	2.731
2.1	1.933	2.929	2.731	7.15	1.935	2.928	2.731
2.15	1.933	2.928	2.731	7.2	1.934	2.928	2.731
2.2	1.933	2.928	2.731	7.25	1.931	2.928	2.731
2.25	1.933	2.928	2.731	7.3	1.932	2.929	2.731
2.3	1.933	2.929	2.731	7.35	1.935	2.929	2.731
2.35	1.933	2.929	2.731	7.4	1.934	2.929	2.731
2.4	1.933	2.929	2.731	7.45	1.931	2.929	2.730
2.45	1.933	2.929	2.731	7.5	1.932	2.929	2.730
2.5	1.933	2.928	2.731	7.55	1.936	2.929	2.730
2.55	1.934	2.929	2.731	7.6	1.934	2.929	2.731
2.6	1.934	2.929	2.731	7.65	1.931	2.929	2.731
2.65	1.933	2.929	2.731	7.7	1.933	2.929	2.731
2.7	1.933	2.929	2.731	7.75	1.935	2.929	2.732
2.75	1.933	2.928	2.731	7.8	1.935	2.929	2.732
2.8	1.933	2.929	2.730	7.85	1.931	2.929	2.731
2.85	1.933	2.928	2.730	7.9	1.932	2.929	2.731
2.9	1.933	2.929	2.731	7.95	1.935	2.928	2.731
2.95	1.933	2.929	2.730	8	1.935	2.928	2.730
3	1.933	2.929	2.730	8.05	1.931	2.928	2.730
3.05	1.933	2.929	2.731	8.1	1.933	2.928	2.730
3.1	1.933	2.929	2.731	8.15	1.935	2.928	2.730
3.15	1.933	2.929	2.731	8.2	1.933	2.929	2.731
3.2	1.933	2.929	2.731	8.25	1.931	2.929	2.731
3.25	1.933	2.929	2.731	8.3	1.932	2.929	2.731
3.3	1.934	2.929	2.731	8.35	1.935	2.929	2.731
3.35	1.933	2.928	2.731	8.4	1.934	2.929	2.731
3.4	1.933	2.929	2.730	8.45	1.932	2.929	2.731
3.45	1.934	2.929	2.730	8.5	1.931	2.929	2.731
3.5	1.933	2.928	2.730	8.55	1.931	2.929	2.731
3.55	1.933	2.928	2.730	8.6	1.933	2.929	2.731
3.6	1.933	2.929	2.731	8.65	1.934	2.929	2.731
3.65	1.933	2.928	2.731	8.7	1.934	2.929	2.730

3.7	1.933	2.929	2.731	8.75	1.930	2.928	2.730
3.75	1.933	2.929	2.731	8.8	1.931	2.928	2.730
3.8	1.933	2.930	2.731	8.85	1.938	2.928	2.731
3.85	1.934	2.929	2.731	8.9	1.937	2.928	2.731
3.9	1.933	2.929	2.731	8.95	1.929	2.928	2.731
3.95	1.933	2.930	2.730	9	1.927	2.929	2.731
4	1.933	2.930	2.730	9.05	1.928	2.929	2.731
4.05	1.933	2.929	2.730	9.1	1.937	2.928	2.731
4.1	1.933	2.929	2.730	9.15	1.924	2.929	2.731
4.15	1.934	2.929	2.731	9.2	1.920	2.929	2.731
4.2	1.933	2.929	2.732	9.25	1.931	2.929	2.731
4.25	1.933	2.928	2.731	9.3	1.936	2.929	2.730
4.3	1.933	2.928	2.731	9.35	1.925	2.929	2.730
4.35	1.933	2.928	2.731	9.4	1.930	2.929	2.730
4.4	1.933	2.928	2.731	9.45	1.936	2.929	2.731
4.45	1.933	2.928	2.731	9.5	1.938	2.929	2.731
4.5	1.933	2.929	2.730	9.55	1.940	2.928	2.731
4.55	1.933	2.929	2.730	9.6	1.928	2.928	2.731
4.6	1.933	2.930	2.731	9.65	1.927	2.928	2.731
4.65	1.933	2.929	2.731	9.7	1.927	2.928	2.731
4.7	1.933	2.929	2.731	9.75	1.937	2.928	2.731
4.75	1.933	2.930	2.731	9.8	1.931	2.929	2.731
4.8	1.933	2.930	2.731	9.85	1.923	2.928	2.731
4.85	1.933	2.929	2.731	9.9	1.933	2.928	2.731
4.9	1.933	2.928	2.731	9.95	1.927	2.928	2.731
4.95	1.933	2.928	2.731	10	1.929	2.928	2.731
5	1.934	2.928	2.731				

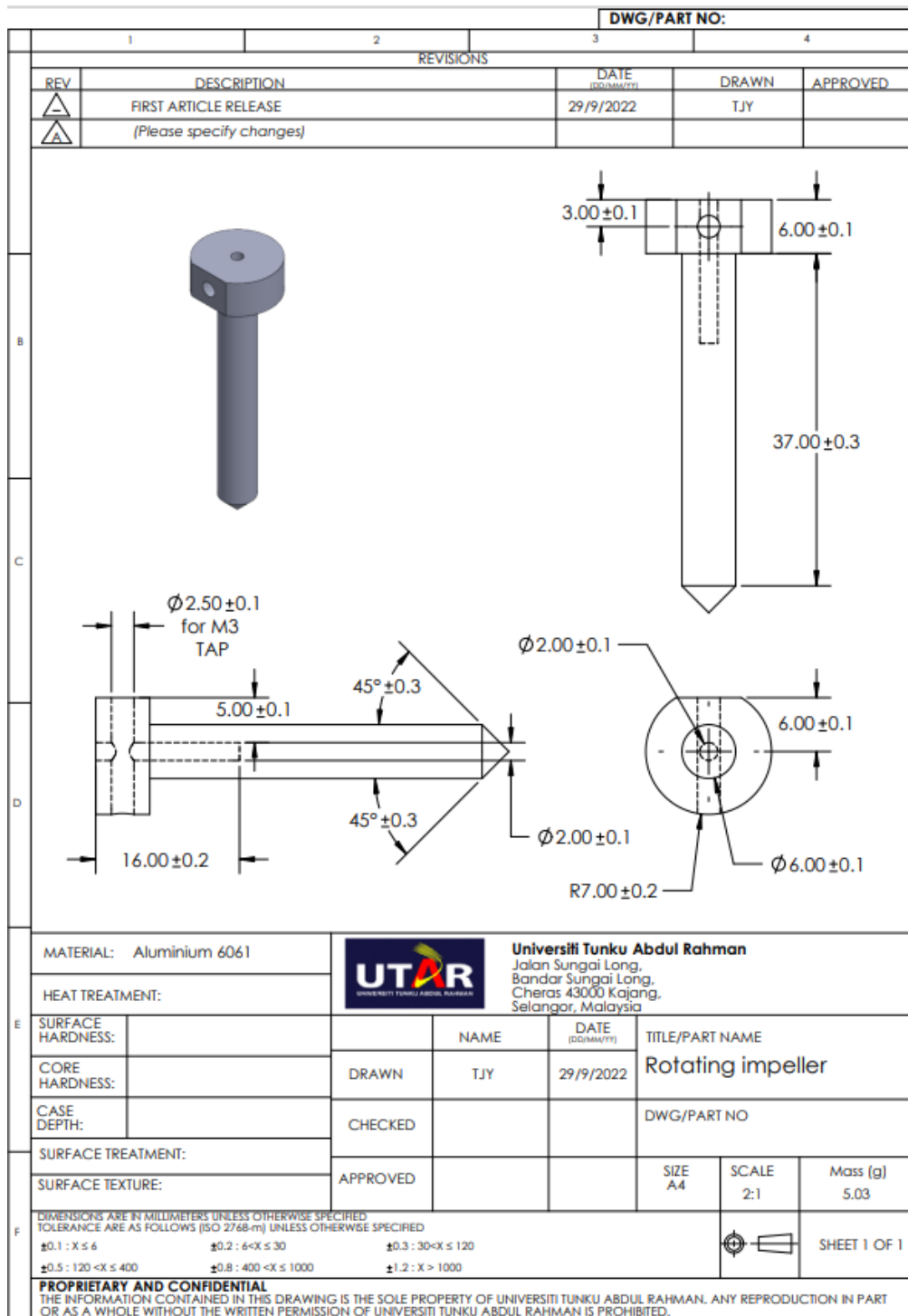
Table B- 9: Results of Wall Shear Stress at different blue silicone ink inlet velocities.

Flow Time, s	Wall Shear Stress, kPa			Flow Time, s	Wall Shear Stress, kPa		
	1 mm/s	3 mm/s	5 mm/s		1 mm/s	3 mm/s	5 mm/s
0	-	-	-	5.05	1.69	1.99	2.31
0.05	6.91	10.13	12.32	5.1	1.69	1.99	2.31
0.1	1.90	2.29	2.72	5.15	1.69	1.99	2.32
0.15	1.51	1.77	2.05	5.2	1.69	1.99	2.32
0.2	1.49	1.75	2.00	5.25	1.69	1.99	2.31
0.25	1.59	1.87	2.14	5.3	1.69	1.99	2.31
0.3	1.65	1.94	2.24	5.35	1.69	1.99	2.31
0.35	1.69	1.98	2.30	5.4	1.69	1.99	2.31
0.4	1.71	2.00	2.33	5.45	1.69	1.99	2.31
0.45	1.71	2.00	2.33	5.5	1.69	1.99	2.31
0.5	1.71	2.00	2.33	5.55	1.69	1.99	2.31
0.55	1.70	2.00	2.32	5.6	1.69	1.99	2.31
0.6	1.70	1.99	2.32	5.65	1.69	1.99	2.31

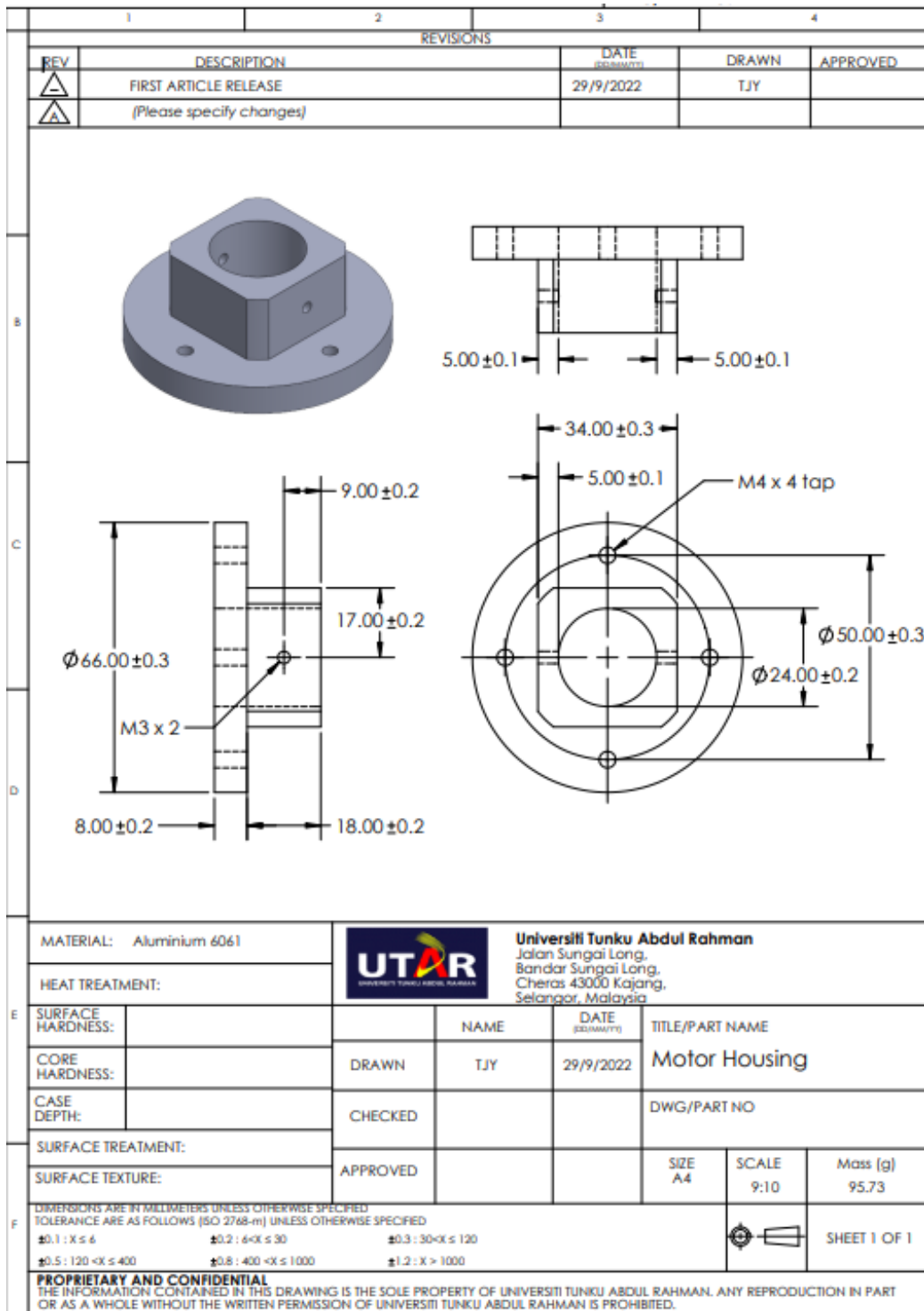
0.65	1.69	1.99	2.31	5.7	1.69	1.99	2.31
0.7	1.69	1.99	2.31	5.75	1.69	1.99	2.31
0.75	1.69	1.99	2.31	5.8	1.69	1.99	2.31
0.8	1.69	1.99	2.31	5.85	1.69	1.99	2.31
0.85	1.69	1.99	2.31	5.9	1.69	1.99	2.31
0.9	1.69	1.99	2.31	5.95	1.69	1.99	2.31
0.95	1.69	1.99	2.31	6	1.69	1.99	2.31
1	1.69	1.99	2.31	6.05	1.69	1.99	2.31
1.05	1.69	1.99	2.31	6.1	1.69	1.99	2.31
1.1	1.69	1.99	2.31	6.15	1.69	1.99	2.31
1.15	1.69	1.99	2.31	6.2	1.69	1.99	2.31
1.2	1.69	1.99	2.31	6.25	1.69	1.99	2.31
1.25	1.69	1.99	2.31	6.3	1.69	1.99	2.31
1.3	1.69	1.99	2.31	6.35	1.69	1.99	2.31
1.35	1.69	1.99	2.31	6.4	1.69	1.99	2.31
1.4	1.69	1.99	2.31	6.45	1.70	1.99	2.31
1.45	1.69	1.99	2.31	6.5	1.69	1.99	2.31
1.5	1.69	1.99	2.31	6.55	1.69	1.99	2.31
1.55	1.69	1.99	2.31	6.6	1.69	1.99	2.31
1.6	1.69	1.99	2.31	6.65	1.70	1.99	2.31
1.65	1.69	1.99	2.31	6.7	1.69	1.99	2.31
1.7	1.69	1.99	2.31	6.75	1.69	1.99	2.31
1.75	1.69	1.99	2.31	6.8	1.69	1.99	2.31
1.8	1.69	1.99	2.31	6.85	1.70	1.99	2.31
1.85	1.69	1.99	2.31	6.9	1.69	1.99	2.31
1.9	1.69	1.99	2.31	6.95	1.69	1.99	2.31
1.95	1.69	1.99	2.31	7	1.69	1.99	2.31
2	1.69	1.99	2.31	7.05	1.70	1.99	2.31
2.05	1.69	1.99	2.31	7.1	1.69	1.99	2.31
2.1	1.69	1.99	2.31	7.15	1.69	1.99	2.31
2.15	1.69	1.99	2.31	7.2	1.69	1.99	2.31
2.2	1.69	1.99	2.31	7.25	1.70	1.99	2.31
2.25	1.69	1.99	2.31	7.3	1.70	1.99	2.31
2.3	1.69	1.99	2.31	7.35	1.69	1.99	2.31
2.35	1.69	1.99	2.31	7.4	1.69	1.99	2.31
2.4	1.69	1.99	2.31	7.45	1.70	1.99	2.31
2.45	1.69	1.99	2.31	7.5	1.70	1.99	2.31
2.5	1.69	1.99	2.31	7.55	1.69	1.99	2.31
2.55	1.69	1.99	2.31	7.6	1.69	1.99	2.31
2.6	1.69	1.99	2.31	7.65	1.70	1.99	2.31
2.65	1.69	1.99	2.31	7.7	1.69	1.99	2.31
2.7	1.69	1.99	2.31	7.75	1.69	1.99	2.31
2.75	1.69	1.99	2.31	7.8	1.69	1.99	2.31
2.8	1.69	1.99	2.31	7.85	1.70	1.99	2.31
2.85	1.69	1.99	2.31	7.9	1.69	1.99	2.31
2.9	1.69	1.99	2.31	7.95	1.69	1.99	2.31

2.95	1.69	1.99	2.31	8	1.69	1.99	2.31
3	1.69	1.99	2.31	8.05	1.69	1.99	2.31
3.05	1.69	1.99	2.31	8.1	1.69	1.99	2.31
3.1	1.69	1.99	2.31	8.15	1.69	1.99	2.31
3.15	1.69	1.99	2.31	8.2	1.69	1.99	2.31
3.2	1.69	1.99	2.31	8.25	1.70	1.99	2.31
3.25	1.69	1.99	2.31	8.3	1.70	1.99	2.31
3.3	1.69	1.99	2.31	8.35	1.69	1.99	2.31
3.35	1.69	1.99	2.31	8.4	1.69	1.99	2.31
3.4	1.69	1.99	2.31	8.45	1.69	1.99	2.31
3.45	1.69	1.99	2.31	8.5	1.70	1.99	2.31
3.5	1.69	1.99	2.31	8.55	1.70	1.99	2.31
3.55	1.69	1.99	2.31	8.6	1.69	1.99	2.31
3.6	1.69	1.99	2.31	8.65	1.69	1.99	2.31
3.65	1.69	1.99	2.31	8.7	1.69	1.99	2.31
3.7	1.69	1.99	2.31	8.75	1.70	1.99	2.31
3.75	1.69	1.99	2.31	8.8	1.70	1.99	2.31
3.8	1.69	1.99	2.31	8.85	1.68	1.99	2.31
3.85	1.69	1.99	2.31	8.9	1.68	1.99	2.31
3.9	1.69	1.99	2.31	8.95	1.70	1.99	2.31
3.95	1.69	1.99	2.31	9	1.70	1.99	2.31
4	1.69	1.99	2.31	9.05	1.70	1.99	2.31
4.05	1.69	1.99	2.31	9.1	1.68	1.99	2.31
4.1	1.69	1.99	2.31	9.15	1.69	1.99	2.31
4.15	1.69	1.99	2.31	9.2	1.71	1.99	2.31
4.2	1.69	1.99	2.31	9.25	1.70	1.99	2.31
4.25	1.69	1.99	2.31	9.3	1.68	1.99	2.31
4.3	1.69	1.99	2.31	9.35	1.70	1.99	2.31
4.35	1.69	1.99	2.31	9.4	1.70	1.99	2.31
4.4	1.69	1.99	2.31	9.45	1.69	1.99	2.31
4.45	1.69	1.99	2.31	9.5	1.68	1.99	2.31
4.5	1.69	1.99	2.31	9.55	1.68	1.99	2.31
4.55	1.69	1.99	2.31	9.6	1.70	1.99	2.31
4.6	1.69	1.99	2.31	9.65	1.70	1.99	2.31
4.65	1.69	1.99	2.31	9.7	1.70	1.99	2.31
4.7	1.69	1.99	2.31	9.75	1.68	1.99	2.31
4.75	1.69	1.99	2.31	9.8	1.69	1.99	2.31
4.8	1.69	1.99	2.31	9.85	1.70	1.99	2.31
4.85	1.69	1.99	2.31	9.9	1.68	1.99	2.31
4.9	1.69	1.99	2.31	9.95	1.69	1.99	2.31
4.95	1.69	1.99	2.31	10	1.70	1.99	2.31
5	1.69	1.99	2.31				

Appendix C: Engineering Drawings

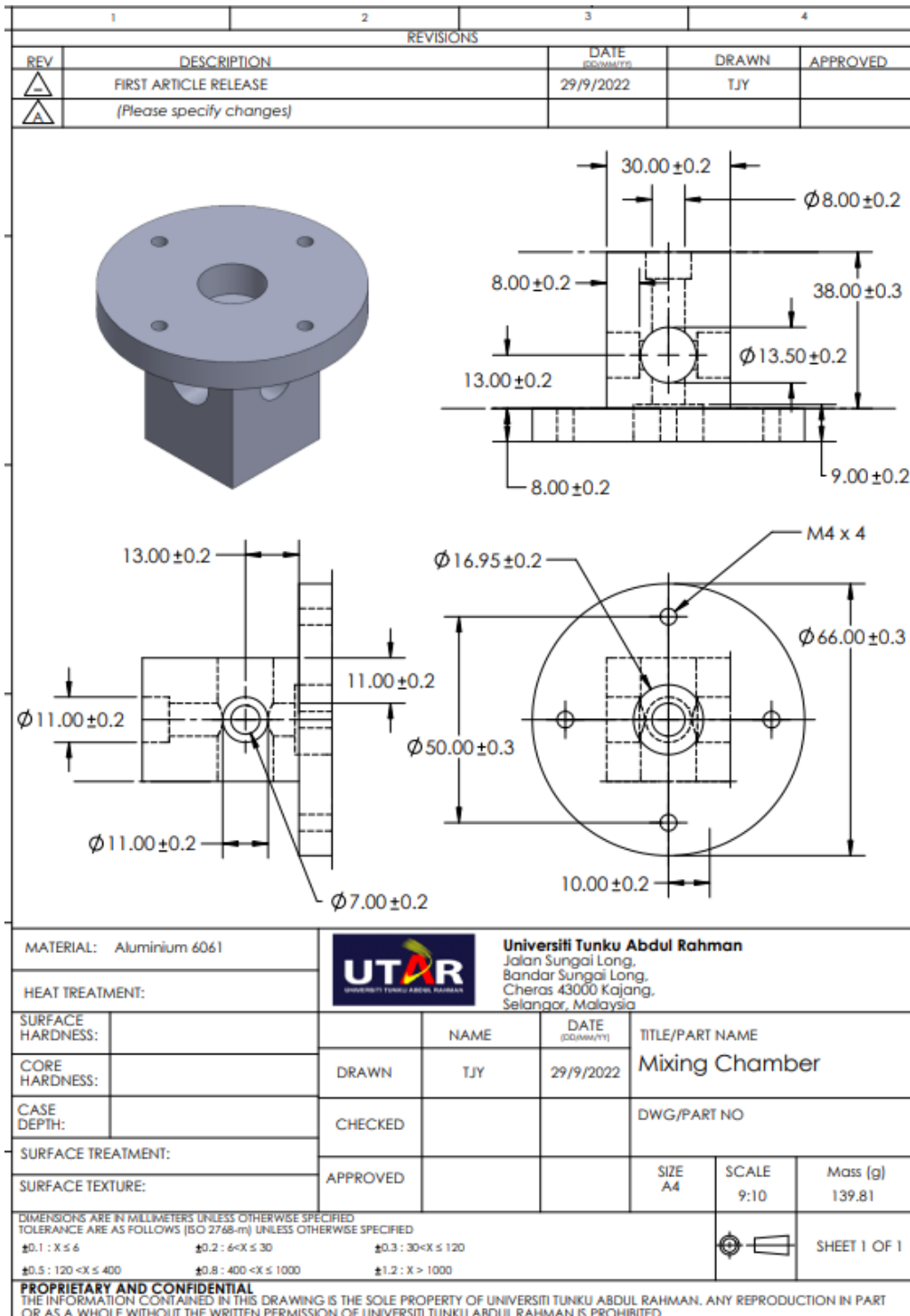


Appendix C- 1: Engineering Drawing of the rotating Impeller.

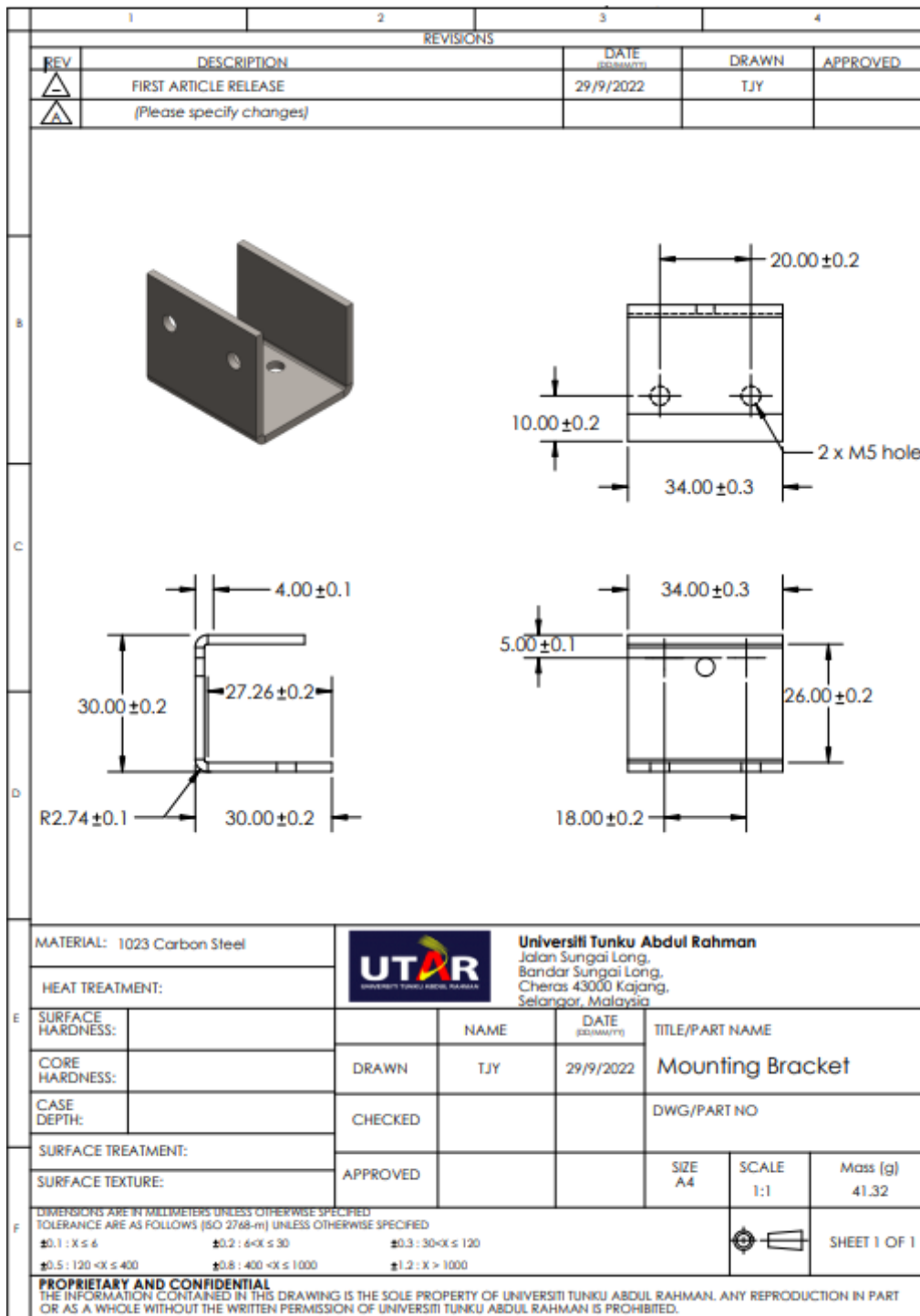


Appendix C- 2: Engineering Drawing of the motor housing,





Appendix C- 3: Engineering Drawing of the mixing chamber.



Appendix C- 4: Engineering Drawing of the Mounting Bracket.

## Appendix D: Costing of the design

Double Ferrule Compression Fitting Male Connector SS304 6mm 8mm 10mm 12mm Tube OD x 1/8" 1/4" 3/8" 1/2" NPT

5.0 ★★★★★ | 15 Ratings | 126 Sold

RM16.94 **RM11.86** 30% OFF

Shop Vouchers: RM2 OFF, RM3 OFF, RM4 OFF, RM5 OFF, RM5 OFF, Show All

Shipping: Free shipping (Free shipping for orders over RM75.00)  
Shipping From: Mainland China to KL City, Kuala Lumpur  
Shipping Fee: RM0.00 - RM4.90

Size:

6mm OD X 1/8"	6mm OD X 1/4"	6mm OD X 3/8"
6mm OD X 1/2"	8mm OD X 1/8"	8mm OD X 1/4"
8mm OD X 3/8"	8mm OD X 1/2"	10mm OD X 1/4"
10mm OD X 3/8"	10mm OD X 1/2"	<b>12mm OD X 1/4"</b>
12mm OD X 3/8"	12mm OD X 1/2"	

Quantity: 1 (5000 pieces available)

10.10 10% CASHBACK

Share: [Facebook](#) [Twitter](#) [Pinterest](#) [LinkedIn](#) | Favorite (39)

Add To Cart Buy Now

### Appendix D- 1: The cost of high-pressure tube fitting to G1/4 Male connector

100pc 18G Dispensing Needle Applicator Tips & 5pc 1:1 Mixing Nozzles Epoxies Acrylic Adhesive AB Glue Resin Static Mixer

4.6 ★★★★★ | 5 Ratings | 16 Sold

**RM24.99**

Shipping: Pre-Order (ships in 10 days)  
Free shipping  
Shipping From: Mainland China to KL City, Kuala Lumpur  
Shipping Fee: RM0.00

Quantity: 1 (84 pieces available)

Add To Cart Buy Now

10.10 FREE SHIPPING MIN. SPEND 15 10% CASHBACK

5x 1:1 mixing nozzles  
100x green 18G Tapered Tip

Shopee Guarantee Get the items you ordered or get your money back.

### Appendix D- 2: The cost of dispensing nozzle.

topplanswatchstore

**1/4** hotsale Metal Nickel Plated Brass Glue Subpackaging Syringe Barrel Luer Lock Adapter bigsale

5.0 ★★★★★ 2 Ratings 2 Sold

RM9.60 **RM5.42** 44% OFF

Shop Vouchers 10% OFF

Shipping Shipping From Mainland China to KL City, Kuala Lumpur Shipping Fee RM1.50 - RM4.90

Size  1/4  M5  M6  1/8

Quantity - 1 + 9999 pieces available

Add To Cart Buy Now

Appendix D- 3: The cost of G1/4 to luer lock adapter.

**606 ZZ**

100% Authentic Guarantee  
Guarantee Authentic or Money Back

Lowest Price Guaranteed  
Found a cheaper option? Claim for FREE Coins!

Shop Vouchers 95% OFF 50% OFF 10% OFF RM2 OFF

Add-On Add-on Deal

Shipping Free shipping Shipping To KL City, Kuala Lumpur Shipping Fee RM0.00

Bearing 1pcs:  606zz 6x17x6mm  607zz 7x19x6mm  608zz 8x22x7mm  609zz 9x24x7mm  623zz 3x10x4mm  624zz 4x13x5mm

Share: Favorite (797)

Appendix D- 4: The cost of 606ZZ radial bearing

Table D- 1: Overall costing for the prototype design.

Item No	Item Name	Quantity	Cost per Item (RM)	Total Cost (RM)
1	Mixing Chamber	1	40.00	40.00
2	Motor Housing	1	30.00	30.00
3	Rotating Impeller	1	2.86	2.86
4	Teflon	1	3.12	3.12
5	606ZZ radial ball bearing	1	1.78	1.78
6	G1/4 to Luer lock fitting	1	5.42	16.21
7	Dispensing nozzle	1	0.25	0.25
8	DC motor	1	2.19	2.19
9	Pressure Plug BSP 3/8	2	0.90	1.80
10	Mounting Bracket	1	0.84	0.84
11	High-Pressure Tube Fitting to G1/4 Male Connector	2	11.86	23.92
Total Cost				122.97